11-1976

Long-Distance Turbidite Correlations in the Horseshoe Abyssal Plain

William H. Hoyt
University at Albany, State University of New York

Long-Distance Turbidite Correlations in the Horseshoe Abyssal Plain

A thesis presented to the Faculty
of the State University of New York
at Albany
in partial fulfillment of the requirements
for the degree of
Master of Science

William H. Hoyt

November, 1976

ABSTRACT

Few studies on modern abyssal plain turbidites have attempted to assess the lateral extent of individual units and few have therefore been able to provide any information on the evolution of turbidity deposits across long abyssal plain distances. In the 4755 m-deep Horseshoe Abyssal Plain, ten distinct lithologic units (six of these Iberian Peninsula-derived turbidites) were delineated in nine piston cores on the basis of stratigraphic position, thickness (range of 20 cm to greater than 500 cm), color, sediment type, sedimentary structures, x-ray mineralogy, and the ubiquitous presence of units in all abyssal plain and supplying canyon piston cores. In order to make this correlation more rigorous, detailed grain size analyses, light and heavy mineralogy of sands, HCl treatment, and volatile solids determinations were performed on three of the six turbidite units, which have volumes of 5.7, 8.0, and 12.1 km^3. These analyses further confirm correlation over the entire 15,000 km^2 area of the Horseshoe Abyssal Plain and certainly provide long-distance correlations for six individual turbidites of over 300 km for each flow. In addition, shallow subbottom reflectors and transparent zones seen on 3.5 kHz-P.D.R. profiles can be tied into the in situ stratigraphy of the piston cores.

The results of previous studies on modern abyssal plain turbidites, ancient turbidite deposits, and experimental lab studies are compared with results from the Horseshoe

Abyssal Plain deposits and it is concluded that minor physiographic disturbances on the otherwise flat abyssal plain floor have resulted in marked sedimentological variation. It was found that regular grain size decrease and thickness decrease with increasing distance from the supplying canyon were not observed for individual bedding units. The ruling notions about lateral variations within turbidites are questioned.

Department of Geological Sciences
State University of New York at Albany
1400 Washington Avenue
Albany, N. Y. 12222

State University of New York at Albany

School of Arts and Sciences

The thesis for the master's degree submitted by

William H. Hoyt

under the title

Long-Distance Turbidite Correlations

in the Horseshoe Abyssal Plain

has been read by the undersigned. It is hereby recommended for acceptance by the Faculty with credit to the amount of six semester hours.

(Signed) Paul J. Fox

(Date) 22 Nov. 1976

(Signed) W. S. Kidd

(Date) 22nd November 1976

(Signed) Kevin Burke

(Date) 22nd November 1976

Recommendation accepted by the Dean of Graduate Studies for the Graduate Academic Council.

(Signed) _____

(Date) _____

ACKNOWLEDGEMENTS

The author wishes to gratefully acknowledge his advisor, Dr. P. J. Fox, for this work. He, along with Drs. D. H. Needham (CENEXO, Brest, France) and W. B. F. Ryan (Lamont-Doherty Geological Observatory), originally formulated this project and collected the data. Without the encouragement and direction of Dr. Fox, this study would have been much less fruitful.

The following faculty from the University at Albany are acknowledged for their advice and assistance: Drs. K. Burke, S. E. DeLong, J. F. Dewey, W. S. F. Kidd, E. H. McLaren, W. D. Means, and G. W. Putman. A. Hajeck, M. E. Bartlett, R. S. Haupt (Vt. Hiwy. Dept.), Drs. F. Shido, J. Olson (Univ. of Vt.), A. Brownlow (B. U.), and T. Shibata are thanked for their professional assistance during various phases of the work. Dr. G. M. Purdy (W.H.O.I.) is thanked for his aid.

Aid in drafting was supplied by P. Medic, E. Grossman, N. Ross, M. Mayrath, and M. Peacock. Aid in typing the original draft was supplied by M. Ayers. Proofreading and typing of the final draft was undertaken by Denise S. Hoyt, who also provided abundant encouragement and support.

Drs. Fox, Burke, Kidd,and Ryan read the manuscript and provided detailed suggestions for improvements, most of which have been incorporated into the final thesis.

The Office of Naval Research Grant #N00014-67-A-0108-004 and the National Science Foundation Grant #GA-29460 are acknowledged for collection of data.

TABLE OF CONTENTS

LIST OF TABLES

LIST OF FIGURES

CHAPTER I.

INTRODUCTION

Although a naturally occurring marine turbidity current has never been directly observed, the hypothesis that these density currents do episodically occur has now gained widespread acceptance among earth scientists. Continuous acoustic sounding of the ocean floor and accurate navigation have recently provided data on the physiography of the ocean floor which have shattered the earlier notion that the sea floor is a naked and featureless abyss (e.g. Heezen and others, 1959b; Heezen and Hollister, 1971). Researchers in the 1930's were startled to discover that precipitous submarine canyons notched the continental margins, some with greater topographic relief than that of the Grand Canyon. With similar surprise and excitement (Heezen, 1956), it was noted that adjacent to many continental margins (and apparently connected to them by submarine canyons) were the flattest regions on the face of the earth (apart from the surface of lakes and oceans). These submarine regions, called abyssal plains, had gradients of less than 1:1000 and were found upon core sampling to contain continentally-derived graded sands and silts intercalated with pelagic clays (Ericson and others, 1952). It has become generally accepted that these continentally-derived sands and silts of abyssal plains have been rapidly deposited by means of turbidity currents which have moved downslope from the continental margins, often

channeled by submarine canyons (Daly, 1936; Heezen, 1956).

The subject of this study is the sedimentology of the Horseshoe Abyssal Plain turbidites. In addition to possessing the above general characteristics (Horn and others, 1972), the Horseshoe Abyssal Plain possesses a rather unique characteristic among the world's abyssal plains: the long axis of the abyssal plain is roughly perpendicular to the regional continental margin trend instead of parallel to it. This fact has resulted in major terrigenous sediment input from only one direction, thus providing an excellent natural flume in which turbidity currents have presumably been deposited. Studying individual turbidite units from a single source is facilitated in such a natural flume by the ease of single-unit correlation.

Figure 1 shows the position of the Horseshoe Abyssal Plain off the southwestern corner of the Iberian Peninsula (about 120 km from Cape St. Vincent to the eastern edge of the abyssal plain).

Review of Studies on the Sedimentology of Turbidity Currents

Previous studies of turbidity currents and their deposits can be divided into three main groups for purposes of this study: 1) modern abyssal plain turbidites; 2) models based on ancient, subaerially exposed turbidites which are applicable to the study of modern turbidites; and 3) experimental studies in the laboratory.

FIGURE 1. General bathymetry of the Horseshoe Abyssal Plain area (after Purdy, 1975).

Contour interval in 100 corrected fathoms.

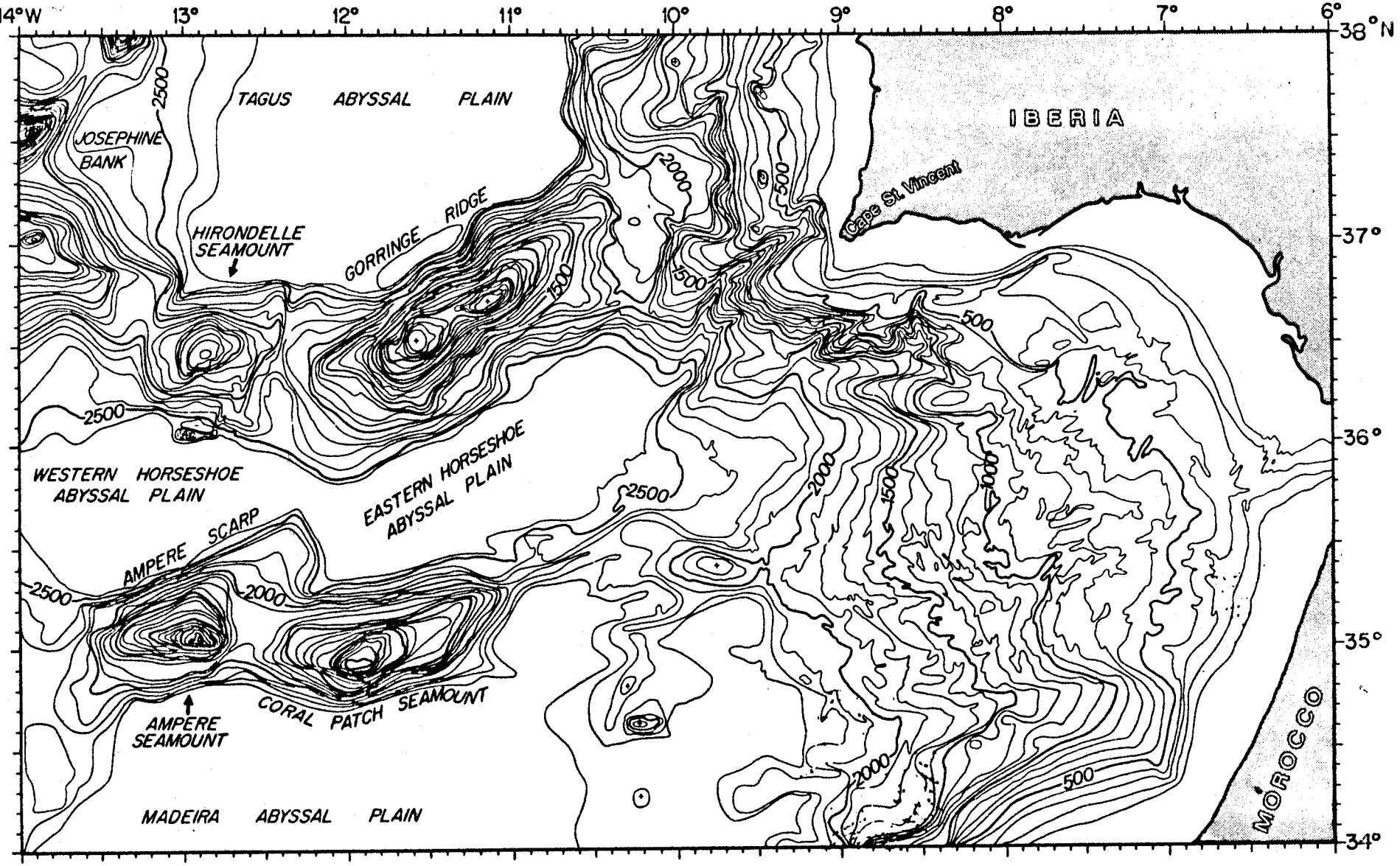
14°W
13°
12°
11°
10°
9°
8°
7°
6°
38°N
37°
36°
35°
34°
IBERIA
Cape St. Vincent
TAGUS ABYSSAL PLAIN
JOSEPHINE BANK
HIRONDELLE SEAMOUNT
GORRINGE RIDGE
WESTERN HORSESHOE ABYSSAL PLAIN
EASTERN HORSESHOE ABYSSAL PLAIN
AMPERE SCARP
AMPERE SEAMOUNT
CORAL PATCH SEAMOUNT
MADEIRA ABYSSAL PLAIN
MOROCCO
2500
2000
1500
1000
500

Modern Abyssal Plain Turbidites

To date, most publications on marine turbidites have been largely concerned with a definition of the sedimentological properties of abyssal plain turbidites. Bouma and Hollister (1973) have compared the sedimentological properties of contourites and turbidites and have distinguished these two types of deposits based on sorting, thickness, bedding contacts, fabric, microfossils, and plant and skeletal remains. In a similar manner, Rupke and Stanley (1974) have distinguished between turbidites and hemipelagic deposits, primarily on the basis of superposition, internal texture, structure, and clay mineralogy differences. The vast majority of studies on turbidites themselves have focused attention on the following characteristics: sediment type, textural properties, primary sedimentary structures, and displaced fauna (e.g. Phleger, 1951; Natland and Kuenen, 1951; Ericson and others, 1952; Gorsline and Emery, 1959; Davidson and Keen, 1963; Hubert, 1964; Hollister and Heezen, 1964; and Horn and others, 1971a, b, 1972). The majority of these studies dealt with abyssal plains which were positioned along continental edges and were characterized by multiple sediment sources and complex interfingering of turbidites (e.g. Hatteras and Sohm Abyssal Plains). Correlation of turbidite beds over great distances proved to be difficult and therefore little was learned about lateral variations of individual turbidites with increasing distance

from the source. Without this kind of knowledge of the turbidite bedding unit, understanding of the depositional processes of marine turbidity currents is imperfect.

However, several noteworthy studies have directly addressed the problem of turbidite long-distance correlation in recent years. In a study of the turbidite that resulted from the Grand Banks earthquake and slump of 1929, and which flowed on to the Sohm Abyssal Plain, Fruth (1965) was able to trace the turbidite some 1700 km. He also calculated the volume of the deposit, 160 km^3, and the area, 470,000 km^2 (this area is roughly equivalent to the area covered by the state of California, whereas, the Horseshoe Abyssal Plain area covers an area about the size of the state of Connecticut). This large turbidite was correlated on the basis of textural parameters, thickness, proximity to the sediment-water interface, and consistent lateral variations in textural parameters. Fruth's analysis of consistent lateral variations in textural parameters was helpful in developing theories about turbidity current evolution; however, these variations were not observed in the turbidites of the Horseshoe Abyssal Plain. Ryan and others (1965) noted "remarkably continuous" (several miles) turbidite beds in the Tyrrhenian Abyssal Plain, but complicated topography, multiple sediment sources and the limited number of cores (four) necessarily limit the certainty of these long-distance correlations. Conolly and Ewing's (1967) study of sedimentation in the narrow Puerto Rico Trench provided

apparent 200 km correlation based on color, texture, and composition of beds from ten cores. Multiple sources of sediment into the Puerto Rico Trench complicate simple turbidite correlation over long distances, but different compositions helped differentiate these units visually. In a study of bioclastic turbidite sedimentation in the Columbus Basin, Bahamas, Bornhold and Pilkey (1971) correlated six turbidites based on color, stratigraphy, ages of pelagics, coiling ratios of G. truncatulinoides, the G. menardii complex, thickness, composition, and texture from data of thirty closely-spaced piston cores. Correlations were possible within about 25 km of the steep banks of the basin, where the turbidites were coarse grained; with greater distance, the turbidites became finer and the units could not be traced further. In contrast, the results of the present study on six turbidites from the Horseshoe Abyssal Plain allow strong correlation of units for distances exceeding 300 km. Moreover, decrease in grain size with increased distance from the source was not observed for the turbidites of the Horseshoe Abyssal Plain. Payne and others (1972) were able to correlate thick (1-to-5 m) turbidites in the Wilkes Abyssal Plain off Antarctica, but were unable to correlate thin turbidites (10-to-50 cm) due to uniformity of coarse-grained constituents. At least one turbidite in the Horseshoe Abyssal Plain is greater than 5 m and provides one of several checks on the visible correlation. Pilkey and Bennetts (1974) correlated three individual turbidites

over 100 km in the Hispaniola-Caicos basin, based on color, thickness, composition, and other parameters. In a study of the Navidad Basin (located between the Puerto Rico Trench and the Hispaniola-Caicos Basin of two previous studies), Seiglie and others (1976) correlated seven sand layers and eleven other stratigraphic horizons in six cores from the 4400 m-deep 35x6 km basin. Correlations over this short distance were based on core stratigraphy, coiling ratios of G. truncatulinoides, percent $CaCO_3$, and various faunal abundances. Most recently, Elmore (1976) has claimed discovery of extensive (400 km) horizontal continuity of a single large, coarse-grained turbidite in the Hatteras Abyssal Plain on the basis of data obtained from 65 piston cores. Unusual black shell fragments were used as an indicator marker for this turbidite, which was also correlated by means of core stratigraphy, grain size, thickness, mineralogy, and acoustic continuity of inferred turbidite reflectors. One characteristic held in common among all of these previous studies is that seaward thinning and/or seaward decrease in grain size was observed, at least in a general fashion. These two observations have become essential components of the ruling paradigm concerning turbidity current evolution (see Appendix I. for details).

Ancient Turbidite Models Applicable to the Study of Modern Abyssal Plain Turbidites

If one accepts as a working hypothesis the tenet that

subaerially exposed deposits with sedimentological characteristics similar to modern turbidites are indeed ancient analogues of Holocene marine turbidites, then sedimentation models based on analyses of these rocks can be applied to modern studies. Many workers have studied large groups of ancient turbidites in an effort to understand how lateral facies changes may reflect original deposition in various morphological provinces in a prograding submarine canyon-fan-channel-abyssal plain sequence (e.g. Mutti and Ricci-Lucchi, 1974, 1975; Nelson and others, 1975). However, the study of the Horseshoe Abyssal Plain does not contain large numbers of turbidity flows (only six major ones) and therefore, these facies models based on ancient Apennine turbidites are not applicable to the present study. Significantly however, Ricci-Lucchi (1975) has claimed great lateral continuity (250 km) of groups of ancient calcareous turbidites exposed in the Apennines of Italy. Parea and Ricci-Lucchi (1975) have further claimed lateral correlations by "... 'walking out in the field' some spectacular turbidite beds for 140-190 km and these beds can be taken not only as stratigraphic markers, but also as paleogeographic and environmental indicators inasmuch as they are found in a well-defined facies association" (p. 235). The emphases of the prior two studies were not on the development of or changes within an individual unit with distance from the source, but as possible indicators of possible paleoenvironments. The data apparently do not allow detailed analysis of a single

bedding unit over great distances.

Many workers have studied the graded beds of the Bavarian "Flysch" Formation in the Alps in an effort to study the supposed turbidite bedding unit. Bouma's (1962) ideal vertical sequence for a turbidite unit was used by many to attempt lateral correlations of turbidites. Hesse (1974) used a petrologically-defined marker bed of the Gault Formation (Alps) to correlate an individual ancient turbidite unit for a distance of 115 km; this evidence suggests that such marker units should exist in modern deposits. Walker (1967) has provided a potentially useful "proximality index" based on textural parameters of ancient turbidites from Maryland, U.S.A.

In conclusion, these studies of flysch may be useful in studying modern turbidites, but it should be pointed out that the complicated structural and deformational setting of most flysch deposits makes the study and interpretation of individual sedimentological units very difficult. Indeed, the author agrees with Walker and Mutti (1973) that further work on modern abyssal plain deposits "...will be necessary before any further synthesis of interpreted ancient environments and actualistic modern environments can be attempted" (p. 146) (see Appendix I.).

Experimental Studies

Many workers have described various mechanisms for transportation of sand and coarser material into deep water

(e.g. Dott, 1963; Middleton and Hampton, 1973). The mechanism of turbidity currents, however, is the only one previously demonstrated beyond a reasonable doubt to be an effective transportation agent for moving large sediment accumulations into deep water (Middleton and Hampton, 1973). Nevertheless, components of other mechanisms are thought to operate in turbidity current initiation, movement, and deposition (e.g. debris flows). For purposes of the present study, only the deposition of turbidity current material will be discussed.

Based on Kuenen and Migliorni's (1950) pioneering hypothesis that turbidity currents are the cause of most graded deposits observed in outcrop, several workers have produced small turbidity currents in the laboratory. Middleton (1966a, b, 1967) used a flume tank 5 m long to study the motion of the head of the turbidity current, the uniform flow of density currents, and deposition of sediment, respectively. These studies provide models for grain size parameters (mean grain size, sorting, skewness, and kurtosis) that one can test by applying the models to modern turbidite deposits. These flume studies may be particularly applicable to the study of the flume-like Horseshoe Abyssal Plain area. Kuenen (1966a) used a circular flume tank to increase the duration of the experiment and was able to produce laminations and other primary sedimentary structures observed in modern turbidites. A fundamentally different approach to turbidity current modeling has been taken by Van der Knaap and Eype (1968):

instead of introducing a slurry of sediment into clear water as earlier workers had done, they rapidly increased pore-water pressure in an existing sediment layer on a slope, which resulted in slumping of the sediment and subsequent development of a turbidity current; many workers have noted that submarine slumping may be caused by earthquake activity and/or oversteepening of the depositional slope (e.g. Heezen and Ewing, 1952; Morgenstern, 1967).

The Ruling Paradigm

In conclusion, the scientific community presently holds to be accurate the following brief model of modern abyssal plain turbidite sedimentation:

1) After being initiated by a variety of mechanisms (usually on the continental shelf/slope), a density current moves downslope toward the abyssal depths (usually through submarine canyons and/or channels).

2) This current, laden with a wide range of sizes and types of material, moves downslope at "catastrophic" geologic rates (up to 55 kts, estimated by Heezen and Ewing, 1952) and spreads out on flat abyssal plain(s).

3) While "fanning out" on the floor of an abyssal plain, the current is thought to decellerate and deposit its load in a manner which is not well understood (it has never been observed).

4) It is thought that this supposed decelleration will manifest itself in the observed deposits by displaying thinning

of the deposit away from the source, fining of the grain size away from the source, and by various other lateral changes, especially in textural parameters.

Purpose of Study

The purpose of studying the turbidites of the Horseshoe Abyssal Plain is to examine an apparently relatively simple sedimentological basin into which turbidity currents have flowed in an effort to shed light on how turbidity currents deposit sediments as they move across the ocean floor. Ascertaining the extent and character of individual turbidites is desirable to achieve this end. Another purpose of this study is to test various published models concerning turbidites: some are based on empirical relationships observed in the laboratory, others are based on studies of ancient turbidite deposits, and a third set are based on studies of Holocene marine turbidites.

More specifically, a testing of the ruling paradigm concerning turbidity current evolution, as outlined in 4 above, will be undertaken. Other aspects of the paradigm here presented are beyond the scope of this study.

CHAPTER II.

SETTING

The Morpho-Tectonic Setting

The Horseshoe Abyssal Plain has an area of about 15,000 km^2, a regional depth of approximately 4755 m (2600 fm corrected), a gradient of less than 1:2000, an average width of 50 km, and a length of 300 km (Figure 1). The plain is bounded on the north by a portion of the seismically active Azores-Gibraltar Ridge (the Gorringe Bank and Hirondelle Seamount), on the west by abyssal hills, on the south by the Ampere Seamount and the Coral Patch Seamount, and on the east by the continental margin of Portugal and Spain (the horseshoe-shaped morphology, with the open end of the horseshoe facing the east, has given rise to the name "Horseshoe Seamount Chain").

The Horseshoe Abyssal Plain area is different from most of the world's abyssal plains in the following characteristics, which are all conducive to the development of a relatively simple sedimentological regime:

1) From published bathymetric data, it appears that the Horseshoe Abyssal Plain has only one major terrigenous sediment source, the large submarine canyon leading up to Cape St. Vincent, Portugal. A single major sediment source means that the common confusing complications characteristic of almost all world abyssal plains (multiple continental

sediment sources, interfingering of turbidity flows from different directions, etc.) will not, in all likelihood, be found in the Horseshoe Abyssal Plain;

2) The long axis of the abyssal plain (east-west) is very nearly linear and runs sub-perpendicular to the continental margin trend. Also, the east-west axis (300 km) is about six times the north-south axis (50 km),and therefore provides an excellent natural flume; and

3) Coupled with the preceding two factors, the seamounts surrounding the Horseshoe Abyssal Plain provide topographic protection from disturbing submarine influences such as turbidity flows external to the Horseshoe Abyssal Plain and regional bottom currents. Theoretically, the above factors provide a setting which permits turbidity currents to evolve in an uncomplicated sedimentological environment.

Many workers have studied the tectonics of the region surrounding the Horseshoe Abyssal Plain. Krause and Watkins (1970) have named the Azores-Gibraltar ridge a "transverse fracture zone" to emphasize their contention (and that of several others) that this plate boundary between the African and Eurasian plates is not a simple oceanic transform fault with only strike-slip motion, but rather a boundary which, along its length from the Azores (west) to Gibraltar (east) expresses: 1) right-handed (dextral) strike-slip motion with some extensional spreading near the Azores; 2) almost exclusively dextral strike-slip motion mid-way between the Azores and Gibraltar, and; 3) strike-slip motion with north-

south compression in the area of the Horseshoe Abyssal Plain and east to Gibraltar.

LePichon and others (1971) took deep-sea photographs of a presently active fault west of the Gibraltar Straits by means of a Troika survey packet which was hauled from northwest to southeast (across the extreme eastern region of the Horseshoe Abyssal Plain up onto a seamount). The sense of displacement observed for this fault and the inferred fault plane solutions for other faults in the area (LePichon and others, 1970) led LePichon and others (1971) to maintain that as the oceanic basement is "swallowed" along the Azores-Gibraltar Ridge by north-over-south thrusting at the bottom of the abyssal plain, the incompetent and lighter sedimentary cover gradually overflows each side of the Horseshoe Abyssal Plain. Gavasci and others (1973) provide independent petrographic evidence (discussed in section on petrography of turbidite sandy bases) which suggests that the Gorringe Ridge has been upthrust as a result of subduction of oceanic crust.

A detailed geophysical study of the eastern end of the Azores—Gibraltar plate boundary by Purdy (1975) indicates that the Horseshoe Abyssal Plain sediments are lying on oceanic crust which is being consumed (in an unusual manner) at the low rate of 1 cm/yr (see Appendix II). Several large earthquakes (greater than 8.0 on the Richter Scale) have been recorded since 1961 in the area of the eastern end of the Horseshoe Abyssal Plain; dozens of smaller quakes have been recorded in the region in the same time interval (Barazangi

and Dorman, 1969; Tarr, 1974). Despite this recent tectonic activity, detailed acoustic profiling in the present study demonstrates that the Holocene turbidites of the Horseshoe Abyssal Plain are undisturbed (see Figures 4,5, and 6).

Geologic Setting

Major terrigenous sediment sources for the turbidites of the Horseshoe Abyssal Plain are the southern and western coastlines of the Iberian Peninsula, predominantly the coastlines of Portugal. The present coastal areas of southern Portugal consist almost entirely of Pleistocene deposits of continental origin, which presumably provided a large portion of sediment to the Horseshoe Abyssal Plain turbidites which are of inferred Holocene age (Carta Geologica Do Quaternario De Portugal, 1969). Pre-Pleistocene rocks of southern Portugal are predominantly Permo-Carboniferous marine deposits termed "flysch", in addition to various metavolcanic rocks (Carta Geologica De Portugal, 1972). The sedimentary rocks include conglomerates, arenites, wackes, limestones, shales, and marls. The Algarve region of southernmost Portugal contains predominantly Mesozoic sedimentary rocks thought to have been deformed during the Alpine Orogeny (Pratsch, 1958).

The common coastal process called long-shore drift doubtlessly has transported material (sand, silt, and clay) from the mouths of the three major rivers in the area (the Tagus River on the west coast and the Guadalquivir and Guadiana Rivers on the south). Duplaix and others (1965) have demon-

strated that the mineralogy of sand in the Tagus River delta is nearly identical to the mineralogy of sand in the Tagus Abyssal Plain, to the north of the Horseshoe Abyssal Plain, which suggests that continental shelf sediment has been redeposited in an adjacent abyssal plain. Although a similar study has not been made for relating the Cape St. Vincent continental shelf sediments to the turbidites of the Horseshoe Abyssal Plain, it is reasonable to suppose that a similar correlation exists.

During the latest glacial stages of the Quaternary, several world-wide low-stands of sea level and high erosion rates probably resulted in large deposits of sediment on the outer continental shelves which provided material for turbidity currents (e.g. Emery, 1969). In many present-day abyssal plains (the Horseshoe included), piston cores reveal a worm-burrowed pelagic sediment top, which indicates an absence of very recent (a few thousand years) turbidite sedimentation. Most of the turbidites of the world's abyssal plains are therefore older than late Quaternary and have been deposited by turbidity currents which were a function of environmental conditions not operating today.

CHAPTER III.

METHODS OF STUDY

Data Collection at Sea

Data for this study were collected on Leg 8 of Colombia University's VEMA Cruise 27 (Lisbon-Madeira) during November of 1969. Acoustic records (seismic reflection profiler, 3.5 kHz precision depth recorder, and 12 kHz records) were all continuously operative as standard underway equipment. Piston cores were taken at nine stations.

Laboratory

Preliminaries to the Present Study.

The nine piston cores were opened, split, and photographed in color at the Lamont-Doherty core repository on 11 June, 1970. The cores were then stored in the core repository until they were sampled in the fall of 1974.

Detailed Lab Analyses of Sediments.

Over 350 sediment samples were taken from the nine cores, on which detailed grain size analyses, volatile solids determinations, HCl-soluble determinations, petrographic mineral determination of sands, and determination of x-ray mineralogy of muds and clays were carried out.

A standard method of grain-size analysis was used (adapted from Schlee, 1957). Samples were deflocculated with sodium

hexametaphosphate water (Calgon) and sieved through a 63 micron (4Ø) brass sieve; the finer than 63 micron fraction was then analyzed by a pipette method based on Stoke's law of settling velocities for spherical particles. Folk's (1968) statistics were used to calculate mean grain size (graphic mean), sorting (inclusive graphic standard deviation), skewness (inclusive graphic skewness), and kurtosis (graphic kurtosis). The standard phi (Ø) scale, based on Wentworth's (1922)size grade scale is used throughout (see Appendix III). Recovery of material from the grain size analyses averaged about 95%.

Volatile solid percentages were determined using method 224-G of the American Health Association, which ashes the agate-ground sample at 650° C for one hour in a muffle furnace.

The percentage of the agate-ground sample soluble in 10% HCl (mostly $CaCO_3$ and organic material) was determined using a standard procedure developed after Ireland (1971). Of the three acids tested (reagent grade glacial acetic acid, 10% hydrochloric acid, and 1:1 nitric acid, H_2O:HNO_3), the 10% solution of HCl was determined to be most efficient for this study (see Appendix III).

The sands from the grain-size analyses were seperated into heavy and light mineral fractions using tetrabromoethane (sp. grav. measured to be 2.96 gm/cc) according to standard gravity-settling methods described by Carver(1971). From the resulting populations of heavy and light minerals,

permanent petrographic microscope slides (grains sprinkled into hot balsam then covered with a glass slip) were made for each sample. Mineralogy of the "light" fraction (less than 2.96 gm/cc density) was determined by counting 100 non-$CaCO_3$ grains in the slide using a mechanical stage. Total point counts ranged between 202 and 958, which provides excellent counting statistics according to the criterion of Hubert (1971, Figure 36 of Appendix III). Due to contamination of the heavy mineral slides and very low concentrations of heavy minerals, quantitative counting of heavy minerals was not performed. Contamination was probably caused by heavy mineral grains dragging down lighter and smaller light mineral grains and biogeneous debris. Apparently some disaggregation procedure must be added to the standard gravity-settling techniques for grains of this size and character (4Ø and angular).

X-ray diffraction of muds and clays were run on a Siemens x-ray diffraction unit using normal instrumental settings. A slide-mounting technique was developed in analyzing the Horseshoe Abyssal Plain sediments. Three agate-ground specimens (one from the top section of each of the large turbidites) were chosen as representative of most samples in these turbidites and were used in a pilot study. A smear-mounting on glass technique seemed advisable (Gibbs, 1968), but five runs were made with disappointing results: reflections of certain minerals, known from previous work (x-ray powder diffraction film studies by the author) to be

in the specimen, were broad and of very low intensity. In a second mounting technique, weighed amounts of sample were added to a measured volume of redistilled water (in test tubes and immersed in an ultrasonic bath for five minutes). Resulting slurrys were then allowed to evaporate to dryness on glass specimen slides. As with the first mounting technique, reflections of minerals known to be in the specimen were broad and low. A third glass slide mounting technique enhanced basal plane reflections by preferred orientations and defined clearer and higher amplitude peaks for most minerals. However, reflections from minor components were not always reproducible when runs were duplicated. One sample from each of the three turbidite tops was weighed (0.1 gm) into a beaker and 30 ml of redistilled water was added. After stirring with a glass rod in an ultrasonic bath for three minutes, the sample was transferred to a 100 ml graduated cylinder and permitted to seperate by settling (method from E. H. McLaren, Dept. of Chemistry SUNY-Albany). One ml aliquots were taken from half way down and from the bottom of this column after periods of 5, 15, and 30 minutes; the six resulting specimens were allowed to evaporate to dryness on specimen slides and then run on the x-ray diffraction instrument with the aforementioned settings (see Appendix III). A careful consideration of the diffractogram results indicated that the two 15 minute samples were unnecessary because they did not contribute to information gained using the other four runs, and thus were dropped in subsequent runs. The sample

drawn from the bottom of the cylinder is henceforth referred to as the Lower Aliquot (LA), whereas the sample taken from half way down is referred to as the Upper Aliquot (UA),(see Table IV). Further XRD profiles were made of these specimens after they were treated with 10% hydrochloric acid to establish the presence of chlorite (see Ireland, 1971 for procedure and to explain the chlorite peak shift upon acid treatment). Slower scans at 1^{o}/10 minutes were made for definite identification of ferririte (a zeolite) and feldspar phases (see Appendix III for details of a sample XRD run). Several x-ray diffractograms were made of standard minerals for aid in identifying common phases (several different sources were used, including the American Petroleum Institute). A gold standard was used to assure that the diffractometer mechanisms were properly aligned.

CHAPTER IV.

DATA AND DISCUSSION

Introduction

After presenting detailed bathymetry of the Horseshoe Abyssal Plain, the VEMA 27 ship track coverage, and the piston core locations, acoustic data of two sorts (seismic reflection profiler and 3.5 kHz-precision depth recorder records) will be presented to establish the acoustic continuity of shallow subbottom reflectors. The acoustic continuity of layers throughout the entire abyssal plain as displayed on the detailed 3.5 kHz-P.D.R. records can be easily tied into the piston core stratigraphy to demonstrate that acoustic reflectors and transparent zones seen in the upper 4-5 fm (7.3-9.1 m) of the 3.5 kHz records match zones in the piston cores where sand and clay, respectively, are found. Macroscopic visual correlation of the piston cores from the abyssal plain are excellent; detailed grain size analyses, thicknesses, color, mineralogy, and other analyses make this nearly 400 km correlation of six individual turbidite deposits much more rigorous and provide a foundation on which to discuss the sedimentological development of each turbidite as it has moved down the length of the Horseshoe Abyssal Plain.

Bathymetry, Ship Track, Core Locations

The abyssal plain is contoured in 5 m intervals (Figure 2,

FIGURE 2. Detailed bathymetry of the Horseshoe Abyssal Plain (contoured in uncorrected meters), showing VEMA 27 ship track and core locations.

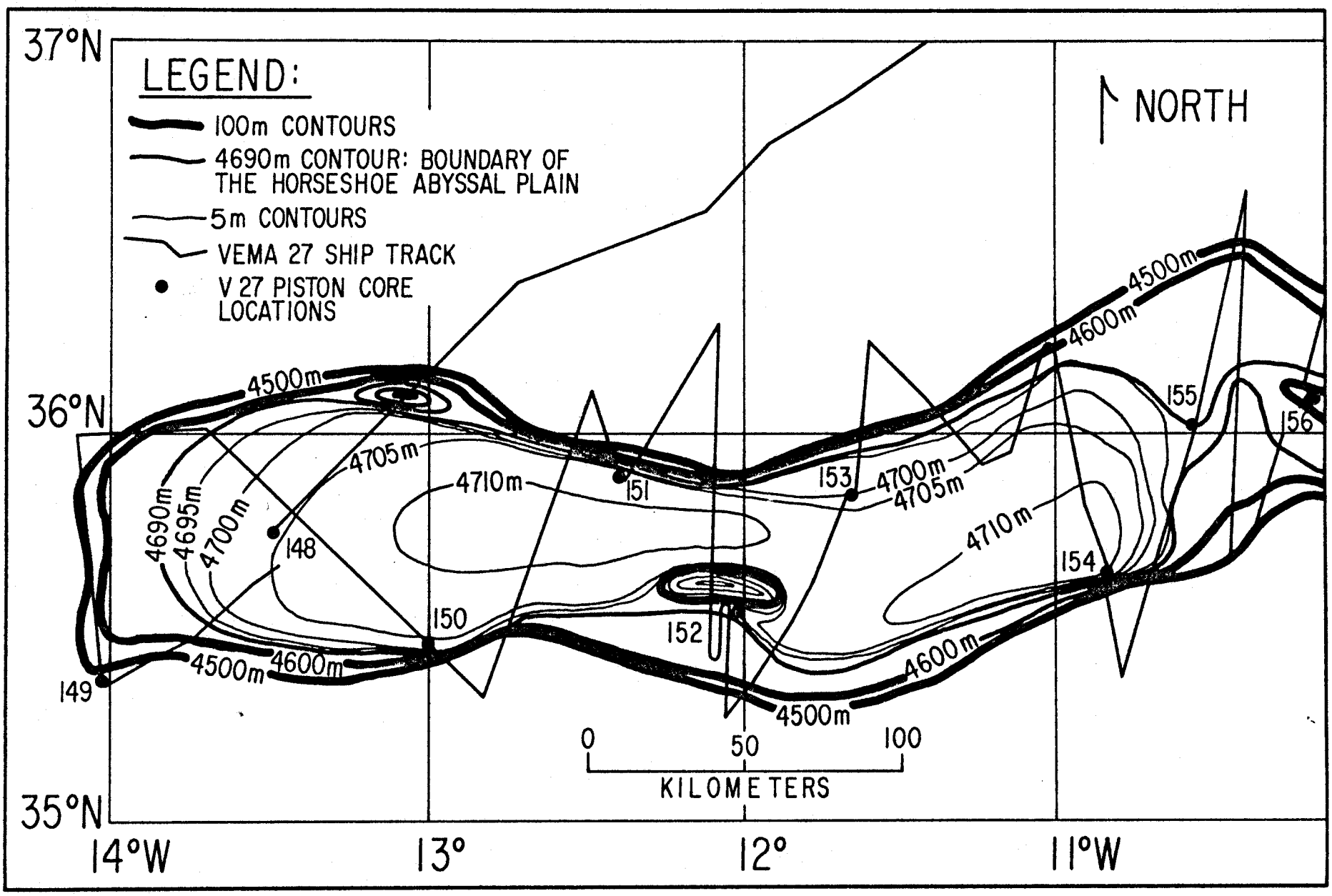
LEGEND:
100m CONTOURS
4690m CONTOUR: BOUNDARY OF THE HORSESHOE ABYSSAL PLAIN
5m CONTOURS
VEMA 27 SHIP TRACK
V 27 PISTON CORE LOCATIONS
NORTH
37°N
36°N
35°N
14°W
13°
12°
11°W
4500m
4600m
4690m
4695m
4700m
4705m
4710m
148
149
150
151
152
153
154
155
156
0
50
100
KILOMETERS

depths uncorrected for local variations in the speed of sound), with 4690 m chosen as the limit of the plain. The 4500 m and 4600 m contours are included to delineate regional bathymetric trends. Except for the two large topographic highs on the south and north boundaries (at 12°W and 13°W, respectively), the gradients in the abyssal plain are some of the lowest found in the world's ocean basins (from 1:1000 to 1:20000). Note the two slight depressions at 4710 m depth, one in the southeast, and one in the west-central part of the abyssal plain; also note the ledge protruding from the northeast margin of the plain (core 153, see Figure 6A). The VEMA 27 ship track coverage on which this bathymetric map is based is superimposed on the map, as well as the nine piston core locations used in this study. Table I lists the VEMA 27 core numbers of this study, their locations, depths (fm and m), and their core lengths. Moving down the table, the cores are arranged west to east and divided by region (abyssal hills, abyssal plain, and supplying channel). Note that all the cores in the abyssal plain are between 4700 and 4709 m depth, and that all but one of the cores (148) are within 10 km of the abyssal plain boundary.

Acoustic Data

Over 1500 km of continuous acoustic data were collected for the study of the Horseshoe Abyssal Plain using the seismic reflection profiler, the 12 kHz sound source, and the 3.5 kHz-P.D.R. sound source. Figure 3 shows the location map for

TABLE I. VEMA 27, LEG 8 CORE DATA.

REGION	CORE	LOCATIONS		DEPTHS		CORE LENGTH
	#	NORTH LATITUDE (DEGREES, MIN.)	WEST LONGITUDE (DEGREES, MIN.)	(FM)	(M)	(CM)
Abyssal Hills	149	35, 20.0	14, 01.9	2355	4307	210
Abyssal Plain	148	35, 45.6	13, 26.7	2572	4704	861
Abyssal Plain	150	35, 26.9	12, 59.2	2572	4704	602
Abyssal Plain	151	35, 52.9	12, 23.3	2573	4706	560
Abyssal Plain	152	35, 32.0	12, 04.4	2570	4700	625
Abyssal Plain	153	35, 50.9	11, 38.0	2570	4700	335
Abyssal Plain	154	35, 37.2	10, 50.6	2575	4709	806
Supplying Channel	155	36, 03.2	10, 33.7	2565	4691	640
Supplying Channel	156	36, 07.7	10, 13.3	2564	4689	915

FIGURE 3. Reference map of the Horseshoe Abyssal Plain showing locations of acoustic profiles displayed in Figures 4, 5, and 6.

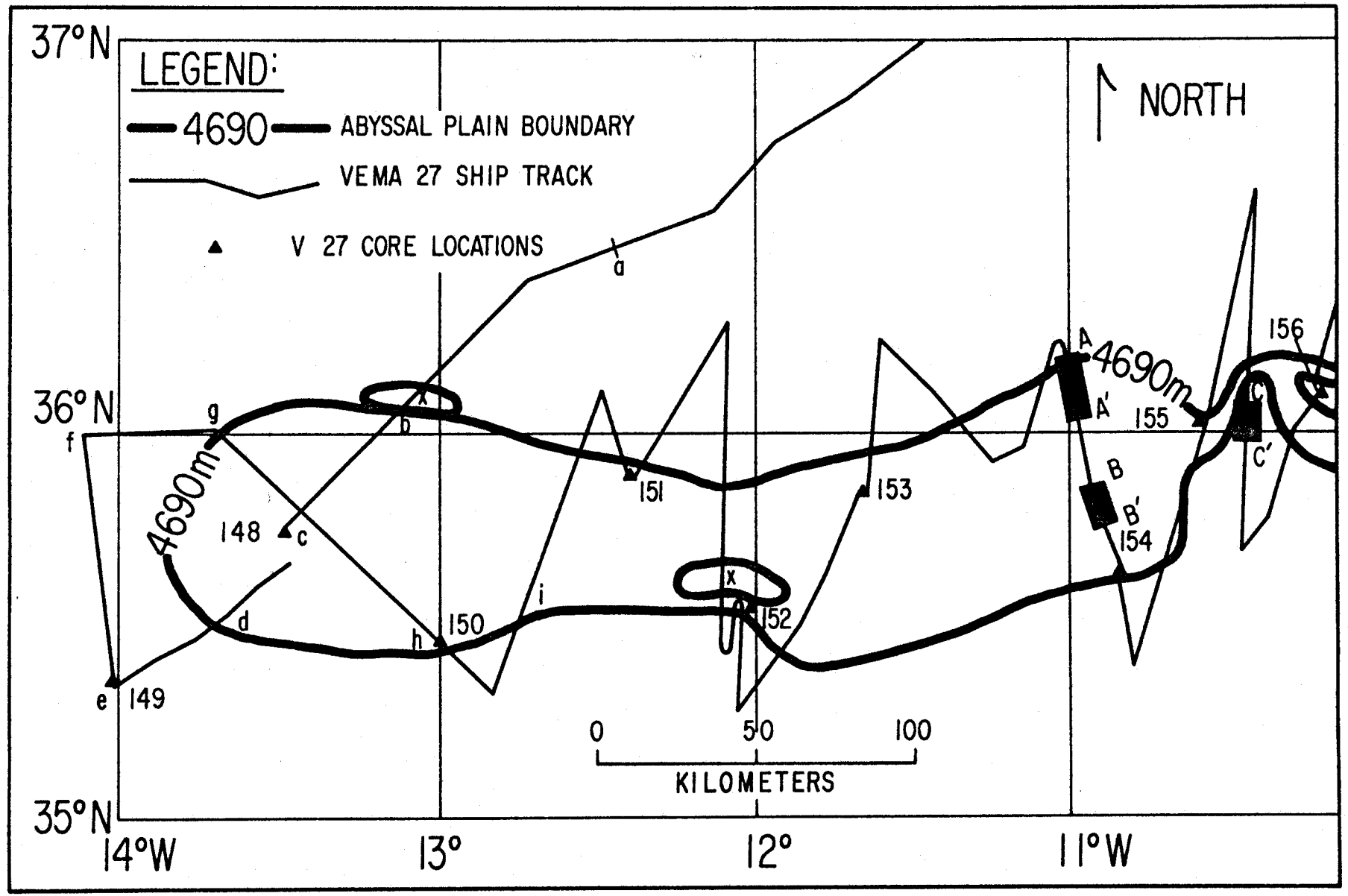
37°N
LEGEND:
4690
ABYSSAL PLAIN BOUNDARY
VEMA 27 SHIP TRACK
V 27 CORE LOCATIONS
NORTH
36°N
35°N
14°W
13°
12°
11°W
4690m
4690m
a
b
c
d
e
f
g
h
i
x
148
149
150
151
152
153
154
155
156
A
A'
B
B'
C
C'
0
50
100
KILOMETERS

acoustic profiles displayed in Figures 4,5, and 6. Figure 4 shows two types of acoustic records going from the largest scale (seismic reflection profile-Figure 4 A),through the intermediate scale (enlarged seismic reflection profiler record, Figure 4 B), to the smallest scale (3.5 kHz-P.D.R., Figure 4 C). The lettered points along the bottom of Figure 4 A refer to points on Figure 3 along the ship track; three core locations are marked and directions of the ship track are noted for orientation purposes. Figure 4 B expands the view of the hill south of the Hirondelle Seamount; note the upwarped sediments at about 2600 fm and the downwarped interface (basement?) at 2800 fm. The upwarped sediments, the presence of an axial ridge, and the upthrust, perched turbidite sediments of Figures 4 B and C suggest that crustal rupture and the initiation of imbricate thrusting described in the Peru-Chile Trench (oceanic crustal compression) by Prince and Kulm (1975) have operated in the Horseshoe Abyssal Plain. In further support of this hypothesis, Purdy (1975), in his study of the geophysical aspects of the Horseshoe Abyssal Plain area, notes that a great density of earthquake epicenters have recently occurred in the eastern Horseshoe Abyssal Plain, suggesting subduction of oceanic crust in this area. Detailed gravity surveys by Purdy also generally support this hypothesis in that they display a gravity high parallel to the subduction zone, as is commonly observed over other trenches. The arrow in Figure 4 B refers to the area expanded on the 3.5 kHz-P.D.R. record shown in Figure 4 C.

FIGURE 4. The two types of acoustic profiles used in the study showing seismic reflection profiler records (A), detail of seismic reflection profiler records (B), and 3.5 kHz-P.D.R. records (C). From A to C shows large to small scale, with the arrow of B referring to the region shown in C (location of Figure 3).

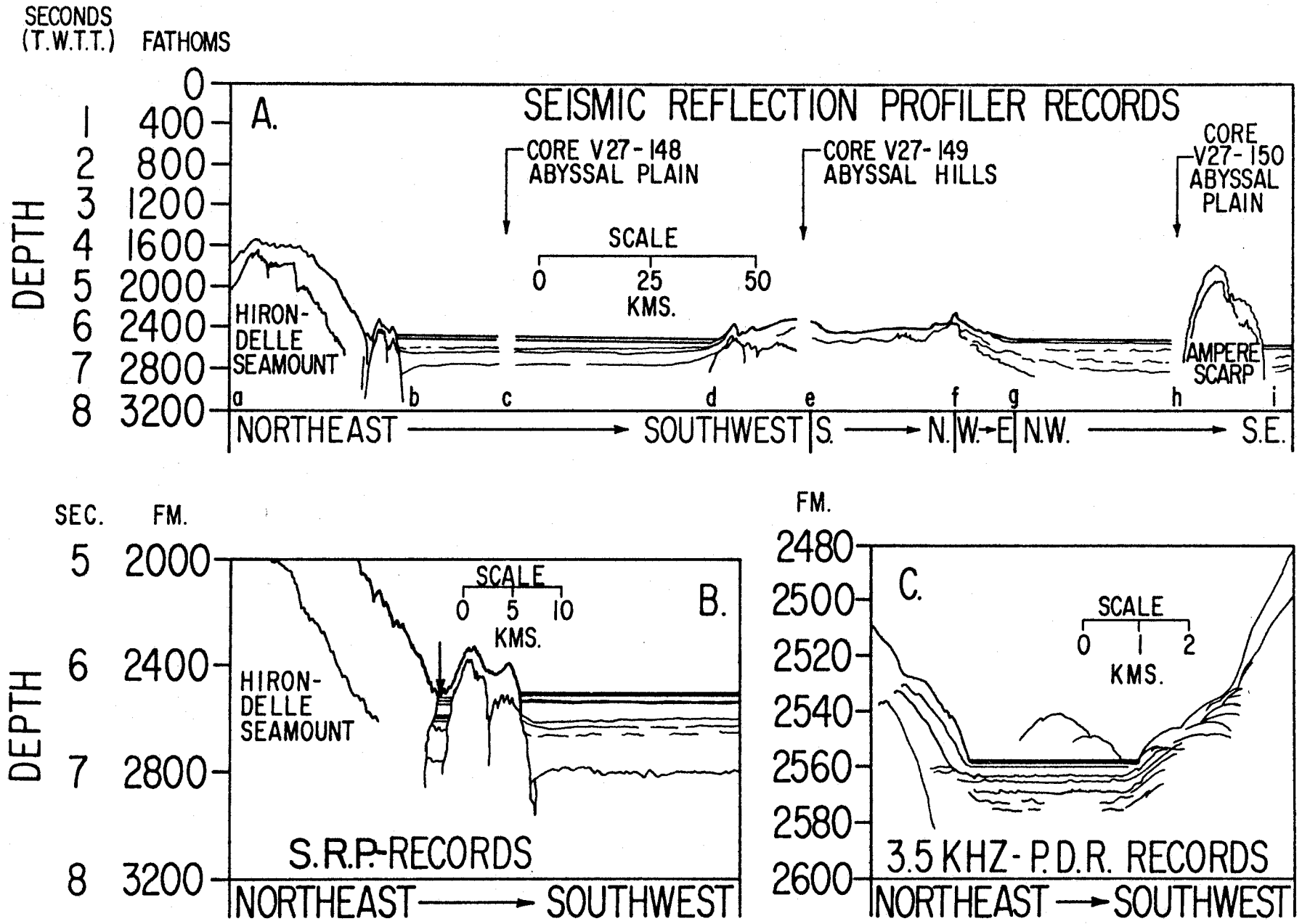
SECONDS (T.W.T.)
FATHOMS
DEPTH
0
1 400
2 800
3 1200
4 1600
5 2000
6 2400
7 2800
8 3200
A.
SEISMIC REFLECTION PROFILER RECORDS
CORE V27-148 ABYSSAL PLAIN
CORE V27-149 ABYSSAL HILLS
CORE V27-150 ABYSSAL PLAIN
SCALE
0 25 50
KMS.
HIRON-DELLE SEAMOUNT
AMPERE SCARP
a b c d e f g h i
NORTHEAST → SOUTHWEST
S. → N.
W.→E
N.W. → S.E.
SEC.
FM.
5 2000
6 2400
7 2800
8 3200
B.
SCALE
0 5 10
KMS.
HIRON-DELLE SEAMOUNT
S.R.P.-RECORDS
NORTHEAST → SOUTHWEST
FM.
2480
2500
2520
2540
2560
2580
2600
C.
SCALE
0 1 2
KMS.
3.5 KHZ-P.D.R. RECORDS
NORTHEAST → SOUTHWEST

Note the continuous subbottom reflectors and the hyperbolic echoes from the steep surrounding walls.

The detailed 3.5 kHz-P.D.R. records of Figure 5 demonstrate the remarkably continuous acoustic character of the upper twenty fathoms of sediments throughout the entire abyssal plain. This nearly identical pattern of acoustic continuity is observed over the 600 km of abyssal plain crossings and at each core location in the abyssal plain and supplying channel. Acoustic continuity continues to the channel-cut eastern extreme of the abyssal plain and, indeed, even up into the supplying canyon (Figures 6 A, B, and C). The locations of the 3.5 kHz-P.D.R. records of Figure 6 are shown on the index map of the abyssal plain (Figure 3) and are marked on the map and in the figure by A-A', B-B', and C-C', respectively. The widths of the channels shown, both relict and active, are a maximum of 2 km, but there are other channels (notably south and west of core 156) which are very broad and shallow, reaching widths up to 15 km and depths of 10 fm. The acoustic character of the sediments in the latter channels cannot be correlated with absolute certainty to the abyssal plain. The Vidal deep-sea channel was studied by Embley and others (1970) and was found to have fed sediments to the Demerara and Barracuda Abyssal Plains. The channels found in the eastern region of the Horseshoe Abyssal Plain are very similar, but are smaller in scale than the Vidal deep-sea channel; this suggests by analogy that these Horseshoe Abyssal Plain channels have also fed

FIGURE 5. Four 3.5 kHz-P.D.R. records from core locations demonstrating acoustic contunuity of the third turbidite top (closed arrows) and the sixth turbidite top (open arrows). Profile locations are shown in Figure 3 and core stratigraphy is shown in Figure 7.

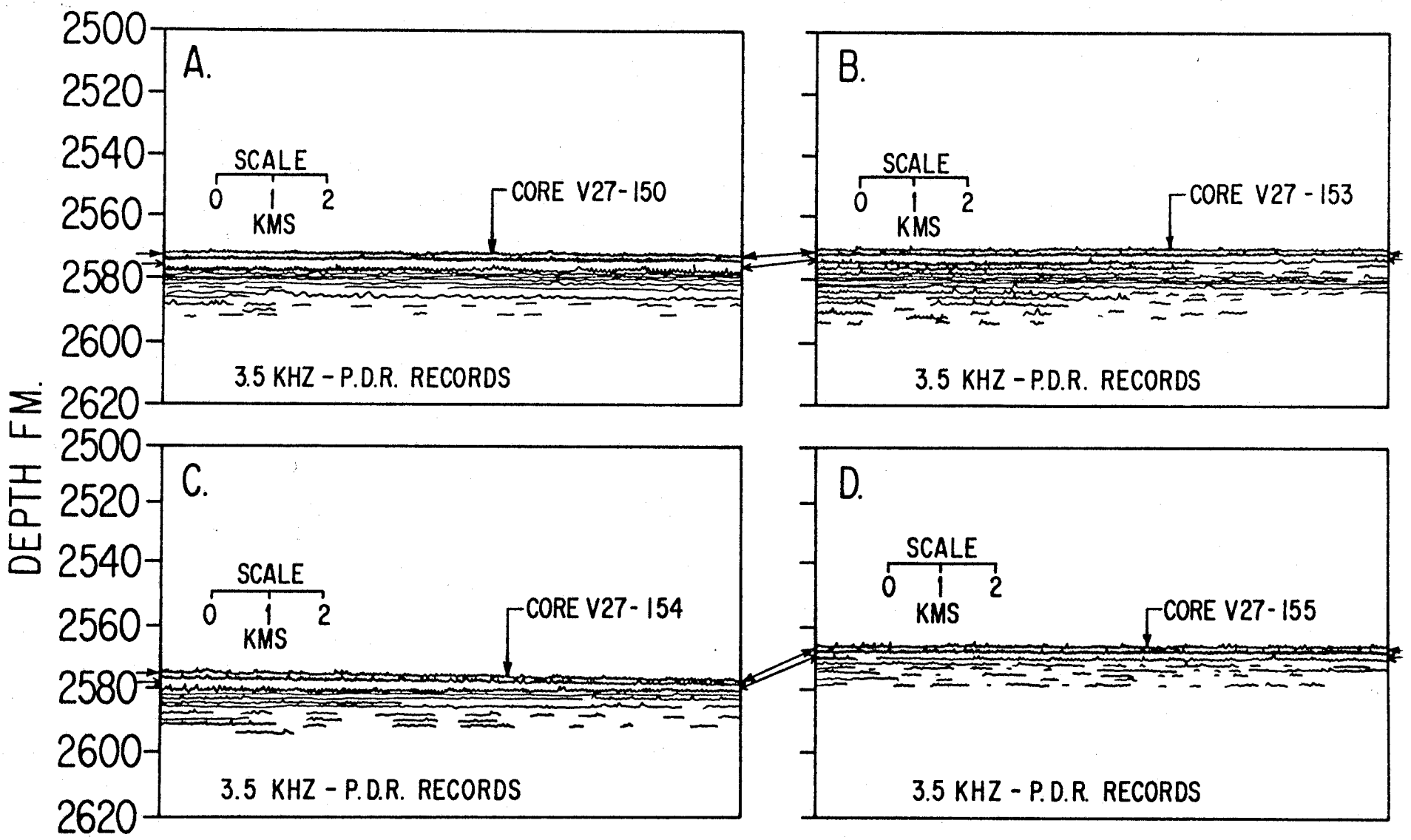
DEPTH FM.
2500
2520
2540
2560
2580
2600
2620
A.
SCALE
0 1 2
KMS
CORE V27-150
3.5 KHZ - P.D.R. RECORDS
B.
SCALE
0 1 2
KMS
CORE V27 - 153
3.5 KHZ - P.D.R. RECORDS
C.
SCALE
0 1 2
KMS
CORE V27-154
3.5 KHZ - P.D.R. RECORDS
D.
SCALE
0 1 2
KMS
CORE V27-155
3.5 KHZ - P.D.R. RECORDS

FIGURE 6. 3.5 kHz-P.D.R. records of channel-cut eastern areas of the abyssal plain (locations on Figure 3). A shows the raised terrace of the northern boundary of the plain, B shows a relict channel which has migrated southward with thme, and C shows a steep-walled channel and a relict channel.

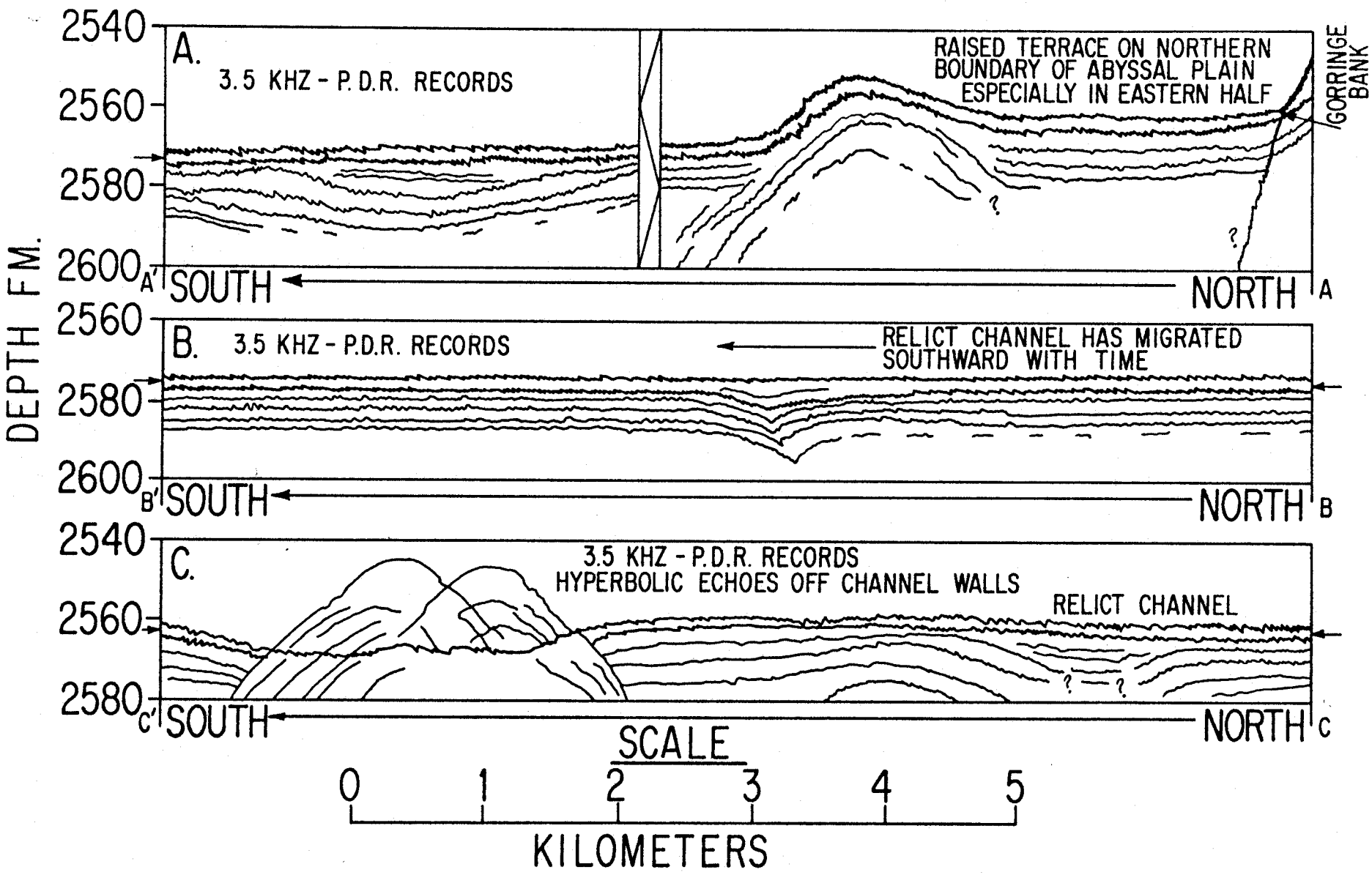
2540
2560
2580
2600
DEPTH FM.
A.
3.5 KHZ - P.D.R. RECORDS
RAISED TERRACE ON NORTHERN BOUNDARY OF ABYSSAL PLAIN ESPECIALLY IN EASTERN HALF
GORRINGE BANK
A'
SOUTH
NORTH
A
B.
3.5 KHZ - P.D.R. RECORDS
RELICT CHANNEL HAS MIGRATED SOUTHWARD WITH TIME
B'
SOUTH
NORTH
B
C.
3.5 KHZ - P.D.R. RECORDS
HYPERBOLIC ECHOES OFF CHANNEL WALLS
RELICT CHANNEL
C'
SOUTH
NORTH
C
SCALE
0 1 2 3 4 5
KILOMETERS

turbidites to an abyssal plain.

Damuth (1975) has classified the echo character of various Western Equatorial Atlantic sediments; the character of the sediments of the Horseshoe Abyssal Plain are almost entirely Type I B, which Damuth describes as distinct, continuous, sharp, parallel subbottom reflectors (10's to 100's of kms continuously). With depth, the reflectors become less distinct and more intermittent (Figure 5).

Piston Core Stratigraphic Correlations

Figure 7 displays the simplified, full-core sketches of the six cores from the abyssal plain, showing color, thickness, texture,and type of sediment. Note the excellent visual correlations of the six turbidites and three pelagic zones, which are based on the above characteristics, in addition to basal erosive character and stratigraphic position. Certainty of correlations becomes more rigorous with detailed size analyses and mineralogic data in the following sections.

A detailed analysis of the reflectivity of subbottom sediments as seen in the 3.5 kHz records (Figure 5) shows that the acoustically transparent zones and the acoustic reflectors correspond to sections of clay and silt/sand in the cores from the abyssal plain (Figure 7). Embley and Bryan (1976) have studied the lithologic and topographic influences on bottom and subbottom reflectivity in deep ocean environments, especially in the vicinities of the Demerara

FIGURE 7. Simplified, full-core sketches of the six abyssal plain cores showing color, thickness, texture, and type of sediment (pelagic, turbiditic, or Gorringe Bank local events). Sediment colors are from GSA rock color chart.

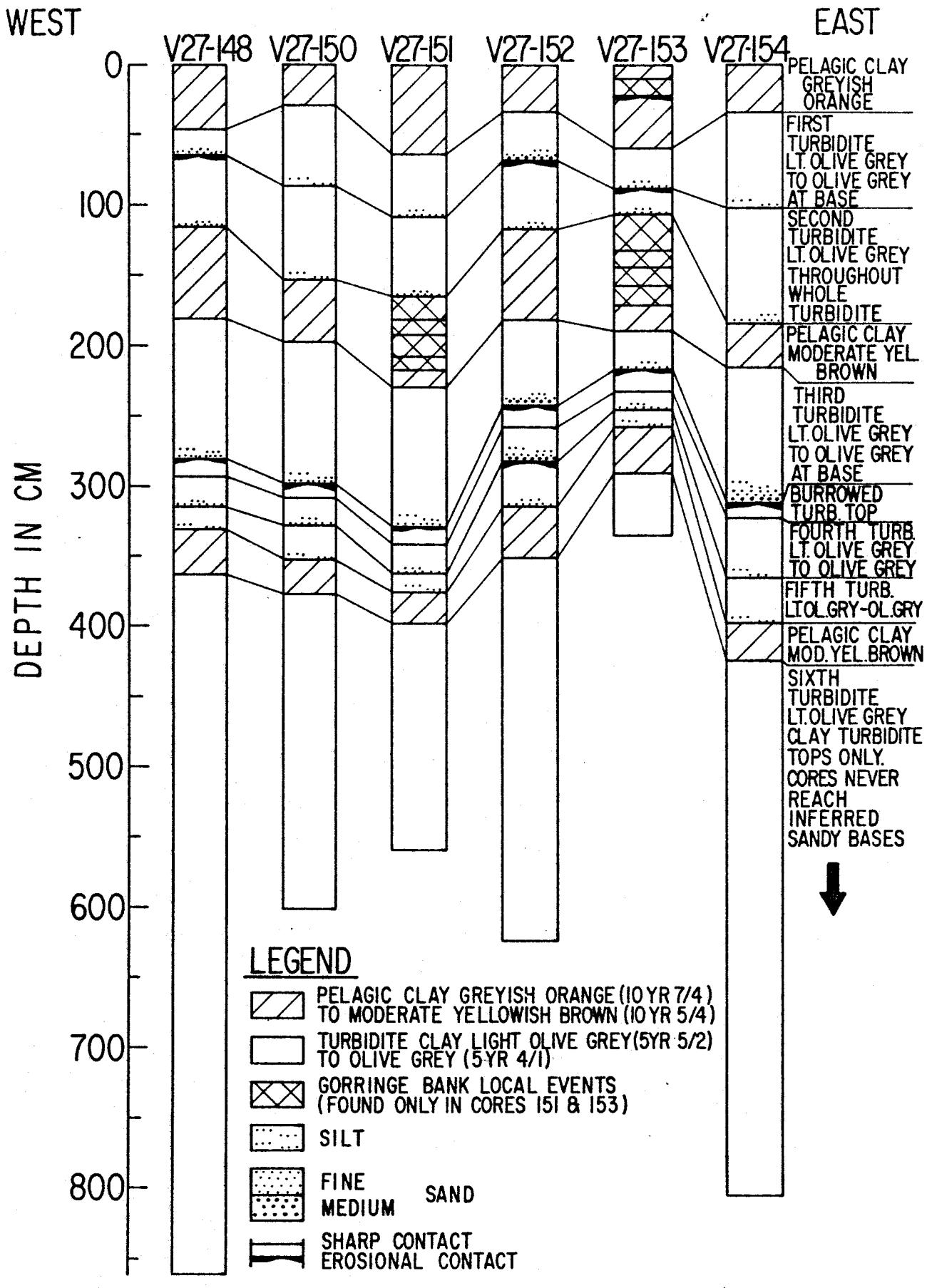
WEST
EAST
V27-148
V27-150
V27-151
V27-152
V27-153
V27-154
DEPTH IN CM
0
100
200
300
400
500
600
700
800
PELAGIC CLAY GREYISH ORANGE
FIRST TURBIDITE LT. OLIVE GREY TO OLIVE GREY AT BASE
SECOND TURBIDITE LT. OLIVE GREY THROUGHOUT WHOLE TURBIDITE
PELAGIC CLAY MODERATE YEL. BROWN
THIRD TURBIDITE LT. OLIVE GREY TO OLIVE GREY AT BASE
BURROWED TURB. TOP
FOURTH TURB. LT. OLIVE GREY TO OLIVE GREY
FIFTH TURB. LT. OL. GRY-OL. GRY
PELAGIC CLAY MOD. YEL. BROWN
SIXTH TURBIDITE LT. OLIVE GREY CLAY TURBIDITE TOPS ONLY. CORES NEVER REACH INFERRED SANDY BASES
LEGEND
PELAGIC CLAY GREYISH ORANGE (10 YR 7/4) TO MODERATE YELLOWISH BROWN (10 YR 5/4)
TURBIDITE CLAY LIGHT OLIVE GREY (5YR 5/2) TO OLIVE GREY (5 YR 4/1)
GORRINGE BANK LOCAL EVENTS (FOUND ONLY IN CORES 151 & 153)
SILT
FINE
MEDIUM
SAND
SHARP CONTACT
EROSIONAL CONTACT

and Ceara Abyssal Plains off the coast of South America. In their study, a subbottom reflector seen on 3.5 kHz echograms was correlated with sand layers found to 10 m subbottom depth in several cores. On the basis of several well documented examples, they conclusively demonstrated that grey clay turbidite tops are acoustically transparent, while sandy bases provide strong reflectors on the 3.5 kHz-P.D.R. records. In the laboratory, they measured the velocity of compressional sound waves in turbidite clays and turbidite sands from the Demerara and Ceara Abyssal Plains. Velocities in clays were found to be about 1.5 km/sec, while those in the thin sand horizons were about 1.7 km/sec. It is assumed that the unconsolidated sediments of the Horseshoe Abyssal Plain (to at least 10 m subbottom depth) have similar compressional wave velocities as the unconsolidated sediments from the Demerara and Ceara Abyssal Plains. Based on the velocity of compressional waves in water (above the Horseshoe Abyssal Plain, this value is about 1.46 km/sec) and the velocity of compressional waves in sediment (1.5-1.7 km/sec), the thickness of the shallow subbottom sediment units of concern in the Horseshoe Abyssal Plain can be calculated. The first acoustically transparent zone is encountered (see 3.5 kHz records of Figure 5) at 0.5-1.5 fm subbottom depth, which is equivalent to 0.9-2.7 m subbottom depth. This acoustically transparent zone is interpreted to represent the clay section atop the third turbidite sandy base, shown in Figure 7 and indicated by filled arrows in Figure 5. Below this, the reflector seen at about

1.60 fm on the 3.5 kHz records (Figure 5) is thought to represent the sandy/silty bases of the 3rd, 4th, and 5th turbidites shown from 2.5-3.5 m (avg. 3.0 m) in Figure 7. The wide acoustically transparent zone, indicated by the open arrows of Figure 5, is found between 2.0-5.0 fm subbottom depth in the 3.5 kHz records (3.7-9.1 m). This corresponds to a zone in the piston cores represented by the clay top of the 6th turbidite. Although the sandy/silty base of this 6th turbidite was not recovered in the piston cores from the abyssal plain, the 3.5 kHz records suggest that it is present further downsection in the uncored sediment. It is predicted that future coring of the abyssal plain will reveal the base of the 6th turbidite between 3.5-5.0 fm subbottom depth (6.4-9.1 m), depending on where in the abyssal plain the core sample is taken. Resolving exact locations of reflectors on the 3.5 kHz records is not possible and therefore, calculated depths are not precise.

Figure 7 shows that cores 151 and 153 contain material visually unlike that found in the other four cores. Figure 2 shows that these two cores were taken from the extreme northern end of the abyssal plain near the steep flanks of the seismically active Gorringe Bank. It is hypothesized that earthquakes on the Gorringe Bank have initiated small, local turbidity current events which have deposited material only very close to the Gorringe Bank source area (i.e. cores 151 and 153). The mineralogy of these local events, as will be discussed later, differs markedly from the mineralogy of

all the other turbidites. This data supports the hypothesis that these local events had a very different source area.

In a previous limited sampling and study of these same cores from the Horseshoe Abyssal Plain, Horn and others (1972) stated that as one sampled to the west down the supplying channel and abyssal plain (156, 155, 154, 153, 152, 151, 150, 148, and 149), one generally observed a greater and greater thickness of non-turbidite material in the cores. Figure 8 plots the percentage of turbidites versus the percentage of non-turbidites for each of the nine cores (down to the sixth turbidite top, where it is seen). Determinations of turbidite or non-turbidite were made on the basis of color, sand mineralogy, and clay x-ray mineralogy. Criterion developed by Bouma (1962) and Hesse (1975) from ancient turbidite deposits were also helpful in making these divisions between turbidite and non-turbidite sediment. Although there appears to be a general increase in percent of non-turbidite material from east to west away from the source, details of Figure 8 suggest great complexity.

The detailed core logs of all nine cores (Figure 9) show the stratigraphy of the cores down to the top of the sixth turbidite which is not included due to the fact that all sixth turbidite material is featureless and homogeneous light-olive-grey clay. Note the correlations in the supplying channel (cores 155 and 156), especially the very great thickness of turbidite layers visually correlated to core 156. Detailed grain size analyses and mineralogic analyses were

FIGURE 8. Percentages of the core length which are turbidite or non-turbidite sediment for all nine cores of the abyssal plain area.

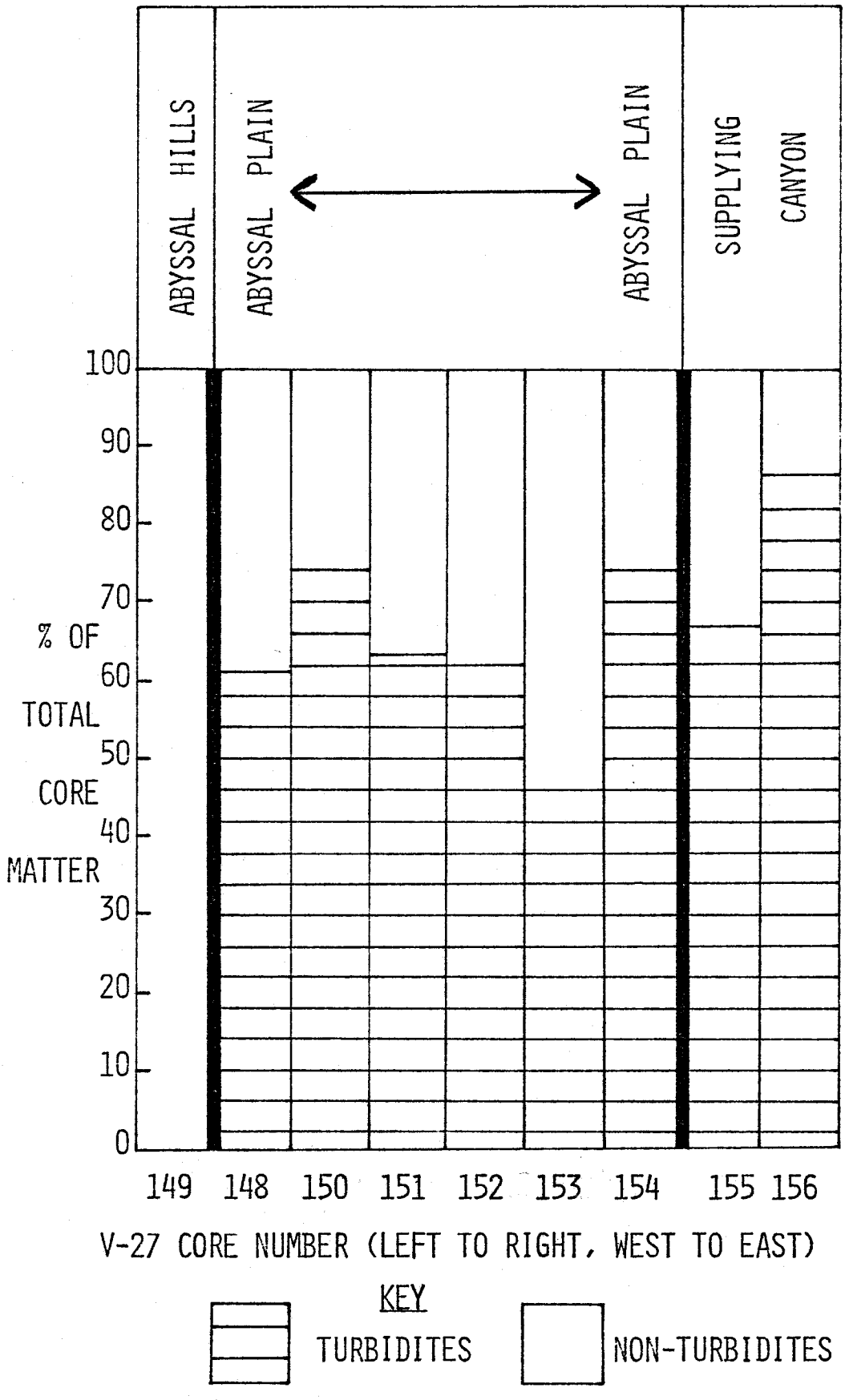
ABYSSAL HILLS
ABYSSAL PLAIN
ABYSSAL PLAIN
SUPPLYING CANYON
100
90
80
70
% OF
60
TOTAL
50
CORE
40
MATTER
30
20
10
0
149
148
150
151
152
153
154
155
156
V-27 CORE NUMBER (LEFT TO RIGHT, WEST TO EAST)
KEY
TURBIDITES
NON-TURBIDITES

FIGURE 9. Detailed core sketches of all nine cores of the abyssal plain area to the top of the sixth turbidite only. Note correlations to the supplying canyon cores 155 and 156.

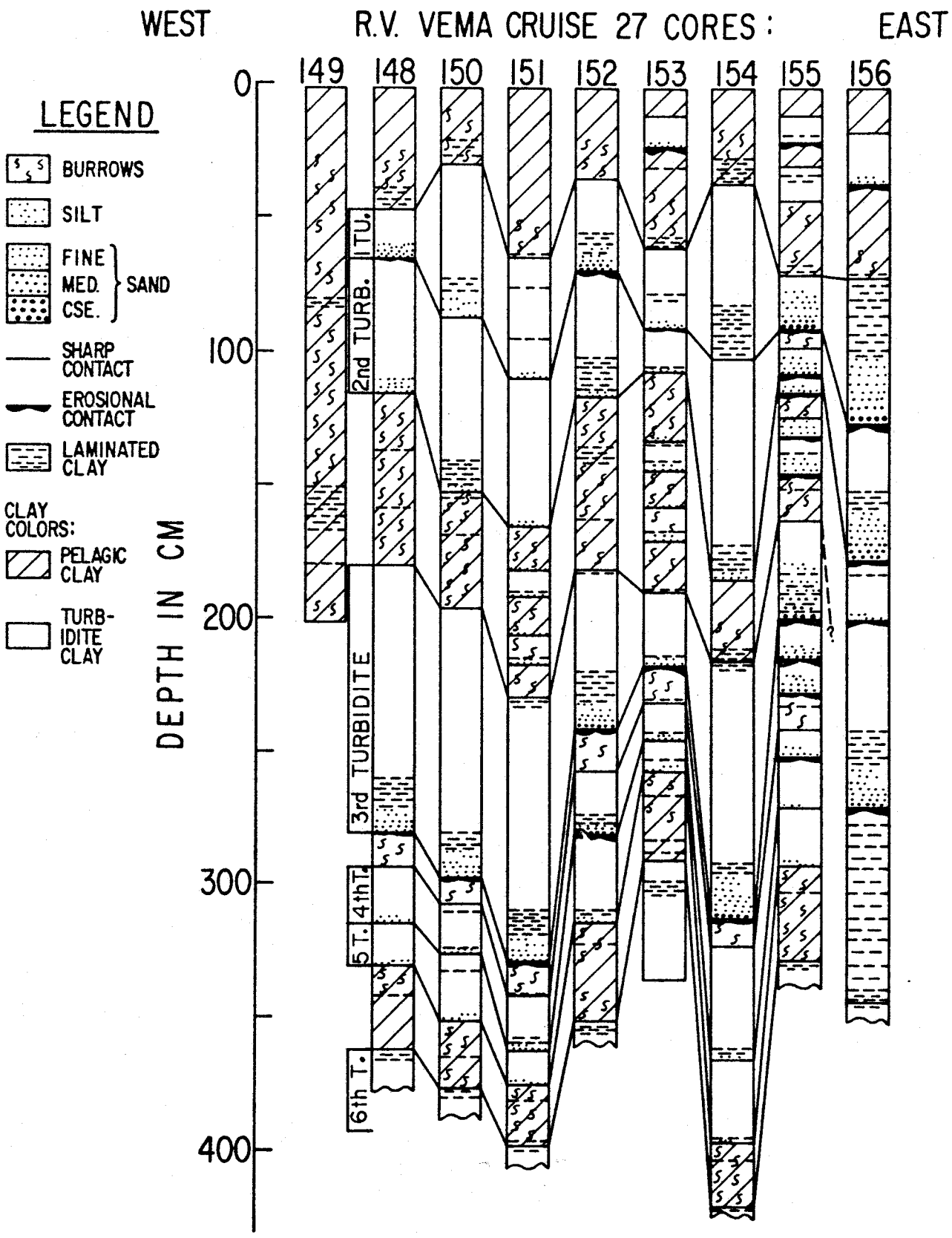
WEST
R.V. VEMA CRUISE 27 CORES :
EAST
149
148
150
151
152
153
154
155
156
LEGEND
BURROWS
SILT
FINE
MED.
CSE.
SAND
SHARP CONTACT
EROSIONAL CONTACT
LAMINATED CLAY
CLAY COLORS:
PELAGIC CLAY
TURB-IDITE CLAY
DEPTH IN CM
0
100
200
300
400
1TU.
2nd TURB.
3rd TURBIDITE
4thT.
5T.
6th T.
?

only carried out for the upper three turbidites, the three largest complete turbidites cored (the first turbidite is the youngest with the second and third being progressively older).

Grain Size Analysis Statistics and their Significance

Mean Grain Size and Thickness Data.

Horn and others (1972) also stated that there was a general decrease in grain size of the Horseshoe Abyssal Plain turbidites from east to west. Again, detailed analyses of the first three turbidites, this time by means of some 115 individual grain size analyses, demonstrate that this conclusion cannot be simply stated and is, indeed, inaccurate. Mean grain size (Folk's 1968 graphic mean grain size) is plotted in phi (Ø) units (Figure 10) for each of four horizons (top, half-way down, two-thirds down, and base) in the top three turbidites; the thicknesses of each of the turbidite units are also represented. Note the similar trend of thickness variation in each of the three turbidites: generally, core 154, the nearest to the eastern supplying channel, is the thickest turbidite and core 153, the next core to the west, is the thinnest. As one moves further away from the source to the west, the turbidite thicknesses increase: in the first turbidite, however, core 148 is the thinnest, probably because the volume of this turbidite is the smallest of the three and may have run out of material to deposit by the location of core 148; the second turbidite

FIGURE 10. Mean grain size for various horizons of the first three turbidites. Averages and standard deviations for each turbidite are presented.

GRAPHIC MEAN GRAIN SIZE=MEAN GRAIN SIZE

M_Z=(Ø16+Ø50+Ø84)/3

FORMULA FROM FOLK, 1968.

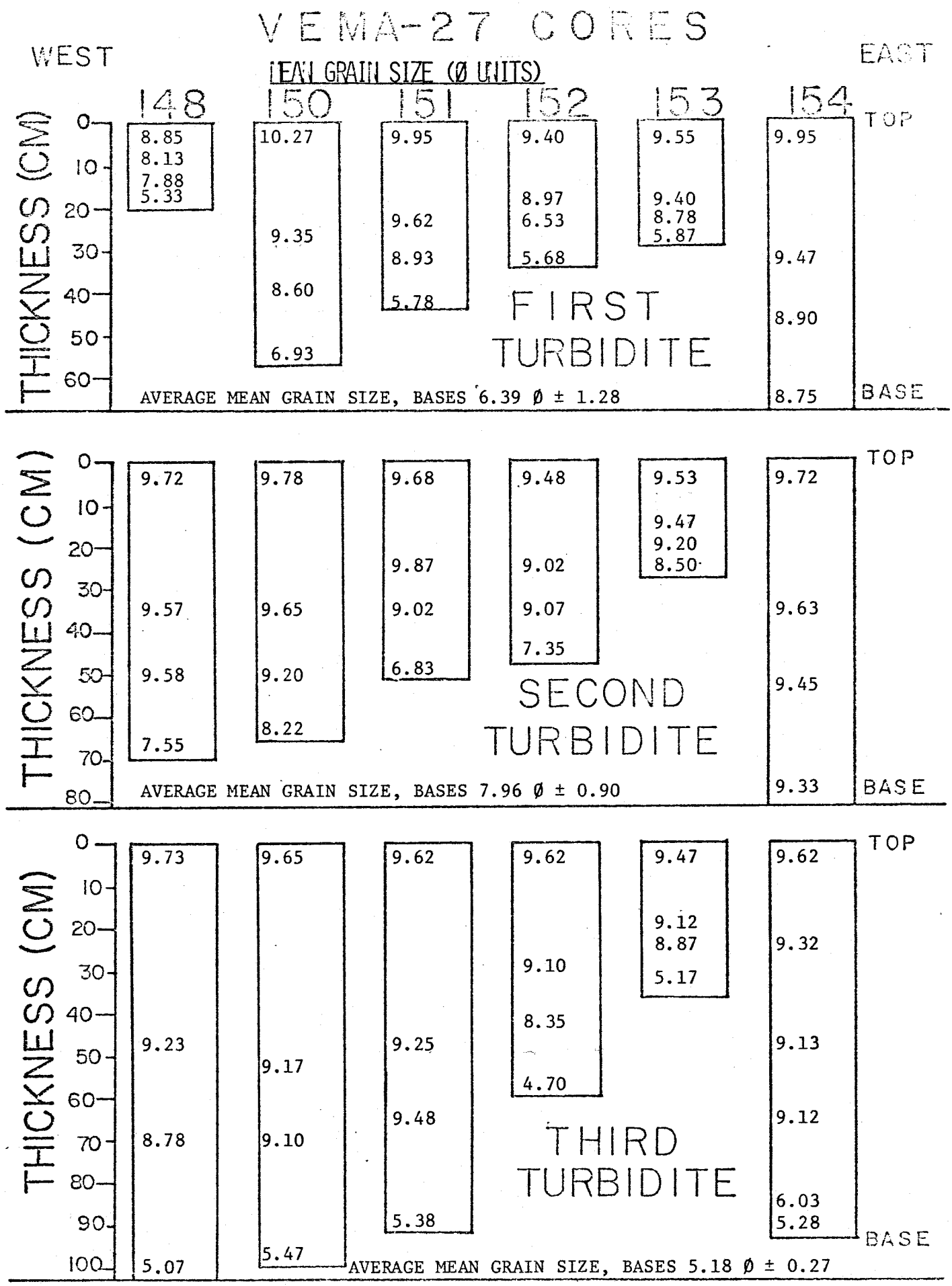
VEMA-27 CORES
WEST
EAST
MEAN GRAIN SIZE (Ø UNITS)
148
150
151
152
153
154
THICKNESS (CM)
0
10
20
30
40
50
60
70
80
90
100
TOP
BASE
8.85
8.13
7.88
5.33
10.27
9.35
8.60
6.93
9.95
9.62
8.93
5.78
9.40
8.97
6.53
5.68
9.55
9.40
8.78
5.87
9.95
9.47
8.90
8.75
FIRST TURBIDITE
AVERAGE MEAN GRAIN SIZE, BASES 6.39 Ø ± 1.28
9.72
9.57
9.58
7.55
9.78
9.65
9.20
8.22
9.68
9.87
9.02
6.83
9.48
9.02
9.07
7.35
9.53
9.47
9.20
8.50
9.72
9.63
9.45
9.33
SECOND TURBIDITE
AVERAGE MEAN GRAIN SIZE, BASES 7.96 Ø ± 0.90
9.73
9.23
8.78
5.07
9.65
9.17
9.10
5.47
9.62
9.25
9.48
5.38
9.62
9.10
8.35
4.70
9.47
9.12
8.87
5.17
9.62
9.32
9.13
9.12
6.03
5.28
THIRD TURBIDITE
AVERAGE MEAN GRAIN SIZE, BASES 5.18 Ø ± 0.27

displays this general trend; the third turbidite follows this same trend, except that cores 150 and 148 are slightly thicker than 154. Based on the average thicknesses of each of these turbidites and the areas they cover (15000 km^2), the calculated turbidite volumes are: first turbidite, 5.7 km^3, second turbidite, 8.0 km^3, and third turbidite, 12.1 km^3.

In every core, the top, middle, and two-thirds horizons of all three turbidites are classified as clay or mud, according to the classification of Folk (1954), Figure 11 (one exception to this is two-thirds down the first turbidite, core 152, which is silt). First turbidite bases are classified as mud (154), silt (148, 151, 153), and sandy silt (150,152). The bases of the second turbidite are all mud except 151 and 152, which are silt. The third turbidite bases are classified as silt (150, 151, 154) and sandy silt (148, 152, 153). Besides the general trend of fining toward turbidite tops, it can be noted that the upper two-thirds of each of the three turbidites are very similar in grain size. Large differences occur only in the coarser-grained bases, which dominate the differences in character of these three turbidites.

Figure 12 shows the grain size mean and standard deviation values of a particular horizon of a turbidite over the entire abyssal plain. For example, the mean grain size of the six sandy bases in the first turbidite is 6.39Ø, with a standard deviation of 1.28Ø. These data demonstrate:

1) there is grain size "overlap" between the same

FIGURE 11. Classification scheme for sand, silt, and clay-sized particles devised by Folk (1954) and used in the present study.

K E Y

S=SAND s=SANDY

Z=SILT z=SILTY

M=MUD m=MUDDY

C=CLAY c=CLAEY

AFTER FOLK, 1954.

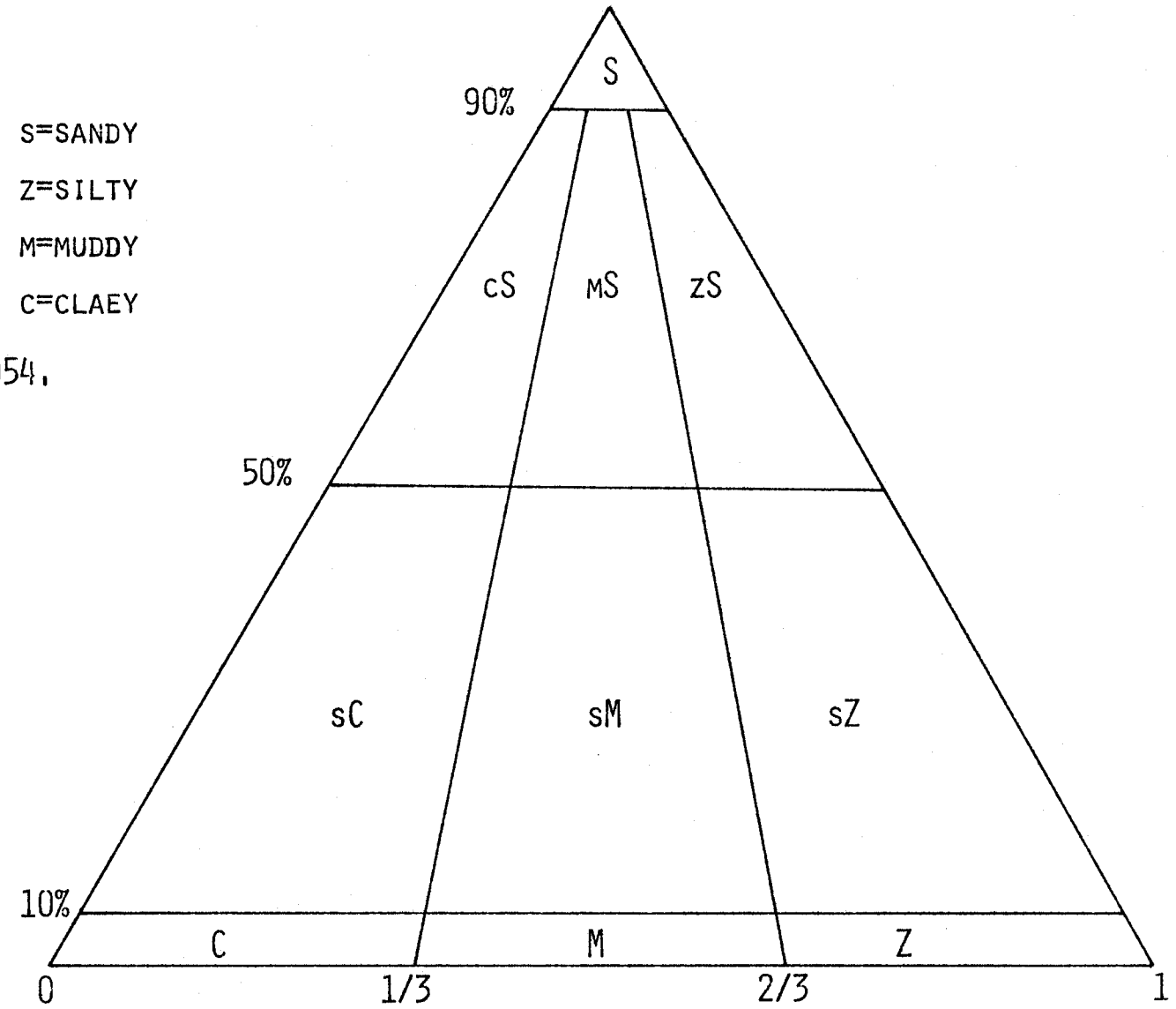

FIGURE 12. Grain size distributions for each of the four horizons of the top three turbidites, showing fining-upwards within each turbidite and consistency of range in sizes within each turbidite.

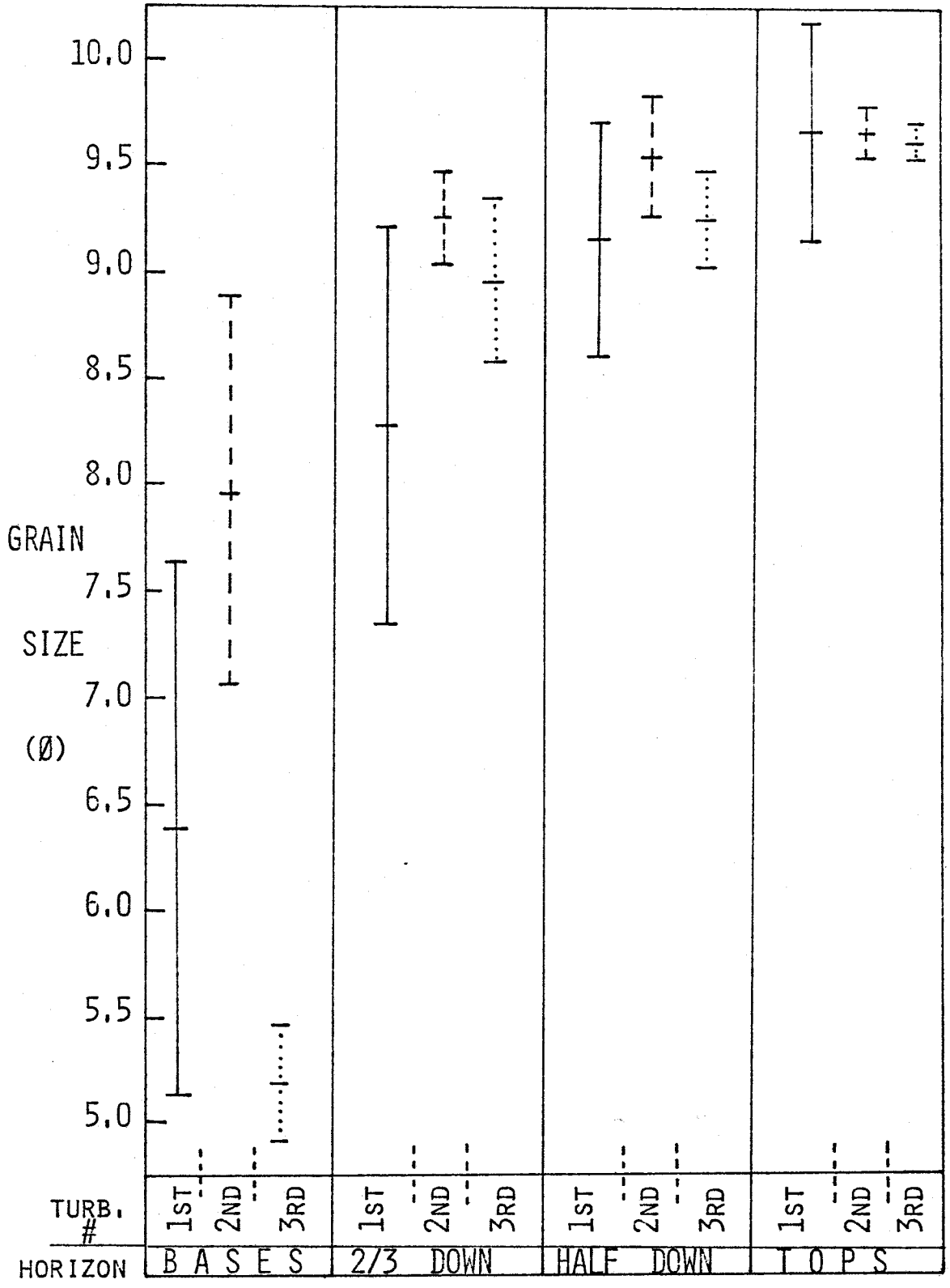
10.0
9.5
9.0
8.5
8.0
GRAIN
7.5
SIZE
7.0
(Ø)
6.5
6.0
5.5
5.0
TURB. #
1ST
2ND
3RD
HORIZON
BASES
2/3 DOWN
HALF DOWN
TOPS

horizons of the three turbidites;

2) the turbidite bases show the widest variation in grain size;

3) the standard deviations are greatest for the first turbidite, lesser for the second turbidite, and least for the third turbidite (one minor exception is in the two-thirds down horizon); and

4) there is much greater variation between the turbidites of any one core than there is down the length of the abyssal plain for a single depositional event (one minor exception is core 151).

It can be concluded from these data that the grain size characteristics of the three turbidites indicate seperate, though statistically overlapping, turbidites of three different characters. This conclusion further corroborates the visual correlation.

For the sake of completeness, several grain size analyses were performed on sediment besides that of the first three turbidites. Most notably, ten samples of pelagic/hemipelagic ooze from various sections of non-turbidite material were found to have average grain-size values very similar to the clay turbidite tops. Also, four samples from the top of the sixth turbidite yielded mean grain sizes identical to those of the first three turbidites. Since the fourth and fifth turbidites are so very thin (avg. about 20 cm each), grain-size analyses were not run on them.

To make the correlation on the basis of grain size data

more rigorous, several figures are presented to display the data. Figure 13 plots percent of sand, silt, and clay down each of the three turbidites for the six cores of the abyssal plain. This graphically displays the size data of Figure 10 and notes differences between the three turbidites. Note, for instance, the lack of appreciable sandy bases in the second turbidite and the general presence of appreciable sandy bases in the first and particularly the third turbidites. Actually, all bases of the turbidites contain some sand, but amounts less than a few percent are not visible on this scale (averages of percent sand in the bases and average amounts based on the same sample size in grams, are recorded in Figure 13). Figures 14 A, B, and C, which correspond to the first, second, and third turbidites, respectively, plot grain size versus the distance above the base of that turbidite. Notice, in each turbidite, that the envelope encompassing each of the six cores has its own distinctive character. The second differs from the first in that it has a greater average thickness, narrower size range, and finer grain size. The third differs from the first and second in its still greater average thickness and still narrower range in grain size. From one turbidite to the next, there is no consistent pattern of arrangement of cores as plotted in Figure 14. When plots of grain size for a particular turbidite horizon versus distance from the eastern source of the abyssal plain were constructed, no simple relationship was observed. In a similar manner, when plots of grain size for

FIGURE 13. Percent sand, silt, and clay for each horizon down the first three turbidites, showing individual character of each turbidite. Average % of sand in each of the three turbidite bases and average amounts (gms) are also displayed to corroborate differences between the three turbidites.

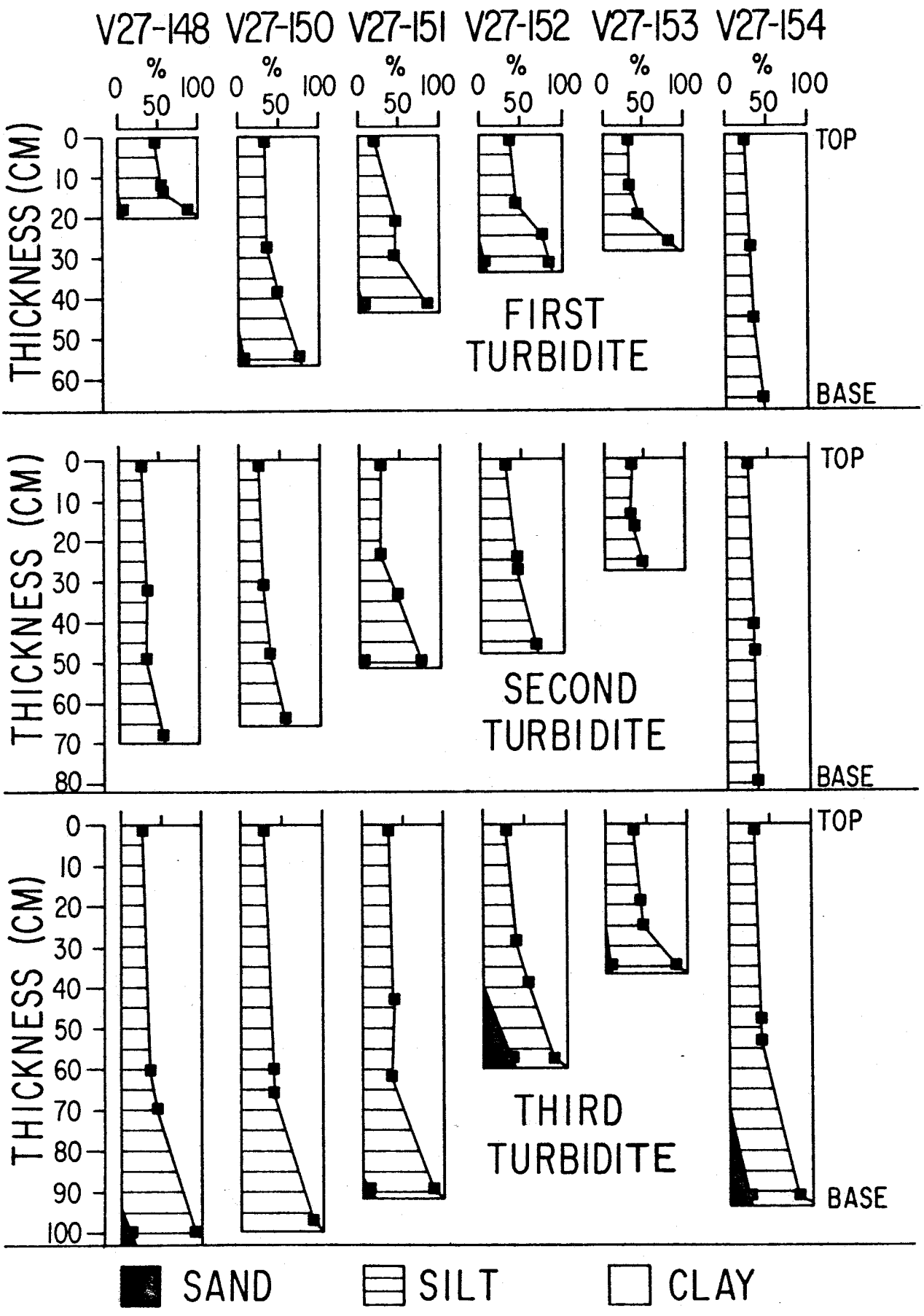
V27-148
V27-150
V27-151
V27-152
V27-153
V27-154
0 % 100
50
THICKNESS (CM)
0
10
20
30
40
50
60
70
80
90
100
TOP
BASE
FIRST TURBIDITE
SECOND TURBIDITE
THIRD TURBIDITE
SAND
SILT
CLAY

FIGURE 14. Envelopes encompassing each of the first three turbidites on plots of grain size versus distance of the sample above the turbidite base.

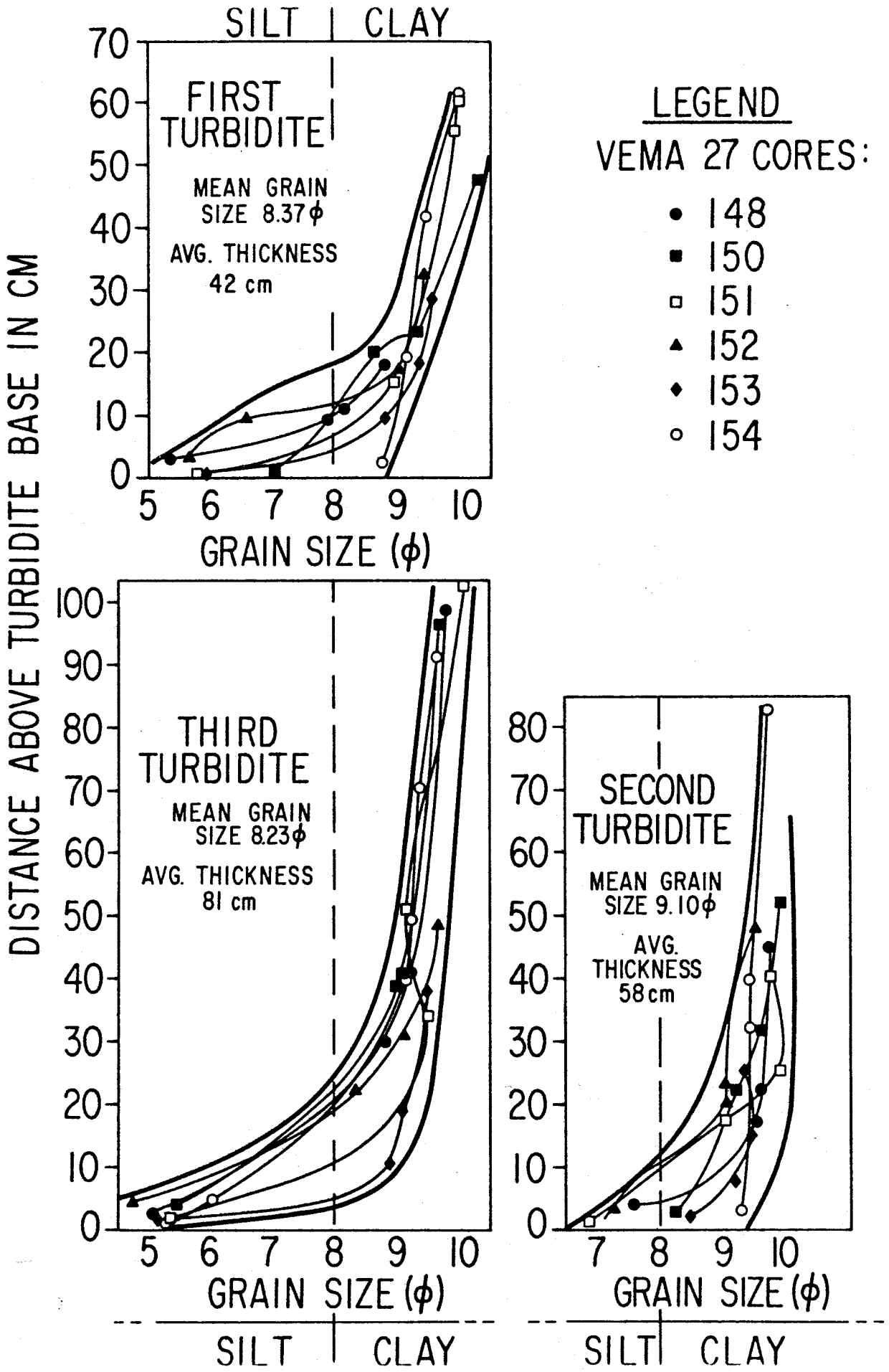
SILT | CLAY
FIRST TURBIDITE
MEAN GRAIN SIZE 8.37φ
AVG. THICKNESS 42 cm
DISTANCE ABOVE TURBIDITE BASE IN CM
GRAIN SIZE (φ)
LEGEND
VEMA 27 CORES:
148
150
151
152
153
154
THIRD TURBIDITE
MEAN GRAIN SIZE 8.23φ
AVG. THICKNESS 81 cm
SECOND TURBIDITE
MEAN GRAIN SIZE 9.10φ
AVG. THICKNESS 58 cm
SILT | CLAY

a particular turbidite horizon versus distance from the geometric center axis of the abyssal plain were constructed, no simple relationship was observed. When turbidite thicknesses were plotted against grain size for a particular turbidite horizon, however, a somewhat linear trend could be observed. Figure 15 displays turbidite thickness versus average grain size values of each of the three turbidites. A weak general trend in each of the three turbidites is for the phi size to increase (become finer grained) as the thickness of the turbidite increases (i.e. the thicker the turbidite, the finer the grain size). Another broad generalization is that as one notes the slope of the trend line from the first turbidite (the thinnest) through the third turbidite (the thickest), it is seen to flatten out, which corresponds to a decrease in range of grain sizes from the first to the third turbidites (previously displayed in Figure 12). Note that the thickness trends of Figure 10 are also graphically displayed, with core 153 being the thinnest core. In the final figure concerning size analysis data, cumulative percent curves are plotted for each of the three turbidite bases in the abyssal plain (Figures 16 A, B, and C, respectively), as well as curves for the base of the first turbidite in the supplying canyon and two types of pelagic sediment (Figure 16 D). Again, the individual character of each group of turbidite bases is displayed (note again the fine grain size of core 154). Turbidites one and three apparently had a relatively coarse-grained source, whereas turbidite two had

FIGURE 15. Grain size versus thickness for all four horizons of the top three turbidites.

KEY

FIRST TURBIDITE INDICATED BY (∘)

SECOND TURBIDITE INDICATED BY (■)

THIRD TURBIDITE INDICATED BY (•)

NOTE: TRENDS ESTIMATED BY EYE.

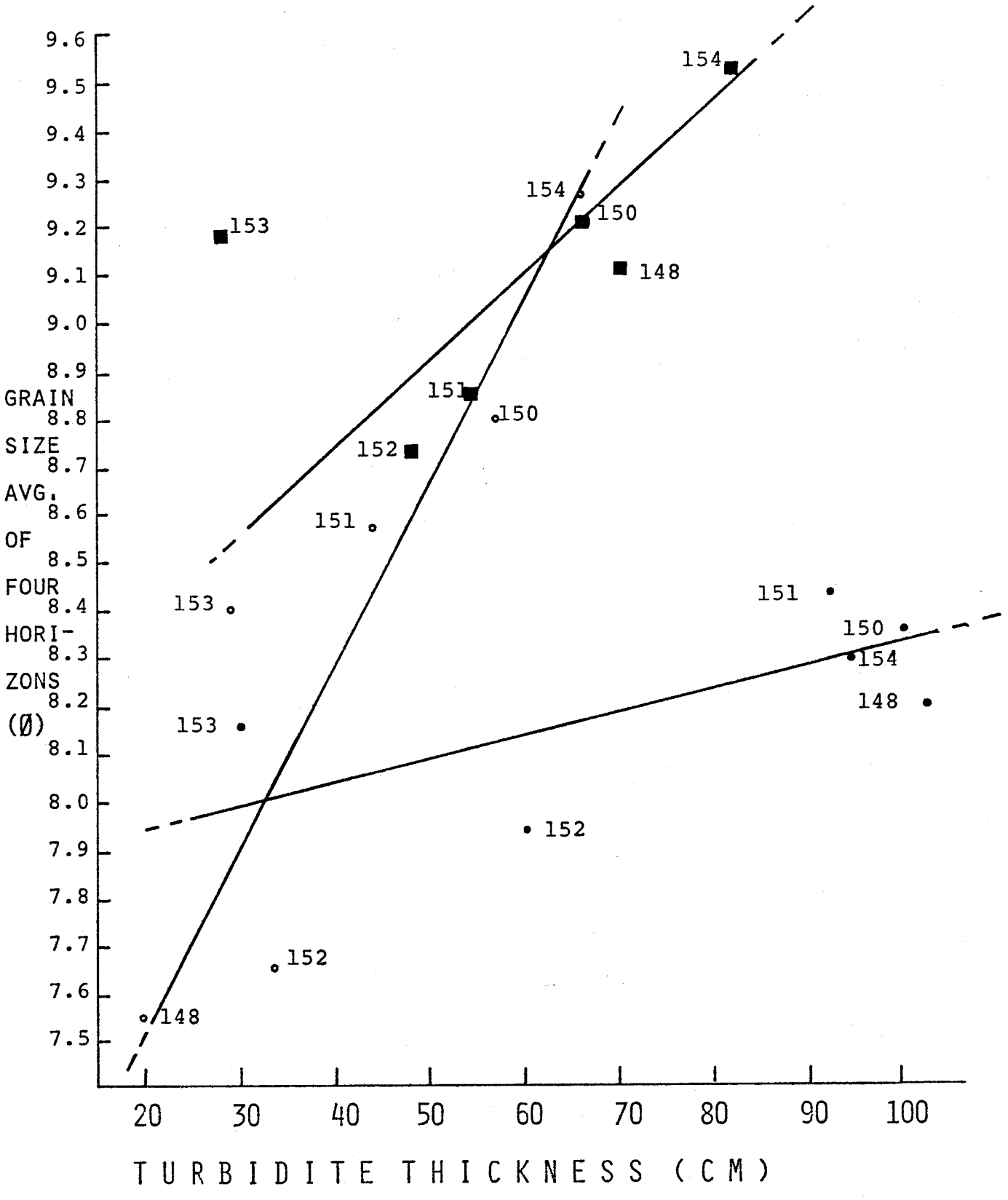
9.6
9.5
9.4
9.3
9.2
9.1
9.0
8.9
8.8
8.7
8.6
8.5
8.4
8.3
8.2
8.1
8.0
7.9
7.8
7.7
7.6
7.5
GRAIN SIZE AVG. OF FOUR HORI-ZONS (Ø)
154
154
150
153
148
151
150
152
151
153
151
150
154
153
148
152
152
148
20
30
40
50
60
70
80
90
100
TURBIDITE THICKNESS (CM)

FIGURE 16. Cumulative frequency curves for the six core locations of the first A, second B, and third C turbidites. Supplying canyon and pelagic samples are displayed in D.

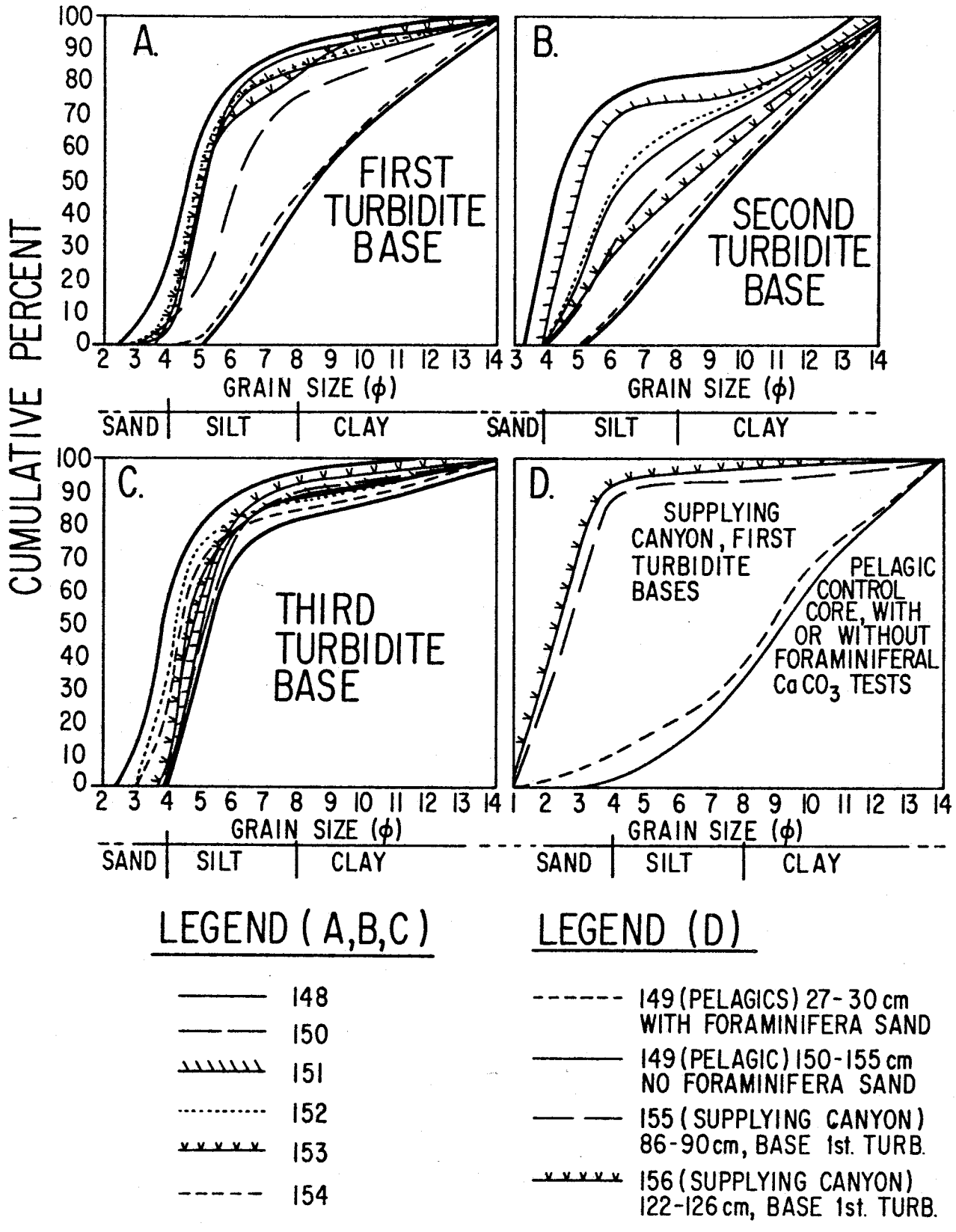
CUMULATIVE PERCENT
100
90
80
70
60
50
40
30
20
10
0
A.
FIRST TURBIDITE BASE
B.
SECOND TURBIDITE BASE
2 3 4 5 6 7 8 9 10 11 12 13 14
GRAIN SIZE (ϕ)
SAND
SILT
CLAY
C.
THIRD TURBIDITE BASE
D.
SUPPLYING CANYON, FIRST TURBIDITE BASES
PELAGIC CONTROL CORE, WITH OR WITHOUT FORAMINIFERAL $CaCO_3$ TESTS
LEGEND (A,B,C)
148
150
151
152
153
154
LEGEND (D)
149 (PELAGICS) 27-30 cm WITH FORAMINIFERA SAND
149 (PELAGIC) 150-155 cm NO FORAMINIFERA SAND
155 (SUPPLYING CANYON) 86-90 cm, BASE 1st. TURB.
156 (SUPPLYING CANYON) 122-126 cm, BASE 1st. TURB.

a fine-grained one. In Figure 16 D, notice the coarser grain sizes of cores 155 and 156 as these two samples move progressively up the canyon to the east along the horizon of the first turbidite base. The two pelagic samples from the pelagic control core to the west of the abyssal plain (core 149) also have a distinctive shape and position, with the sample containing abundant foraminifera being the more coarse-grained.

Discussion of Grain Size and Thickness Results.

To the reader ingrained with the tenet that grain size and thickness of turbidites decrease with increasing distance from the source, many of the results from the six abyssal plain cores previously described are inconsistent with conclusions of other studies of Holocene turbidites; among the most notable are Ryan and others (1965, sediments of the Tyrrhenian Abyssal Plain), Fruth (1965, the 1929 Grand Banks earthquake and sediments of the Sohm Abyssal Plain), Conolly and Ewing (1967, sedimentation in the Puerto Rico Trench), Bornhold and Pilkey (1971, bioclastic turbidite sedimentation in the Columbus Basin, Bahamas), Horn and others (1971a, turbidites of the Northeast Pacific; 1971b, turbidites of the Hatteras and Sohm Abyssal Plains; and 1972, graded bed-sequences emplaced by turbidity currents north of 20° North in the Pacific, Atlantic, and Mediterranean), Bennetts and Pilkey (1974, characteristics of three turbidites; Hispaniola-Caicos Basin), and Elmore (1976,

extensive horizontal continuity of a single turbidite, Hatteras Abyssal Plain). However, if one divides the core samples from the Horseshoe Abyssal Plain area into two groups, those from the supplying canyon (average of cores 155 and 156) and those from the abyssal plain proper (average of cores 148 and 150-154), the very general decrease in grain size can be observed (see Figure 8). Horn (1971a, b, 1972) has outlined general characteristics of proximal versus distal turbidite deposits; cores 155 and 156 from the Horseshoe Abyssal Plain supplying canyon area have the following "proximal" characteristics: 1) presence of sand, 2) overall greater thicknesses of individual coarse layers, and 3) a wide range of layer thicknesses. Many of the turbidites from the abyssal plain basin display characteristics 1 and 3 above, but never 2. A few others display purely distal characteristics (e.g. core 153 turbidite two), which Horn and others (1971a, b, 1972) define as graded, thin-layered silts and clays. The vast majority of turbidites, however, do not fit either of these definitions, but rather share a mixture of characteristics of both distal and proximal groups (e.g. the silts and clays of turbidite two found in rather thick beds--see Fugures 9 and 10). In an attempt to define and quantify these concepts of proximal and distal facies, the turbidites were evaluated by means of Walker's (1967) P_1 index, where groups of beds which are most proximal will have values approaching 100 and those most distal, values approaching 0. The P_1 index

evaluates the percentage of beds beginning with Bouma's interval A, B, or "A--E" (the latter denotes beds less than 3 cm thick with perfect grading from A--E). With the six core samples from the abyssal plain as the data base, this P_1 index was calculated for each of the five complete turbidites, with the results shown in Table II.

TABLE II.

P_1 INDEX FOR FIVE TURBIDITES FROM THE HORSESHOE ABYSSAL PLAIN.

TURBIDITE NUMBER DOWN FROM THE TOP OF EACH CORE	P_1 VALUE	FACIES
THIRD TURBIDITE	50	MOST PROXIMAL ↓ MOST DISTAL
FIRST TURBIDITE	41.5	
FOURTH TURBIDITE	41.5	
SECOND TURBIDITE	25	
FIFTH TURBIDITE	25	

When these five turbidites are plotted on Walker's (1967) ABC flow regime ternary diagram (based on flow regimes used by Simmons and others (1961) and Harms and Fahnestock (1965)), each of the five turbidites fall in a small part of the diagram designated as a mixture of upper and lower flow regimes. The usefulness of Walker's index is severely limited by the small number (six) of core samples from the Horseshoe Abyssal Plain turbidites.

From observations of the bases of any one turbidite

horizon down the length of the abyssal plain (both visually in Figure 9 and statistically as discussed immediately above), the simple inference is that the depositional dynamics and inferred flow regimes for any one turbidite event vary profoundly down the length of the abyssal plain from one core location to the next. For example, in the first turbidite, core 154 contains essentially no sand, yet is the thickest and nearest to the supplying channel (Figure 2). Further down the abyssal plain on the same south boundary, core 152 has the thickest section of sand cored in the first turbidite and one of the two coarsest grain sizes. A possible explanation for this behavior lies in the location of these cores and the local bottom relief in these areas (Figure 2). Notice that core 154 is located in the deepest part of the basin (4709 m) where there is a slight north-to-south slope to the abyssal plain across its entire length; the southerly slope to the abyssal plain may be due to subsidence of this area as a result of the high seismicity and possible oceanic crust subduction of this zone observed by Purdy (1975). If the major deposition of sediment occurs after the passage of the main head wave of sediment as Middleton (1967) has inferred from scaled laboratory experiments, then a low-velocity current with fine-grained material may "slop" the sediment toward the southerly slope where a very thick deposit of fine-grained sediment would be deposited, as observed in core 154. The absence of sand indicates that the inferred main avenue of turbidite flow did not pass by the location

of core 154 with the material, and/or that the portion of the flow carrying sand had a velocity too high to deposit sand at that locality. However, since erosional bases are generally not observed in core 154, the former explanation is accepted.

Further detailed investigation of the bottom topography in the area of core 153 helps explain why this core always contains the thinnest turbidite. As Figures 2 and 6 A display, core 153 is located on an elevated terrace nearly 10 m above the abyssal plain floor. It is reasonable to expect that the main avenue of turbidite flow would have sought the lowest point and consequently, the raised terrace would have been starved of sediment from the turbidity current.

The coarse grain size and thickness of sand at the location of core 152 can also be explained by the local bottom topography (Figure 2), which shows a nearby physiographic barrier to the westward-advancing current. Ericson and others (1961) and Hersey (1965) have suggested that turbidity currents may be "turned back" on themselves at physiographic barriers and that sediment ponding over small areas may account for some of the thickness irregularities observed in marine turbidites (e.g. Horn and others, 1971b; Bornhold and Pilkey, 1971; and Bennetts and Pilkey, 1974). However, no bedding irregularities are observed in core 152 (e.g. graded bed reversals), and therefore, it is more likely that as the turbidite climbs upslope onto the hill west of core 152, it also slows down and deposits coarser-grained material in

greater thicknesses.

The thickness of the first turbidite increases from core 153 to 150 (east to west), but then the thickness drops off sharply at core 148. It should be noted, by way of explanation, that the volume of the first turbidite is the lowest of the three studied in detail and that perhaps the turbidity current had nearly expended its material at the western extreme of the abyssal plain near the area of core 148. Again, as in core 152, as the turbidity current moved upslope toward the western limit of the abyssal plain, the thickness of the sandy base and the coarseness of the grain size increased (Figures 2 and 10).

The thickness and grain size variations of the second and third turbidite cores (Figure 10) are nearly identical to those of the first turbidite and the inferences on the effects of local topography are likewise identical. One exception is that core 148 follows the thickening trend in both the second and third turbidite, suggesting that ample material was available to result in a thicker deposit at the far end of the abyssal plain. Again, the thicker deposit is thought to have resulted from deposition out of a slower-moving turbidity flow. Another exception is the third turbidite base of core 154, which contains large amounts of sand and is coarse-grained, unlike the younger two turbidites. The third turbidite bases contain 72 times more sand than the second turbidite bases and 3.68 times more sand than the first turbidite bases. Therefore, it is likely that

the sand of the third turbidite would travel further to reach core 154, which is consistent with Kuenen and Migliorni's (1950) observation in the laboratory that sandy turbidites travel further than silt-and-clay-rich ones. Thus, it is not necessary to hypothesize a main avenue of turbidite flow for the third turbidite different from that of the first two turbidites.

Middleton (1966a) provides a possible experimental explanation for the thickness variations observed in the turbidites of the Horseshoe Abyssal Plain (Figure 17); he released into an aqueous flume a dense slurry of material and then photographed the advancing turbidity current head. The results of his experiment (Figure 17) showed that the thickest turbidity current head was observed the furthest distance away from the point of entry of the material. If one makes the assumption that the observed thickness of the head of the turbidity current is directly proportional to the final thickness of the deposit, then Middleton's results can be used to compare the thicknesses of turbidites on the Horseshoe Abyssal Plain versus distance from the supplying canyon. The thickness trends for the first turbidite, as previously discussed (Figure 10), can only be placed into the framework of Middleton's curves (Figure 17) if cores 153-150 are located on the positive slope of the curves further than 3 m from the gate. As aforementioned, it is probable that the first turbidite of core 148 was deposited as the small-volume turbidity flow was running out of material

FIGURE 17. Variation in thickness of the advancing head of the turbidity current (d_2) with distance from the gate (from Middleton, 1966a, Figure 11). Data represent two seperate flows.

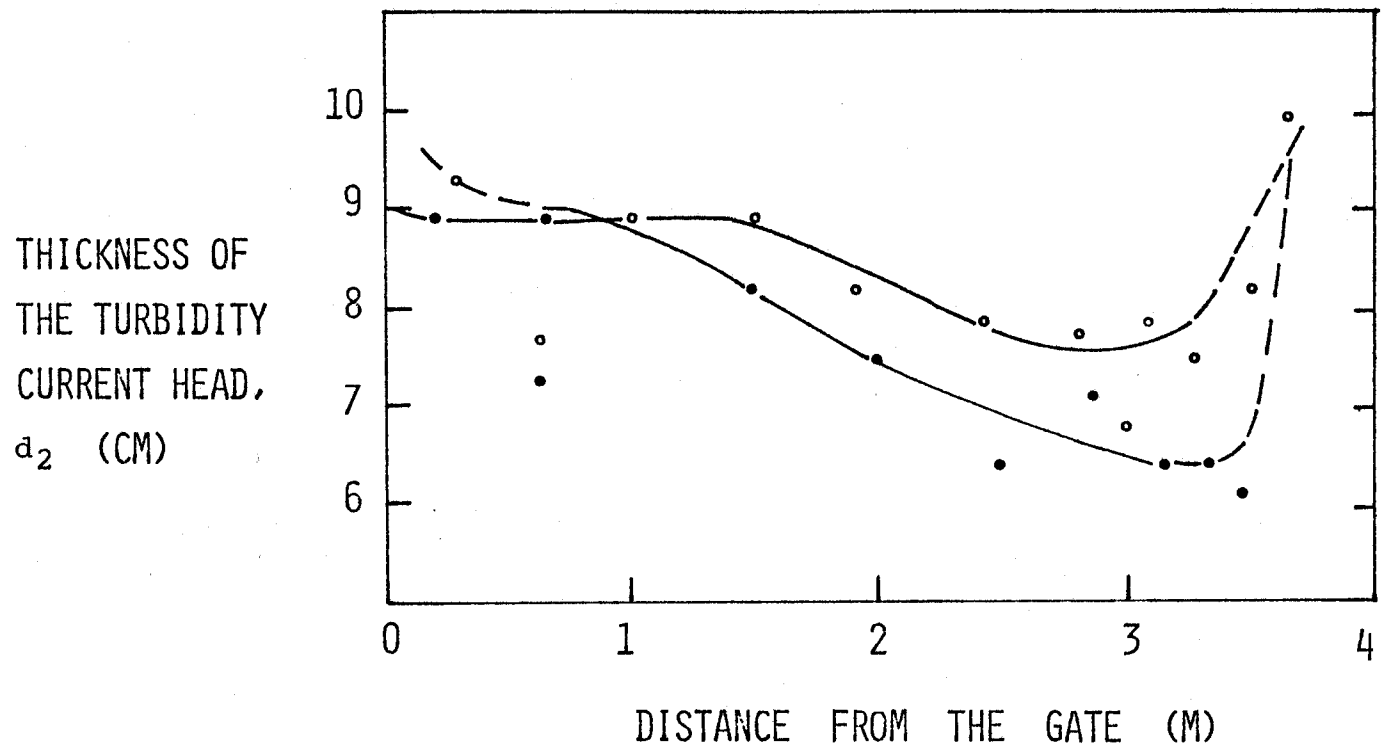
THICKNESS OF
THE TURBIDITY
CURRENT HEAD,
d_2 (CM)
10
9
8
7
6
0
1
2
3
4
DISTANCE FROM THE GATE (M)

and approaching zero velocity. The second and third turbidites (Figure 10) are seen to follow nearly identical thickness trends to that of the first turbidite, except that the much larger volumes of the second and third turbidites (8.0 km^3 and 12.1 km^3) apparently provided more than ample material to deposit a very thick bed at the "distal" reaches, as the upturned tail of Middleton's curve suggests.

Using Kuelegan's (1958) model laws for density currents, Middleton (1966a) experimented (in the laboratory flume previously mentioned) on the velocity of the head of small turbidity currents. Based on these models, estimates of velocities of larger flows can be attempted; however, several assumptions must be made, and therefore the results are highly speculative.

For high salinity flows on slopes of less than 4°, the following formula was applied: $v=0.75\sqrt{(\Delta\rho/\rho)(gd_2)}$. V is the velocity of the advancing density current head, 0.75 is a constant calculated on the basis of experiments, $\Delta\rho$ is the difference between the density of the current (ρ) and that of the overlying water, d_2 is the thickness of the head and g is the acceleration due to gravity (9.8 m/sec^2). In order to arrive at estimations of possible velocity, one must first estimate values for turbidite density and thickness. Menard (1964) has maintained that high density (greater than 1.10 gm/cc) turbidity currents have not occurred in the ocean or in experiments, but Kuenen (1966a) has convincingly argued, based on experimental studies and sampling of suspended river

loads, that turbidity currents can be as dense as 1.5-2.0 gm/cc. Kuenen argues that a thin, high-density turbidity current is most probable and that, in the case of the large (50 km^3) Grand Banks Turbidite, the thickness was probably about 40 m. The volumes calculated for the three turbidites studied in detail from the Horseshoe Abyssal Plain are 5.7 km^3, 8.0 km^3, and 12.1 km^3 for the first, second, and third turbidites, respectively. I will use the third turbidite as an example for velocity calculations and assume, for simplicity, that this turbidite is presently 1 m thick throughout the abyssal plain (actual average thickness of the third turbidite in the cores is 0.81 m). I will use 1.5 gm/cc as approximating the present density of the turbidite (average) and arbitrarily choose 1.25 gm/cc as the density of the turbidity current flow, which is quite a reasonable value according to many authors (e.g. Kuenen, 1966a). Therefore, from the present thickness and density of the deposit, I can calculate the thickness of the deposit when it was suspended as a density current of 1.25 gm/cc. The resulting thickness (T) is : $\frac{1.50 \text{ gm/cc}}{1.25 \text{ gm/cc}} = \frac{T}{1m}$, where solving for T yields an average thickness over the entire abyssal plain area (5100 km^2) of 1.2 m. However, this was probably not distributed over the entire abyssal plain area instantaneously, but rather occupied a much smaller area of the supplying canyon to the east. If I could assume this area to have been 510 km^2 (one tenth of abyssal plain area), for example, this would require that the suspension (approximated to equal the

thickness of the advancing turbidity current head) was about 12 m thick. Finally, the density of sea water is taken to be 1.0 for this general calculation:

$$\text{velocity}=0.75\sqrt{((1.25-1.0)\,\text{gm/cc}/1.25\,\text{gm/cc})(9.8\,\text{m/sec}^2)(12\,\text{m})}$$

$$\text{velocity}=0.75\sqrt{(23.52\ \text{m}^2/\text{sec}^2)}$$

velocity=3.6 m/sec or 13 km/hr

This calculated velocity is based on assumptions which have not been unambiguously and rigorously tested in this study or any other study of modern turbidites. The only constraint on this problem is that provided by small-scale simulations of turbidity currents run in laboratory flumes, most notably the studies of Middleton (1966a). Although scaling problems make inferences from these laboratory studies rather tenuous, first-order inferences may be at least partially valid for modern turbidity flows. For example, Middleton (1966a) shows that the initial velocity and density of a turbidity flow upon entering a basin is maintained without decrease until the supply of material is exhausted, at which time the velocity and density of the current drops rapidly to zero, as does the thickness. These results are similar to those concerning velocity put forth in quantitative form by Kuenen (1965,1966a). Certainly, reliable velocity calculations of the heads of advancing turbidity currents cannot confidently be made until thicknesses and densities of modern marine turbidity currents can be accurately determined by direct observations.

The relative velocities of the three turbidites from

the Horseshoe Abyssal Plain can, however, be ranked on the basis of erosional basal contacts and coarseness of bases. Ericson and others (1961) have maintained that the velocity of the turbidity current controls the grain size being transported; higher velocities are associated with larger grain sizes. On this basis, the third turbidite ought to have had the highest velocity (all six cores have erosional bases, Figure 7) and coarsest grain size, the first turbidite a slightly lesser velocity (three erosional bases and coarse grain size), and the second turbidite a much lower velocity (no erosional bases and a very fine grain size). Based on the same criterion, the fourth turbidite appears similar to the first (inferred similar velocity) and the fifth turbidite appears similar to the second (inferred similar velocity). These results are consistent with the application of Walker's (1967) P_1 index as presented in Table II.

In summary then, the local bottom topography of the Horseshoe Abyssal Plain is an important control on the details of sedimentation at the core localities observed. It is thought that upon moving upslope, a turbidity current would decellerate and therefore deposit more sandy material. In addition to velocity, the volume of material being transported is of primary importance. Locally, topographic lows in the abyssal plain appear to receive thick sections of fine-grained material, while topographic highs appear to receive thin sections of fine-grained material.

Sorting Index Data.

The sorting index data (Folk's 1968 inclusive graphic standard deviation) is presented in Figure 18 for each of the first three turbidites of the six cores taken from the abyssal plain. Again, as was the case with mean grain size, the top, middle, and two-thirds horizons are quite uniform, but the bases display marked differences. All of the upper three horizons are very poorly sorted (between 2.31 and 3.16 ø sorting index). The bases, however, vary from poorly sorted to very poorly sorted from sample to sample and indicate a distinctive character of each of the three turbidites.

The average sorting index for the first turbidite bases is 2.23 ± 0.38 ø. As one moves up from the bases of the first turbidite, a small increase in the sorting index indicates that the upper sections are generally more poorly sorted. Horn and others (1971a, b), in studies of turbidites on world abyssal plains suggest that poorer sorting of silts and clays is probably due to an inferred longer time interval required for deposition. On the other hand, Middleton (1967) observed in the laboratory that sorting generally improves (index decreases) as one moves up the bed. Such is not the case, however, with the first turbidite, but only because the bases do not follow this trend. A general sorting improvement is observed for each horizon above the base as Middleton (1967) notes. Laterally, the variations within the first turbidite appear to be insignificant, except for the low index (1.61 ø) in the base of core 148. As aforementioned, sediment was

FIGURE 18. Sorting index for various horizons in each of the first three turbidites. The average sorting index of the bases and standard deviations are displayed to corroborate individual characters of the three turbidites.

INCLUSIVE GRAPHIC STANDARD DEVIATION=SORTING INDEX

$$\sigma_I = \frac{\phi 84 - \phi 16}{4} + \frac{\phi 95 - \phi 5}{6.6}$$

FORMULA FROM FOLK, 1968.

VALUE	VERBAL DESCRIPTION
LESS THAN 0.35	VERY WELL SORTED
0.35 TO 0.50	WELL SORTED
0.50 TO 0.71	MODERATELY WELL SORTED
0.71 TO 1.00	MODERATELY SORTED
1.00 TO 2.00	POORLY SORTED
2.00 TO 4.00	VERY POORLY SORTED
GREATER THAN 4	EXTREMELY POORLY SORTED

VEMA-27 CORES

WEST — SORTING INDEX (Ø UNITS) — EAST

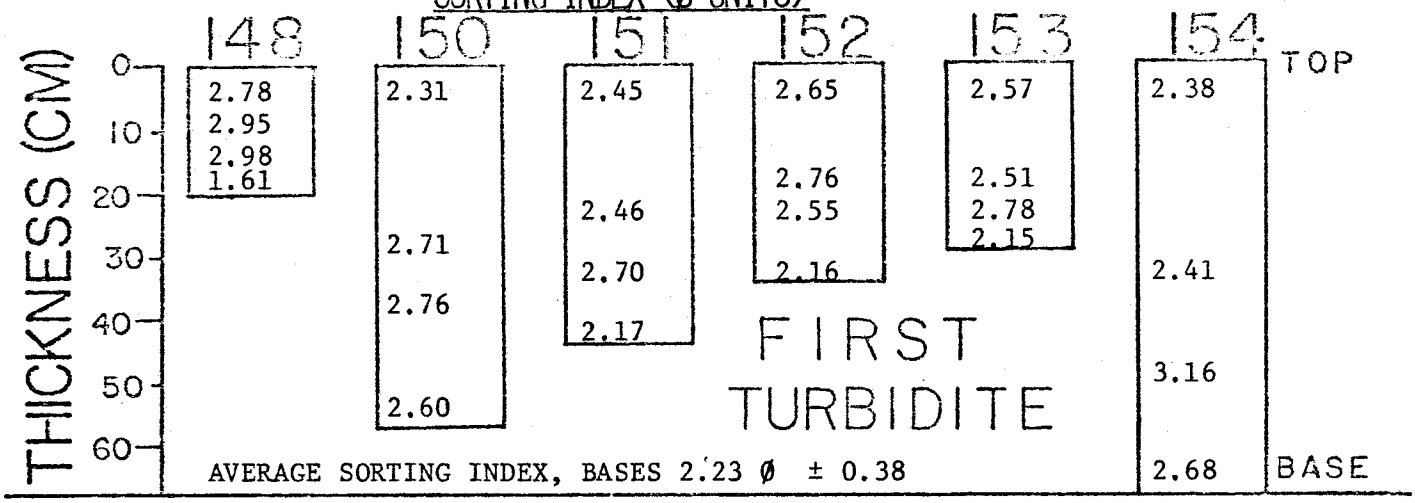

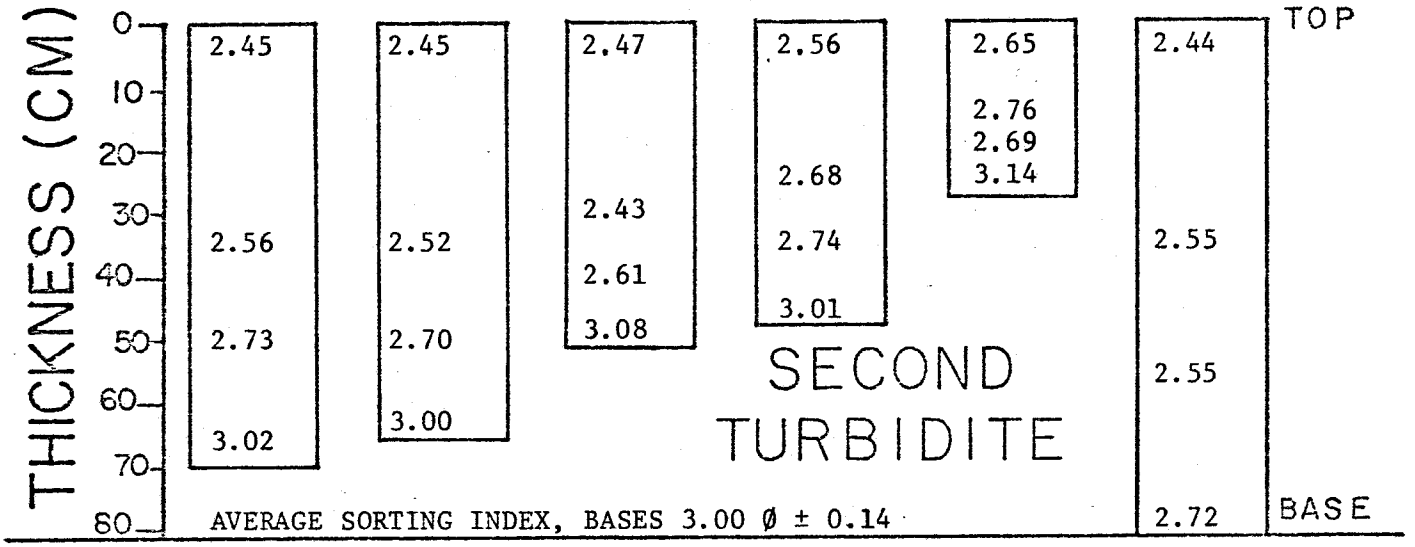

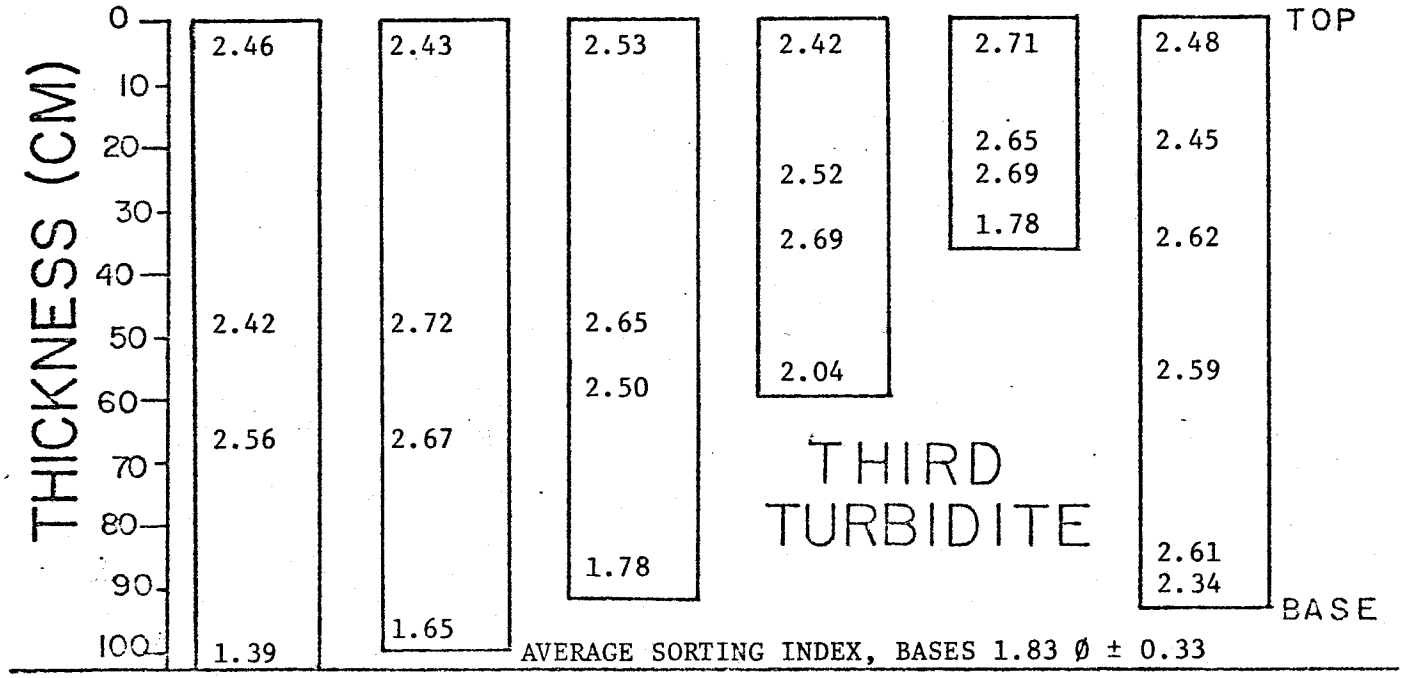

probably deposited rapidly as the current decellerated quickly, giving rise to better sorting than in the bases of other cores.

The average sorting for the second turbidite bases is 3.00 ± 0.14 Ø, which is very poorly sorted (and the most poorly sorted of the three turbidites). This value does not bracket the value for the bases of the first or third turbidites. Horn and others (1971a, b) observed poorer sorting in silts and clays than in sands. This trend is observed for the second turbidite, which contains essentially no sand. Middleton's (1967) observation that sorting generally improves upward from the base is clearly displayed in the second turbidite, the only such case of the three turbidites. Except for core 154, there is almost no lateral variation in sorting of the bases. The better sorting of core 154 may be due to preferential deposition of a relatively homogeneous sediment.

The average sorting index of the third turbidite bases is 1.83 ± 0.33 Ø, which is poorly sorted (and the most highly sorted of the three turbidites). This value overlaps the first turbidite base values. As the coarsest-grained of the turbidites, the third turbidite appears to support Horn and others' (1971a,b) observation of better sorting for coarser-grained turbidites. As with the first turbidite, above the two-thirds horizon, Middleton's (1967) claim of better sorting upward from the base is vaguely suggested.

Pelagic samples display a wider size range than turbidites, due to finer pelagic clay and large foraminiferal tests;

thus, sorting is generally poorer than in turbidites.

In summary, the above sorting data is consistent with the correlation previously demonstrated. It appears, however, that local environmental factors in the various core locations are significant, as was likewise concluded in the grain size and thickness discussion (e.g. note uniformity of sorting in the three turbidites of core 154). Many workers have claimed for Holocene turbidity currents (e.g. Pilkey and Bennetts, 1974; Elmore, 1976) that there are regular lateral sorting variations within an individual bed over its aerial extent, where sorting generally improves with increasing distance from the source. This trend, in general, cannot be observed based on the limited data from the Horseshoe Abyssal Plain cores.

Skewness Index Data.

Skewness index data (Folk's 1968 inclusive graphic skewness) are presented for the top three turbidites of the six abyssal plain cores (Figure 19). Values for the three turbidites vary from nearly symmetrical, through fine skewed, to strongly fine skewed, with all turbidites having a positive skewness. Pelagic samples are nearly symmetrical, but most often have a negative skewness. This further substantiates these trends observed for skewness of turbidite deposits and intercalated pelagics by Horn and others (1971a, b). Middleton's (1967) observed skewness values ranged from a positive skewness (fine skewed) at the base, through a maximum positive

FIGURE 19. Skewness index for various horizons of the first three turbidites. The average skewness index of the bases and standard deviations are displayed.

INCLUSIVE GRAPHIC SKEWNESS=SKEWNESS INDEX

$$SK_I = \frac{Ø16+Ø84-2Ø50}{2(Ø84-Ø16)} + \frac{Ø5+Ø95-2Ø50}{2(Ø95-Ø5)}$$

FORMULA FROM FOLK, 1968.

VALUE	VERBAL DESCRIPTION
1.0TO0.3	STRONGLY FINE SKEWED
0.3TO0.1	FINE SKEWED
0.1TO-0.1	NEARLY SYMMETRICAL
-0.1TO-0.3	COARSE SKEWED
-0.3TO-1.0	STRONGLY COARSE SKEWED

THOSE WITH EXCESS FINE MATERIAL (A TAIL TO THE RIGHT ON CUMULATIVE % CURVES) HAVE POSITIVE SKEWNESS. THOSE WITH EXCESS COARSE MATERIAL (A TAIL TO THE LEFT ON CUMULATIVE % CURVES) HAVE NEGATIVE SKEWNESS.

VEMA-27 CORES

WEST — SKEWNESS INDEX — EAST

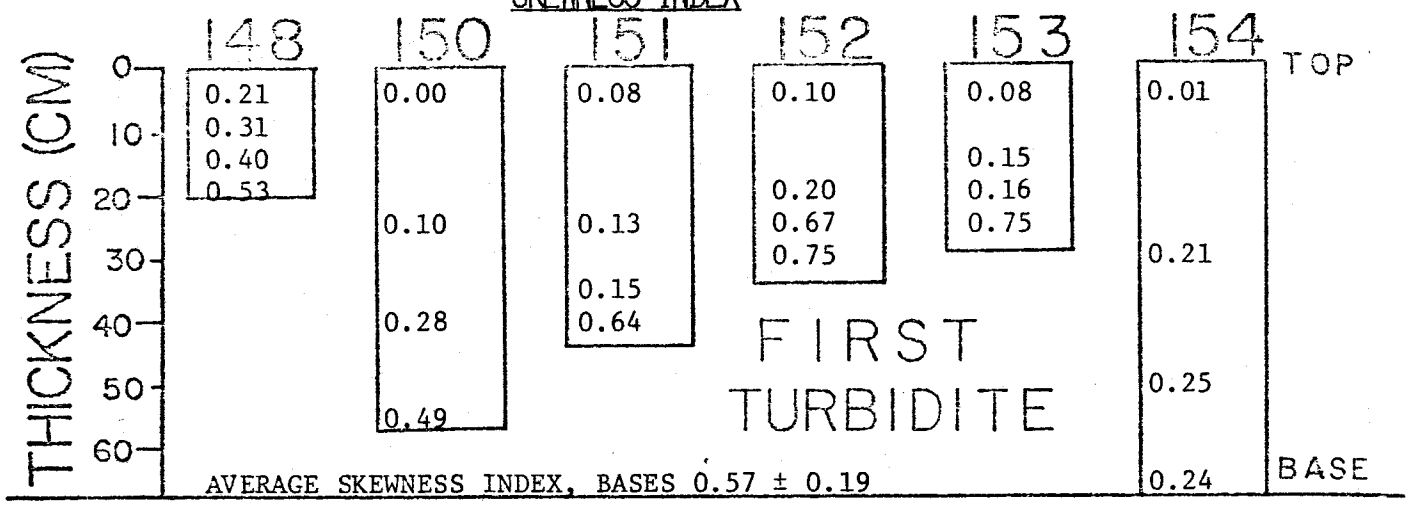

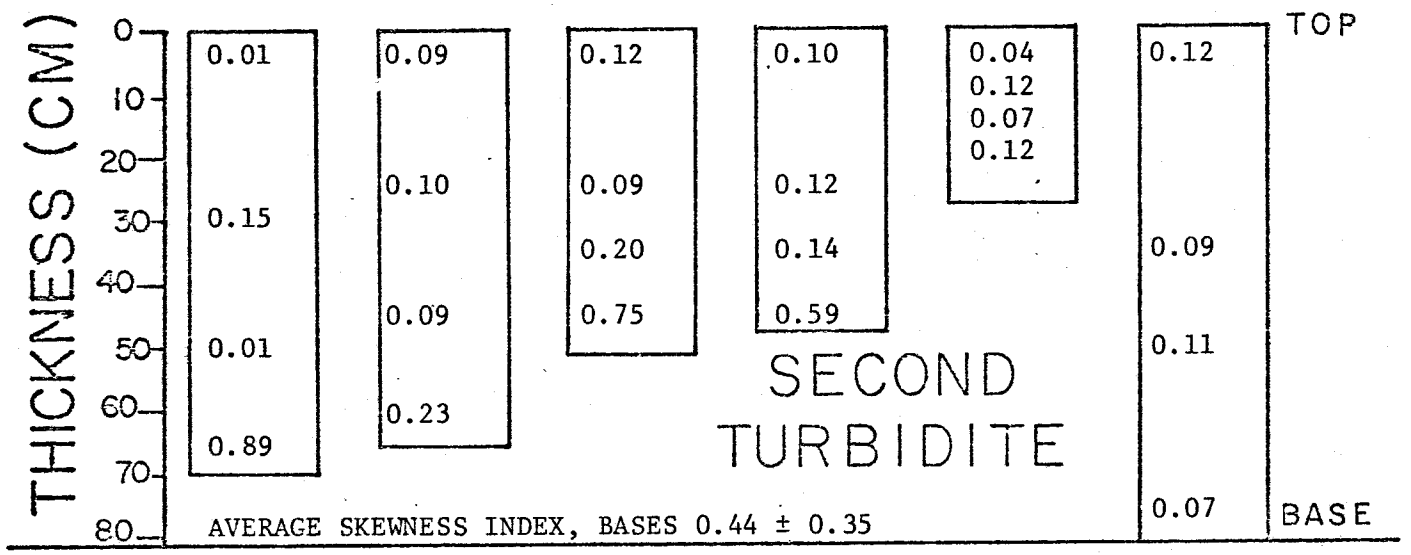

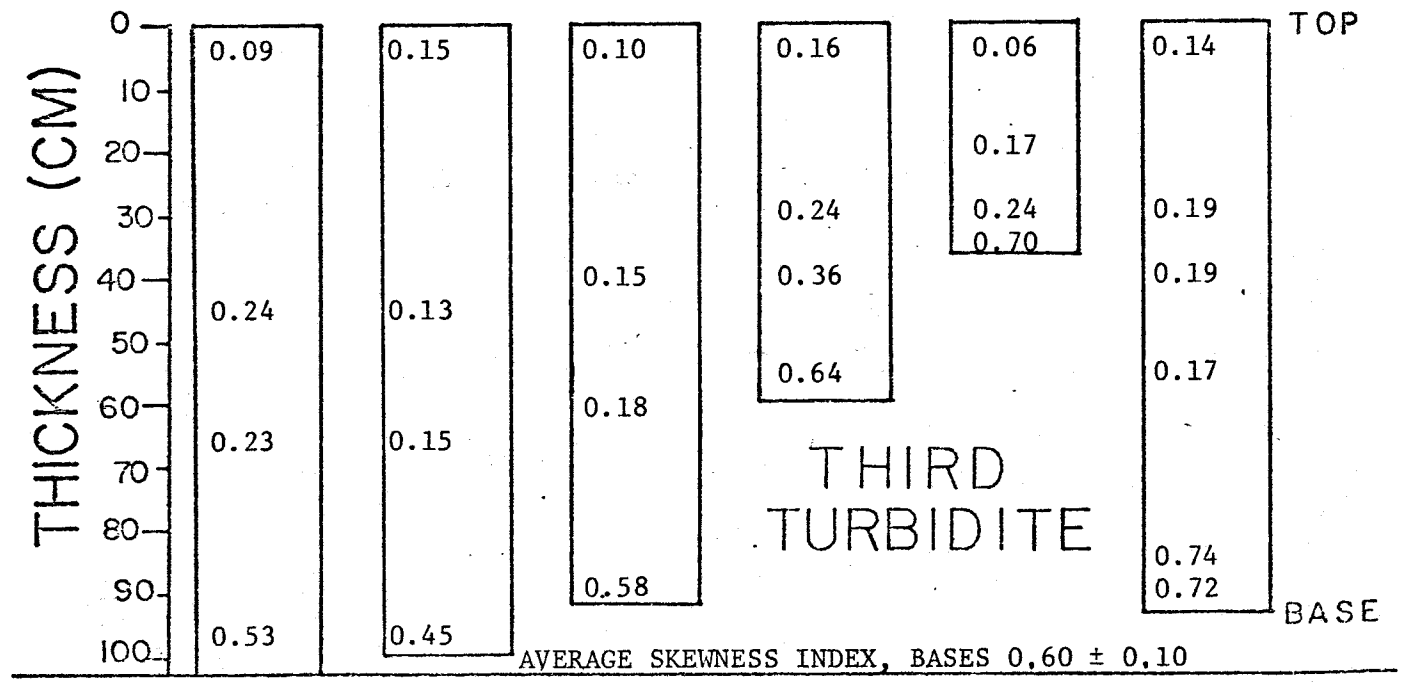

skewness near the center, to a zero skewness (symmetrical) at the turbidite tops. However, in nearly every case of the present study, the bases (18 total) are strongly fine skewed (three are fine skewed and one is nearly symmetrical). Variations such as this have been observed in other basins (Horn and others, 1971a, b, 1972). Instead of observing a maximum positive skewness near the center of the turbidite, this maximum value is observed in the bases (all except four cases), with skewnesses decreasing up the turbidite. All the turbidite tops are nearly symmetrical (or very close to it), as Middleton (1967) has experimentally observed in the laboratory.

Ericson and others (1961) have explained the ubiquitous positive skewnesses (fine skewed) found in turbidites to be explained by the upper size limit of particles being strongly regimented by the velocity of the turbidite flow. That is, the velocity of the current appears to be sensitively related to the coarsest size being transported, as previously discussed (coarsest grain sizes associated with highest velocity).

There are no general trends in skewness down the length of any one turbidite flow nor down any one core from first to third turbidite. Therefore, these data cannot be used to support the individual character of these three turbidites, but this appears to be a common result as skewness data are not used elsewhere to demonstrate correlations of units in studies of Holocene turbidites.

Kurtosis (Peakedness) Data.

Kurtosis data (Folk's 1968 graphic kurtosis) is presented in Figure 20, which again displays great homogeneity of the upper three horizons of the first three turbidites. All of the samples from the upper three horizons, save one, are platykurtic (the one exception is mesokurtic). Again, as in the other three grain size statistics parameters, the turbidite bases dominate the character of each flow, although individual characters are not as distinctive as in mean grain size or sorting parameters.

The values of kurtosis for the first turbidite range from platykurtic, through mesokurtic and leptokurtic, to very leptokurtic (well peaked histogram). The average value of the bases is 1.71 ± 0.69 (very leptokurtic), which overlaps both the second turbidite on the low side and the third turbidite on the high side. No general trends can be observed for lateral variations within any of the turbidite bases, although it can be generally stated that the coarser the grain size, the greater the kurtosis.

The second turbidite bases display an average kurtosis of 0.79 ± 0.14 (platykurtic) which is a low peakedness compared with the other two turbidites. Except for core 151, remarkable uniformity of kurtosis values characterizes this turbidite.

The third turbidite bases' average kurtosis values, 2.33 ± 0.44, are classified as very leptokurtic and are much

FIGURE 20. Kurtosis (Peakedness) index for various horizons of the first three turbidites. The average kurtosis index of the bases and standard deviations are displayed to corroborate individual characters of the three turbidites.

GRAPHIC KURTOSIS=KURTOSIS INDEX

$$K_G = \frac{\emptyset 95 - \emptyset 5}{2.44(\emptyset 75 - \emptyset 25)}$$

FORMULA FROM FOLK, 1968.

VALUE	VERBAL DESCRIPTION
LESS THAN 0.67	VERY PLATYKURTIC
0.67 TO 0.90	PLATYKURTIC
0.90 TO 1.11	MESOKURTIC
1.11 TO 1.50	LEPTOKURTIC
1.50 TO 3.00	VERY LEPTOKURTIC
GREATER THAN 3	EXTREMELY LEPTOKURTIC

INCREASING PEAKEDNESS ↓

VEMA-27 CORES

WEST — KURTOSIS (PEAKEDNESS) INDEX — EAST

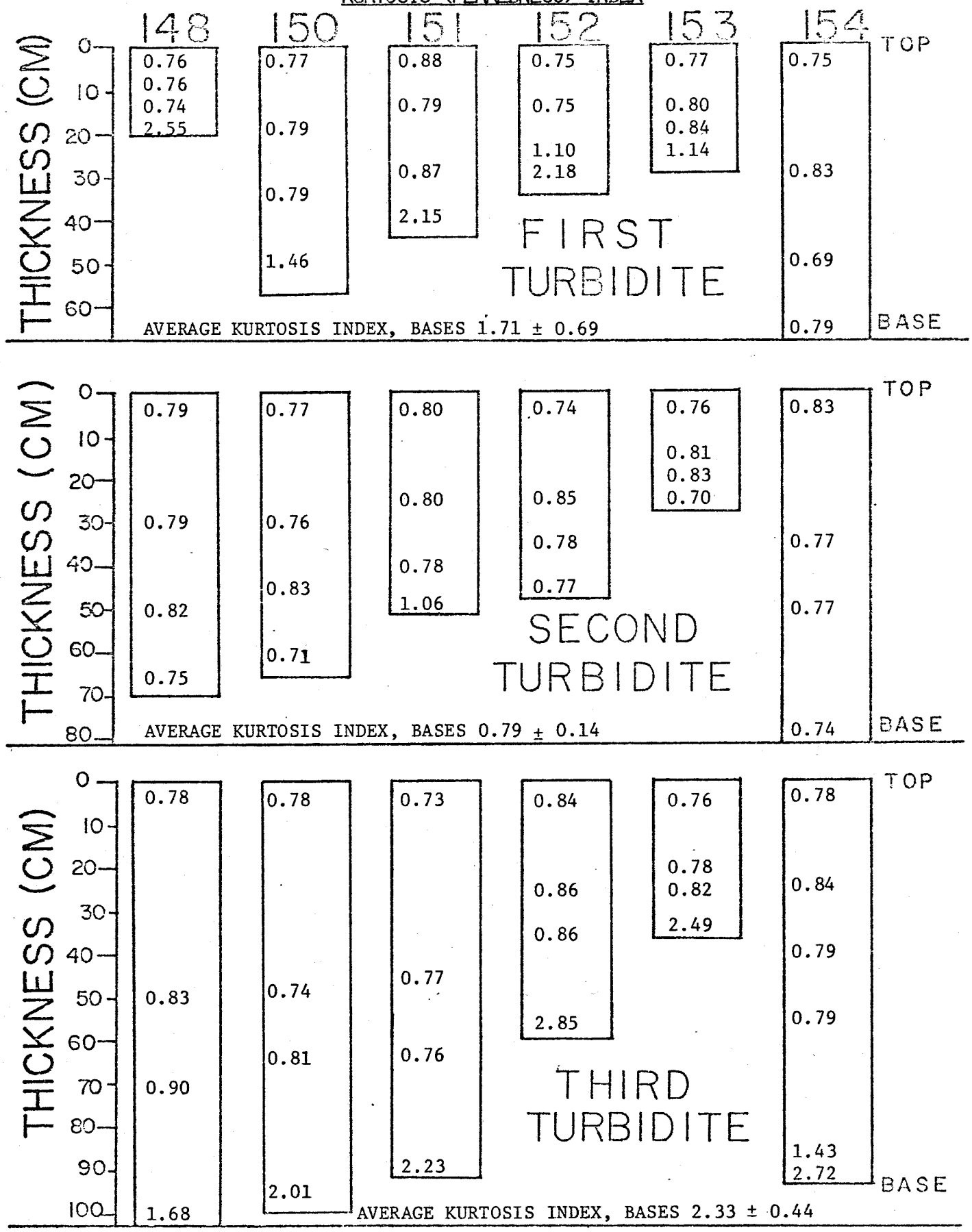

more peaked than the first turbidite (very leptokurtic also) and second turbidite (platykurtic). Again, no general trends are apparent down the plain.

The most commonly observed kurtosis values on Holocene turbidites (Horn and others, 1971a, b) are leptokurtic for sands and very leptokurtic for silts. The results for the first and third turbidites are consistent with results for very leptokurtic values for silts and sandy silts. The second turbidite, however, fits neither the silt nor the sand category, but rather defines its own clay-like platykurtic peakedness.

Plots of One Grain Size Parameter Against Another.

By combining two grain size parameters on the same plot, it is often possible to define relations of geologic significance (e.g. Folk and Ward, 1957; Horn and others, 1971b). All three turbidites from the Horseshoe Abyssal Plain plot in a segment of Horn and others' (1971b) curve for turbidites of the Sohm and Hatteras Abyssal Plains: this segment is termed Phase 3, which consists entirely of graded silts and finer-grained sections above graded sands. In a like manner, the three turbidites of the present study appear to be the products of orderly gravity settling of fine-grained particles. The turbidite bases alone (Figure 21) display part of the sinusoidal trend observed by Folk and Ward (1957) and are explained by bimodal sorting developed in distal turbidites, which allowed sufficient time

FIGURE 21. Plot of mean grain size versus standard deviation (sorting) for the bases of the first three turbidites.

K E Y

FIRST TURBIDITE INDICATED BY (∘)

SECOND TURBIDITE INDICATED BY (■)

THIRD TURBIDITE INDICATED BY (•)

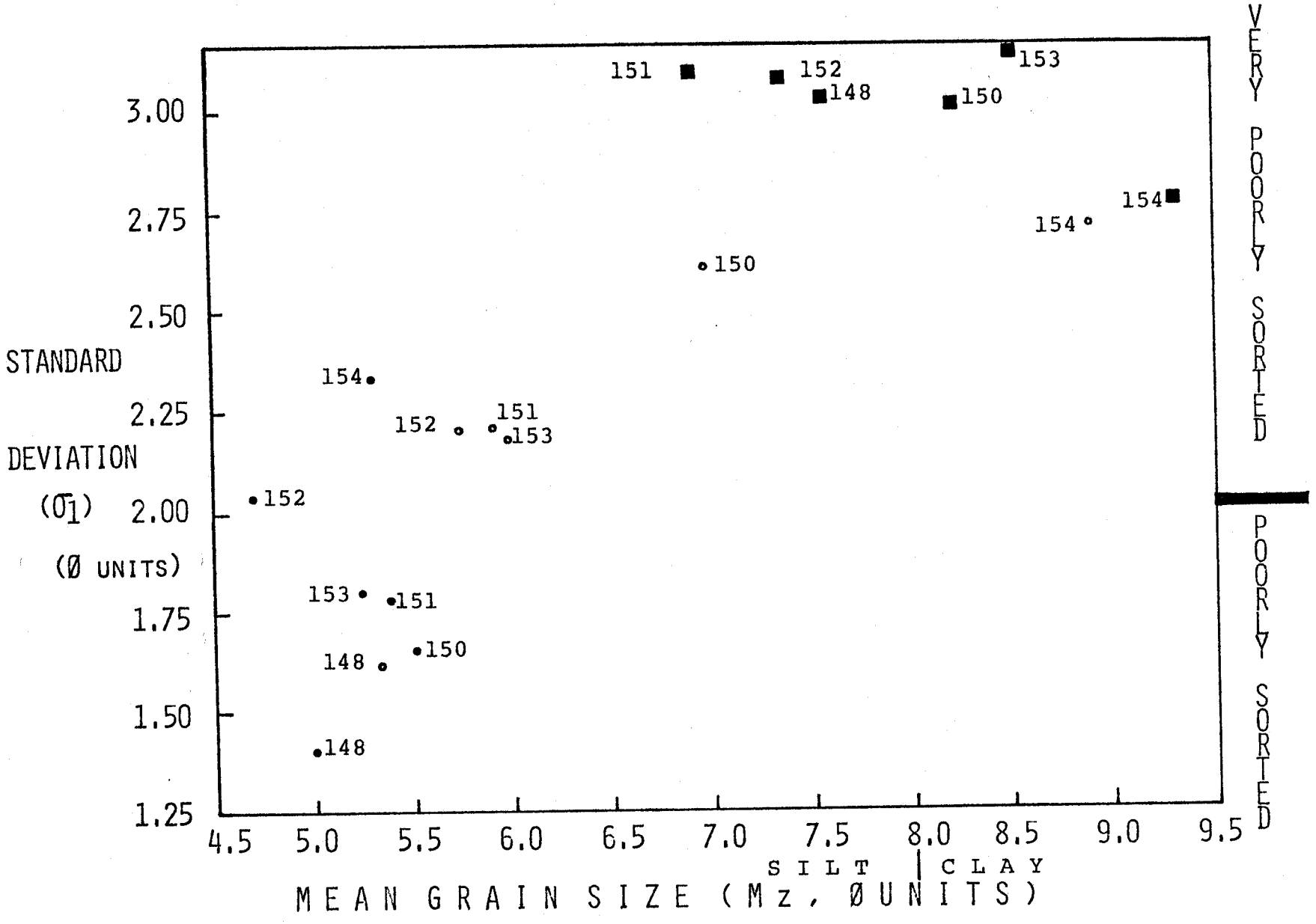
3.00
2.75
2.50
2.25
2.00
1.75
1.50
1.25
STANDARD
DEVIATION
(σ1)
(Ø UNITS)
151
152
153
148
150
154
154
150
154
152
151
153
152
153
151
150
148
148
4.5
5.0
5.5
6.0
6.5
7.0
7.5
8.0
8.5
9.0
9.5
SILT | CLAY
MEAN GRAIN SIZE (Mz, ØUNITS)
VERY POORLY SORTED
POORLY SORTED

for segregation of sizes. Each of the three turbidites displays its own chatacter on this plot, with the coarsest turbidites (first and third) displaying the widest range of standard deviations (sorting), and the finest turbidite (second) displaying the narrowest range of standard deviations (Figure 21). All these data are consistent with the findings of previous workers who have discussed mean grain size versus standard deviation (sorting) plots.

Figure 22 is a plot of mean grain size versus kurtosis index for the bases of each of the three turbidite bases. A few generalizations can be drawn from this plot. The coarser the turbidite, the higher the peakedness, which has been explained previously as a function of the velocity-controlled, sharp upper limit to grain sizes carried by turbidity currents (Ericson and others, 1961). From these data, the larger the grain size (and hence, the higher the inferred velocity), the more peaked or abrupt the truncation of large grain sizes. Again, the distinctive character of each of the three turbidites confirms the visual and acoustic correlation.

Figure 23 displays standard deviation (sorting) versus kurtosis for the bases of the first three turbidites. Although each turbidite expresses its own character, trends for the second and third turbidites appear to be opposite to the trend of the first turbidite. The latter suggests that as the standard deviation gets greater (worse sorting), the kurtosis gets larger, whereas the second and third tur-

FIGURE 22. Plot of mean grain size versus kurtosis for the bases of the first three turbidites.

K E Y

FIRST TURBIDITE INDICATED BY (•)

SECOND TURBIDITE INDICATED BY (■)

THIRD TURBIDITE INDICATED BY (•)

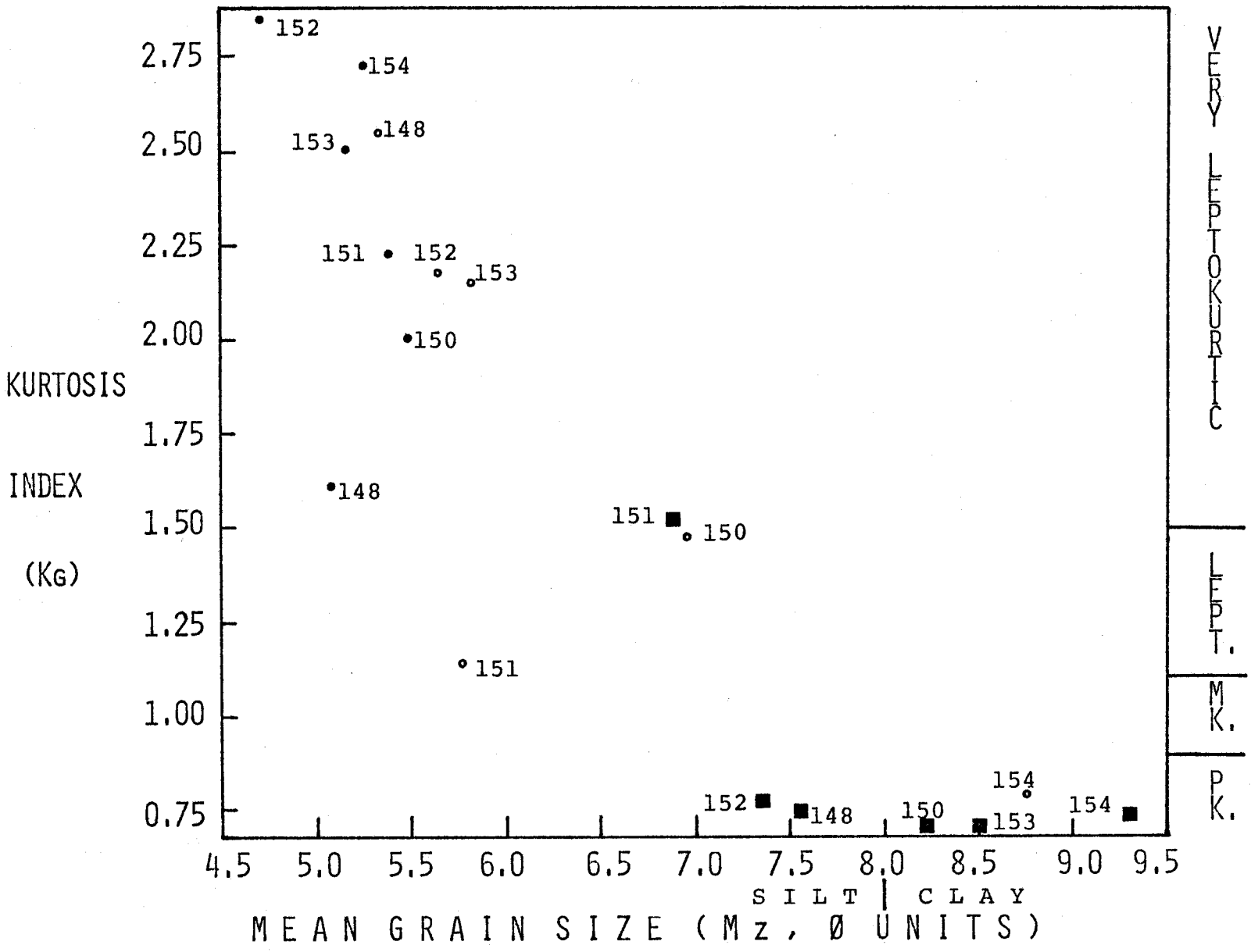
KURTOSIS INDEX (KG)
2.75
2.50
2.25
2.00
1.75
1.50
1.25
1.00
0.75
152
154
153
148
151
152
153
150
148
151
150
151
152
148
150
153
154
154
VERY LEPTOKURTIC
LEPT.
MK.
PK.
4.5
5.0
5.5
6.0
6.5
7.0
7.5
8.0
8.5
9.0
9.5
SILT | CLAY
MEAN GRAIN SIZE (Mz, Ø UNITS)

FIGURE 23. Plot of standard deviation versus kurtosis fot the bases of the first three turbidites.

FIRST TURBIDITE INDICATED BY (•)
SECOND TURBIDITE INDICATED BY (■)
THIRD TURBIDITE INDICATED BY (•)

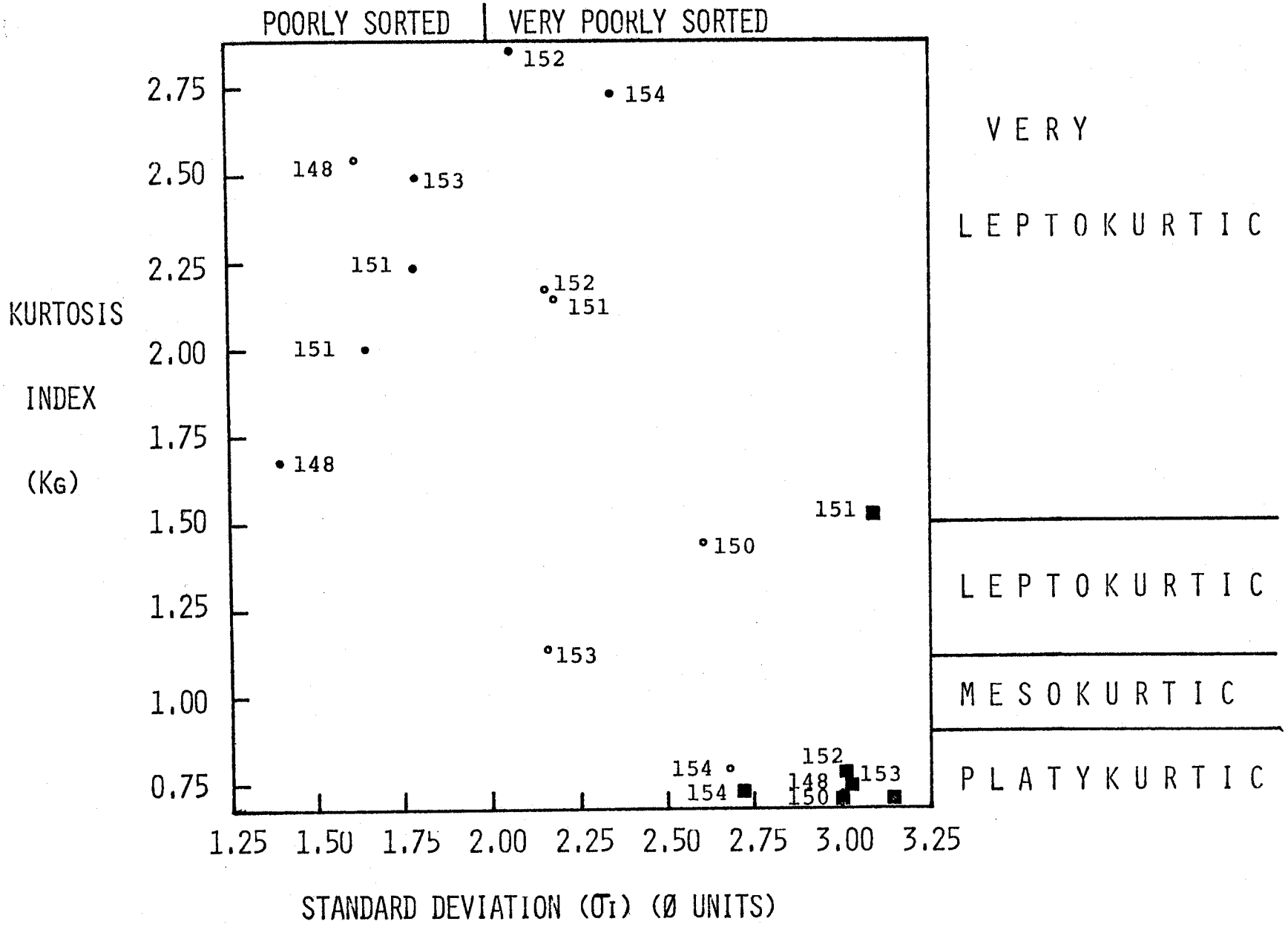
POORLY SORTED
VERY POORLY SORTED
VERY LEPTOKURTIC
LEPTOKURTIC
MESOKURTIC
PLATYKURTIC
KURTOSIS INDEX (KG)
2.75
2.50
2.25
2.00
1.75
1.50
1.25
1.00
0.75
1.25 1.50 1.75 2.00 2.25 2.50 2.75 3.00 3.25
STANDARD DEVIATION (σI) (Ø UNITS)
152
154
148
153
151
152
151
151
148
151
150
153
154
152
148
153
154
150

bidites express the opposite relationship.

In all three plots of grain size parameters (Figures 21, 22, and 23), the trends for the second and third turbidites are better defined (or more closely spaced) than those trends for the first turbidite. This suggests that the flow regime for the first turbidite gave rise to a wider range of depositional fluid dynamics than in either of the two earlier turbidites. This is probably a function of the smaller volume of material in the first turbidite and suggests that larger turbidites develop with a more uniform sedimentological character, probably because they "overpower" microtopographic influences.

Character of Clay and Mud Turbidite Tops

Analyses were performed on the first three turbidites' clay and mud tops (to one-third down the turbidite) to ascertain whether differences existed with regard to hydrochloric acid treatment, volatile solids determinations, or x-ray diffraction mineralogy. Pelagic samples were also run for comparison purposes and, in addition, x-ray mineralogy and volatile solids were determined for the tops of the fourth, fifth, and sixth turbidites.

Hydrochloric Acid Treatment.

Agate-ground samples were treated with 10% hydrochloric acid to determine approximate concentrations of calcite and organic material. A normal pelagic sample from the section

above the third turbidite in core 151 was found to contain 94.7% HCl-soluble material, as one would expect of carbonate ooze. A sandy base of the third turbidite, core 148, was found to contain 62.6% HCl-soluble material. Tops of the first three turbidites are remarkably uniform with regard to HCl-soluble material, having between 29.4% to 33.0% soluble (average of samples from all three turbidites 31.5%$\pm$1.1%, see Table III). No differences between the three turbidites or down the length of the abyssal plain within one turbidite are discernable and thus, the observed correlation is not defined by these data. A slight increase in percent of soluble material may be found in the supplying canyon (155 and perhaps 156).

Volatile Solids Treatment.

Samples from the tops (to one-third down) of all six of the turbidites are remarkably uniform with respect to volatile solids burned off for one hour at 650^{o} C in a muffle furnace (average of samples from all six turbidites is 13.2 $\pm$ 1.3%, see Table III). Hence, volatile solids data cannot be used to substantiate the observed correlation. Pelagic samples have nearly the same volatile solids content as the turbidite tops. The supplying channel samples (cores 155 and 156), however, have turbidite tops with a lower percentage of volatile solids, indicating a much lower percentage of combustible organic material than in the turbidite tops.

TABLE III. HCl-SOLUBLE MATERIAL (%) AND VOLATILE SOLIDS (%).

TURBIDITE NUMBER	CORE NUMBER	HCl-SOLUBLE MATERIAL (%)	VOLATILE SOLIDS (%)
Top First	148	32.3	11.2
Top First	150	30.7	12.9
Top First	151	30.2	14.4
1/3 First	152	33.0	11.0
1/3 First	153	31.1	14.2
Top First	154	29.4	12.5
Top Second	148	30.9	13.2
Top Second	150	32.4	13.9
Top Second	151	32.6	14.5
Top Second	152	30.9	14.9
1/3 Second	153	31.8	13.6
Top Second	154	32.1	15.5
1/3 Third	148	30.2	12.2
Top Third	150	31.8	12.3
Top Third	151	31.9	13.1
1/3 Third	152	31.3	12.1
Top Third	153	30.0	11.6
1/3 Third	154	31.1	13.2
Top Pelagic Of Third	151	94.7	11.5*
Top First, Channel	155	35.3	8.8#
Top First, Channel	156	32.5	9.7@
Base Third	148	62.6	2.7**
Top Forth	148	----	13.3
Top Fifth	150	----	12.8
Top Sixth	152	----	14.2

X-Ray Diffraction Mineralogy.

One hundred and thirty-six x-ray diffraction scans were run on clays of the six turbidites, on pelagics, and on supplying canyon clays. Results are presented in Table IV by core number, west to east in the abyssal plain, in order down the table. Each sample (e.g. 148, first turbidite) was split into four seperate specimens for complete x-ray diffraction analysis, as previously described in the methods section. "UA" refers to the "upper aliquot" and "LA" refers to the "lower aliquot", both taken at specified time intervals (5, 30, and occasionally 15 minutes) from a column of settling sediment. The purpose of taking upper and lower aliquots at different times was to isolate groups of minerals for x-ray analysis. For example, dense, large-grained silts would be predominant in the 5 minute lower aliquot whereas light, small-grained clays would be predominant in the 30 minute upper aliquot. Combining all results from the four specimens, a uniform mineralogy was found for the clay and mud tops of the first, second, third, fifth, and sixth turbidites. These turbidites were found to contain, on the basis of at least three x-ray peaks identified, muscovite (or its fine-grained equivalent illite), ferririte (a zeolite mineral), kaolinite, chlorite, orthoclase feldspar, albite feldspar, microcline feldspar, quartz, calcite, and dolomite. The fourth turbidite was distinct in that microcline feldspar was not identified from the above list of minerals. Figures 24 and 25 show, respectively, sections of typical scans of the

TABLE IV. X-RAY DIFFRACTION MINERALOGY OF CLAY TURBIDITE TOPS.

MINERALS:	MUSCOVITE (ILLITE)	FERRIRITE (A ZEOLITE)	KAOLINITE	CHLORITE	ORTHOCLASE	ALBITE	QUARTZ	MICROCLINE	CALCITE	DOLOMITE
148,1st,UA,5	x	x	x	x	x	x	x1	x	x2	x3
" , " ,LA,5	x	x	x	x	x	x	x1		x2	x3
" , " ,UA,30	x	x	x	x	x	x	x3		x2	x1
" , " ,LA,30	x	x	x	x	x	x	x1	x	x2	x3
148,2nd,UA,5	x	x	x	x		x	x1	x	x2	x3
" , " ,LA,5	x	x	x	x	?	x	x1	x	x2	x
" , " ,UA,30	x	x	x	x	x	x	x1	x	x2	
" , " ,LA,30	x	x	x	x	x	x	x1		x2	x3
148,3rd,UA,5	x	x	x	x	x	x	x1	x	x2	x3
" , " ,LA,5	x	x	x	x	x	x	x1		x2	x3
" , " ,UA,30	x	x	x	x	x	x	x1	x	x2	x3
" , " ,LA,30	x	x	x	x	x	x	x1	x	x2	
150,1st,UA,5	x	x	x	x	x	x	x1	x	x2	x3
" , " ,LA,5	x	x	x	x	?	x	x1	x	x3	x2
" , " ,UA,30	x	x	x	x	x?	x?	x1	x	x2	x3
" , " ,LA,30	x	x	x	x	x	x	x1	x	x3	x2
150,2nd,UA,5	x	x	x	x	x	x	x1	x	x2	x3
" , " ,LA,5	x	x	x	x	x	x	x1	x	x2	x3
" , " ,UA,30	x	x	x	x			x1		x2	x3
" , " ,LA,30	x	x	x	x	x	x	x1	x	x2	x3

TABLE IV. (cont.)

MINERALS:	MUS.	FER.	KA.	CH.	OR.	AB.	Q.	MIC.	CA.	DO.
150,3rd,UA,5	x	x	x	x	x	x	xl		x2	x3
" , " ,LA,5	x	x	x	x	x	x	xl	x	x3	x2
" , " ,UA,30	x	x	x	x	x	x	xl	x	x2	x3
" , " ,LA,30	x	x	x	x	x	x	xl		x2	x3
151,1st,UA,5	x	x	x	x	x	x	xl	x	x2	x3
" , " ,LA,5	x	x	x	x	x	x	xl	x	x3	x2
" , " ,UA,30	x	x	x				x	TRUNCATED		
" , " ,LA,30	x	x	x	x	x		xl	x	x2	x3
151,2nd,UA,5	x	x	x	x	x	x	xl	x	x2	x3
" , " ,LA,5	x	x	x	x	x	x	xl	x	x2	x3
" , " ,UA,30	x	x	x	x		x	xl	x	x2	x3
" , " ,LA,30	x	x	x	x	x	x	xl	x	x2	x3
151,3rd,UA,5	x	x	x	x	?	?	xl	x	x2	x3
" , " ,LA,5	x	x	x	x	x	x	xl	x	x2	x3
" , " ,UA,30	x	x	x	x	?	?	xl	?	x2	x3
" , " ,LA,30	x	x	x	x	x	x	xl	x	x2	x3
152,1st,UA,5	x	x	x	x	x	x	xl	x	x2	x3
" , " ,LA,5	x	x	x	x	x	x	xl	x	x3	x2
" , " ,UA,30	x	x	x	x	x	?	xl	x	x2	x3
" , " ,LA,30	x	x	x	x	x	x	xl	x	x3	x2
152,2nd,UA,5	x	x	x	x	x	x	xl	x	x2	x3
" , " ,LA,5	x	x	x	x	x	x	xl	x	x2	x3
" , " ,UA,30	x	x	x	x	x	x	x	x	TRUNCATED	
" , " ,LA,30	x	x	x	x	x	x	xl	x	x2	x3

TABLE IV. (cont.)

MINERALS:	MUS.	FER.	KA.	CH.	OR.	AB.	Q.	MIC.	CA.	DO.
152,3rd,UA,5	x	x	x	x	?		xl	x	x2	x3
" , " ,LA,5	x	x	x	x	x	x	xl	x	x3	x2
" , " ,UA,30	x	x	x	x	?	?	xl	x	x2	x3
" , " ,LA,30	x	x	x	x	x	x	xl	x	x3	x2
153,1st,UA,5	x	x	x	x	x	x	xl	x	x2	x3
" , " ,LA,5	x	x	x	x	x	x	xl	x	x3	x2
" , " ,UA,30	x	x	x	x	x	x	xl	x	x2	x3
" , " ,LA,30	x	x	x	x	x	x	xl	x	x2	x3
153,2nd,UA,5	x	x	x	x	x	x	xl	x	x2	x3
" , " ,LA,5	x	x	x	x	x	x	xl	x	x2	x3
" , " ,UA,30	x	x	x	x	x	x	xl	x	x2	x3
" , " ,LA,30	x	x	x	x	x	x	xl	x	x3	x2
153,3rd,UA,5	x	x	x	x	x	x	xl	x	x2	x3
" , " ,LA,5	x	x	x	x	x	x	xl	x	x3	x2
" , " ,UA,30	x	x	x	x		x	xl	x	x2	x3
" , " ,LA,30	x	x	x	x	x	x	xl	x	x2	x3
154,1st,UA,5	x	x	x	x	x	x	xl	x	x2	x3
" , " ,LA,5	x	x	x	x	x	x	xl	x	x3	x2
" , " ,UA,30	x	x	x	x		?	xl	x	x2	x3
" , " ,LA,30	x	x	x	x	x	x	xl	x	x2	x3
154,2nd,UA,5	x	x	x	x	x	x	x2	x	xl	x3
" , " ,LA,5	x	x	x	x	x	x	xl	x	x2	x3
" , " ,UA,30	x	x	x	x			x	TRUNCATED		
" , " ,LA,30	x	x	x	x	x	x	xl	x	x2	x3

TABLE IV. (cont.)

MINERALS:	MUS.	FER.	KA.	CH.	OR.	AB.	Q.	MIC.	CA.	DO.
154,3rd,UA,5	x	x	x	x	x	x	x	x	TRUNCATED	
" , " ,LA,5	x	x	x	x	x	x	x1	x	x2	x3
" , " ,UA,30	x	x	x	x			x	x	TRUNCATED	
" , " ,LA,30	x	x	x	x	x	x	x1	x	x2	x3
148,3rd,UA,15	x	x	x	x	x	x	x2	x	x1	x3
" , " ,LA,15	x	x	x	x	x	x	x2	x	x1	x3
148,1st,HCl Smear	x	x	x	x	x	x	x1		x2	x3
148,3rd,HCl Smear	x	x	x	x	x	x	x1	x	x2	x3
148,2nd,HCl Smear	x	x	x	x	x	x	x1	x	x2	x3
148,3rd, Smear	x	x	x	x	x	x	x1	x	TRUNCATED	
148,3rd,UA,HCl 5	x	x	x	x	x	x	x1	x	x2	
" , " ,LA,HCl 5	x	x	x	x	x	x	x1	x	?	?
FELDSPAR RUNS 21-28°,27-29°;ALSO 8-10° FOR MUS. AND FER.										
148,2nd,New Mount #2	x	x				x	x	x		
152,4th,UA,5	x	x	x			?	x1		x2	x3
" , " ,LA,5	x	x	x	x	x	x	x1		x3	x2
" , " ,UA,30	x	x	x	x		x	x1		x2	x3
" , " ,LA,30	x	x	x	x	x	x	x1		x2	x3
152,5th,UA,5	x	x	x	x			x1	x	x2	x3
" , " ,LA,5	x	x	x	x	x	x	x1	x	x3	x2
" , " ,UA,30	x	x	x	x			x2		x1	x3
" , " ,LA,30	x	x	x	x	x	x	x1		x2	x3

TABLE IV. (cont.)

MINERALS:	MUS.	FER.	KA.	CH.	OR.	AB.	Q.	MIC.	CA.	DO.
152, 6th,UA,5	x	x	x	x	x	x	x1	x	x2	
" , " ,LA,5	x	x	x	x	x	x	x1		x2	x3
" , " ,UA,30	x	x	x	x	x	x	x1		x2	x3
" , " ,LA,30	x	x	x	x	x	x	x1	x	x2	x3
153,4th,UA,5	x	x	x	x		x	x2		x1	x3
" , " ,LA,5	x	x	x	x	x	x	x1	?	x2	x3
" , " ,UA,30	x	x	x	x	x	x	x1		x2	x3
" , " ,LA,30	x	x	x	x	x	x	x1		x2	x3
153,5th,UA,5	x	x	x	x	x	x	x1		x2	x3
" , " ,LA,5	x	x	x	x	x	x	x1	x	x3	x2
" , " ,UA,30	x		x	x	x	x	x1		x2	x3
" , " ,LA,30	x	x	x	x	x	x	x1	x	x2	x3
155,3rd,UA,5	x	x	x	x			x1		x2	x3
" , " ,LA,5	x	x	x	x	x	x	x1		x2	x3
" , " ,UA,30	x					x	x1	TRUNCATED		
" , " ,LA,30	x	x	x	x	x	x	x1	x	x2	x3
156,3rd,UA,5	x	x	x	x	x	x	x2		x1	x3
" , " ,LA,5	x	x	x	x	x	x	x1	x	x3	x2
" , " ,UA,30	x	x			x	x	x1	TRUNCATED		
" , " ,LA,30	x	x	x	x	x	x	x1		x2	x3
153,Gor.,UA,5	x	x	x	x		x	x2		x1	x3
" , " ,LA,5	x	x	x	x	x	x	x1	x	x2	x3
" , " ,UA,30			x		x	x	x	x	TRUNCATED	
" , " ,LA,30	x	x	x	x	x	x	x1	x	x2	x3

TABLE IV. (cont.)

MINERALS:	MUS.	FER.	KA.	CH.	OR.	AB.	Q.	MIC.	CA.	DO.
153,UKA,UA	x	x	x	x			x1		x2	x3
" , " ,LA	x	x	x	x	x	x	x1	x	x2	x3
154,UKB,UA	x	x	x	x			x1		x2	
" , " ,LA	x	x	x	x	x	x	x2		x1	
156,UKC.	x	x	x	x			x1		x2	
149,Top Pel.,UA,5	x	x	x		?		x2		x1	
" , " " ,LA,5	x	x	x		x	x	x3		x1	x2
" , " " ,UA,30			x	x			x2		x1	
" , " " ,LA,30	x		x	x	x		x2	x	x1	x3
148,B.3,Bur,LA,5	x	x	x	x	x	x	x1	x	x3	x2
150, " " ,LA,5	x	x	x	x	x	x	x1	x	x2	x3
151, " " ,LA,5	x	x	x	x	x	x	x1	x	x2	x3
152, " " ,LA,5	x	x	x	x	x	x	x2	x	x1	x3
153, " " ,LA,5	x	x	x	x	x	x	x1	x?	x2	x3
154, " " ,LA,5	x	x	x	x	x?	x?	x2	x?	x1	x3
148,3rd Pel.,LA,5				x			x2		x1	x3
150, " " ,LA,5				x			x2		x1	x3
151, " " ,LA,5				x			x2		x1	x3
152, " " ,LA,5				x			x2		x1	x3
153, " " ,LA,5				x			x2		x1	x3
154, " " ,LA,5				x			x2		x1	x3

FIGURE 24. Example of a typical x-ray mineralogy scan representing part of the mineralogy found in the first, second, third, fifth, and sixth turbidite tops.

The sample is from the top of the second turbidite (core 150, 97-100cm, LA 5 min.).

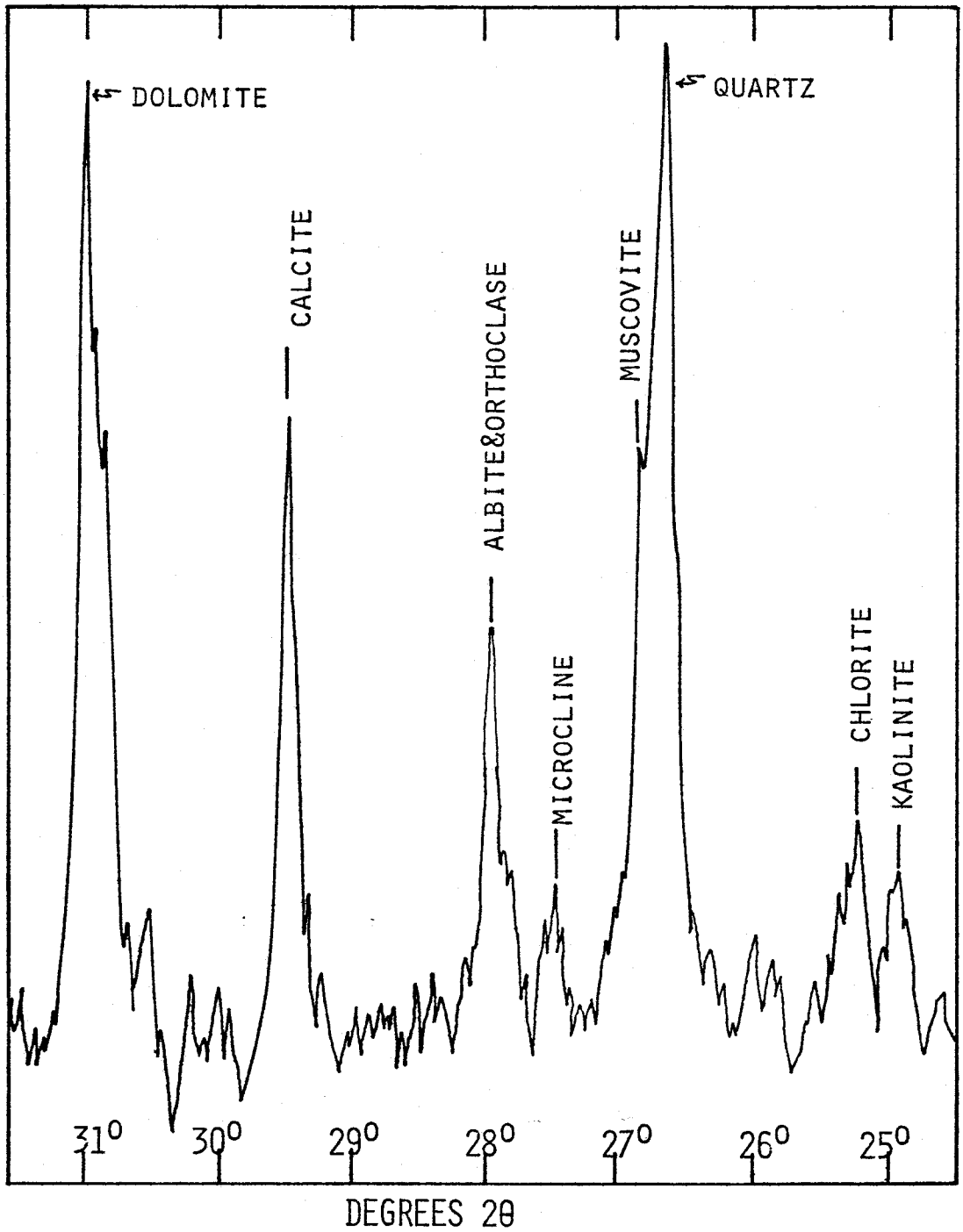
DOLOMITE
CALCITE
ALBITE&ORTHOCLASE
MICROCLINE
MUSCOVITE
QUARTZ
CHLORITE
KAOLINITE
31°
30°
29°
28°
27°
26°
25°
DEGREES 2θ

FIGURE 25. Example of a typical x-ray mineralogy scan representing part of the mineralogy found in the fourth turbidite tops.

The sample is from the top of the fourth turbidite (core 152, 259-260 cm, LA, 5 min.).

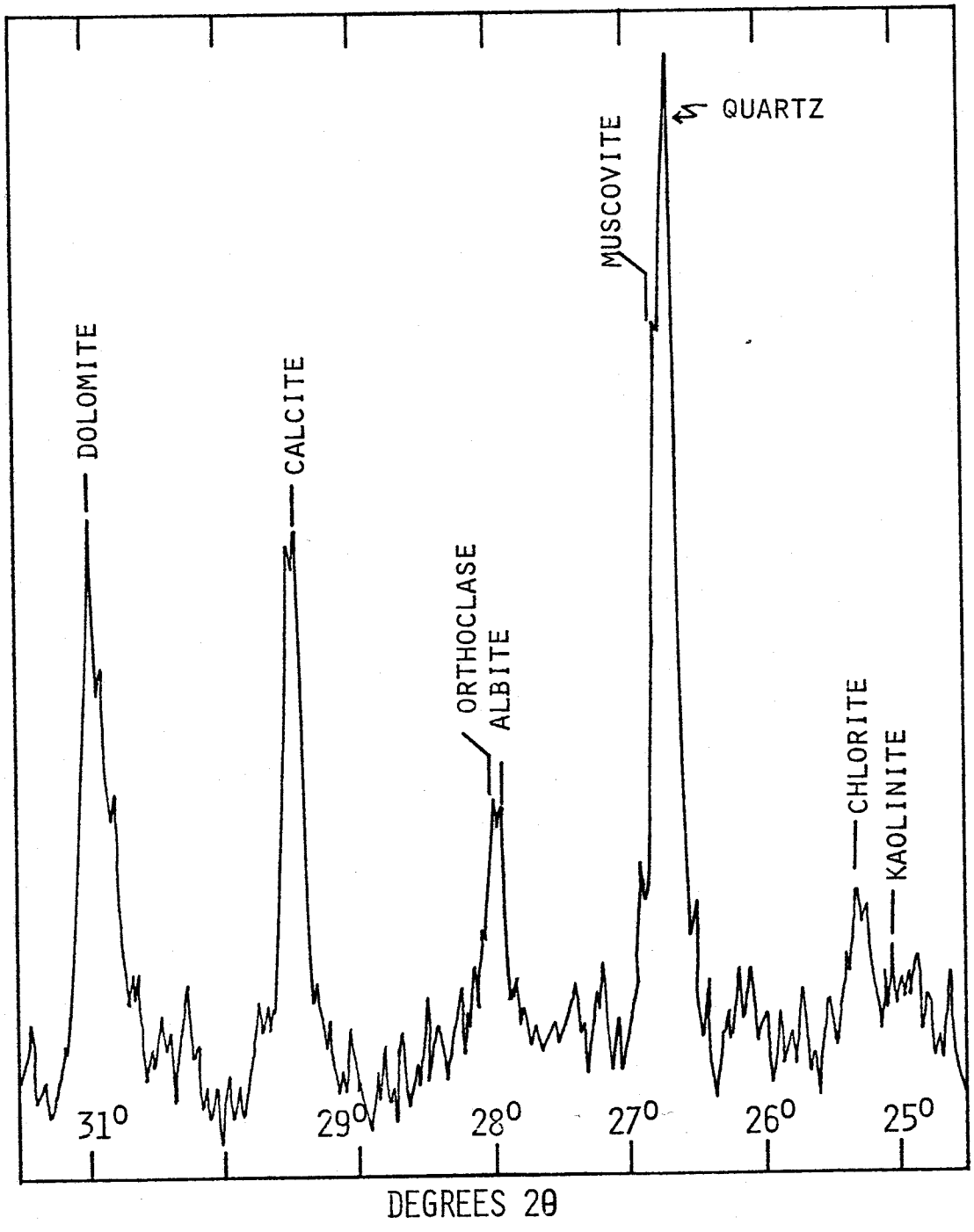
DOLOMITE
CALCITE
ORTHOCLASE
ALBITE
MUSCOVITE
QUARTZ
CHLORITE
KAOLINITE
31°
29°
28°
27°
26°
25°
DEGREES 2θ

predominant mineralogy found in the first, second, third, fifth and sixth turbidites and the microcline-lacking mineralogy of the fourth turbidite. All x-ray diffraction scans displayed were run at the same instrumental settings. No quantitative x-ray mineralogy was attempted and, where the identification of certain minerals was uncertain, a question mark is indicated.

A typical scan of a pelagic sample (from core 149, the pelagic control core) is reproduced in Figure 26. In addition to the minerals identified in Figure 26 (quartz, muscovite, microcline, calcite, dolomite, and chlorite), ferririte, kaolinite, orthoclase feldspar, and albite feldspar were found to be present in other sections of the scan. Although the mineralogy of pelagics is very similar, the character and intensity of most component minerals are strikingly different (e.g. compare quartz, calcite, and dolomite of Figure 26 with the same minerals of Figure 25).

A representative x-ray diffraction scan from a Gorringe Bank event of core 153 (Figure 27) has the identical mineralogy of most of the other turbidites, but the intensities of the components are much higher. This may be due to the relative absence of continentally-derived organic material in the Gorringe Bank events; with little organic material, the intensity of mineral peaks is enhanced (see Figures 30 and 31).

Sections of the core which were of dubious nature (either pelagic or turbidite) were analyzed by means of

FIGURE 26. Part of a typical x-ray scan showing mineralogy of pelagic clay.

The sample is from the pelagic control core section west of the abyssal plain in the abyssal hills (core 149, 27-30 cm, LA, 30 min.).

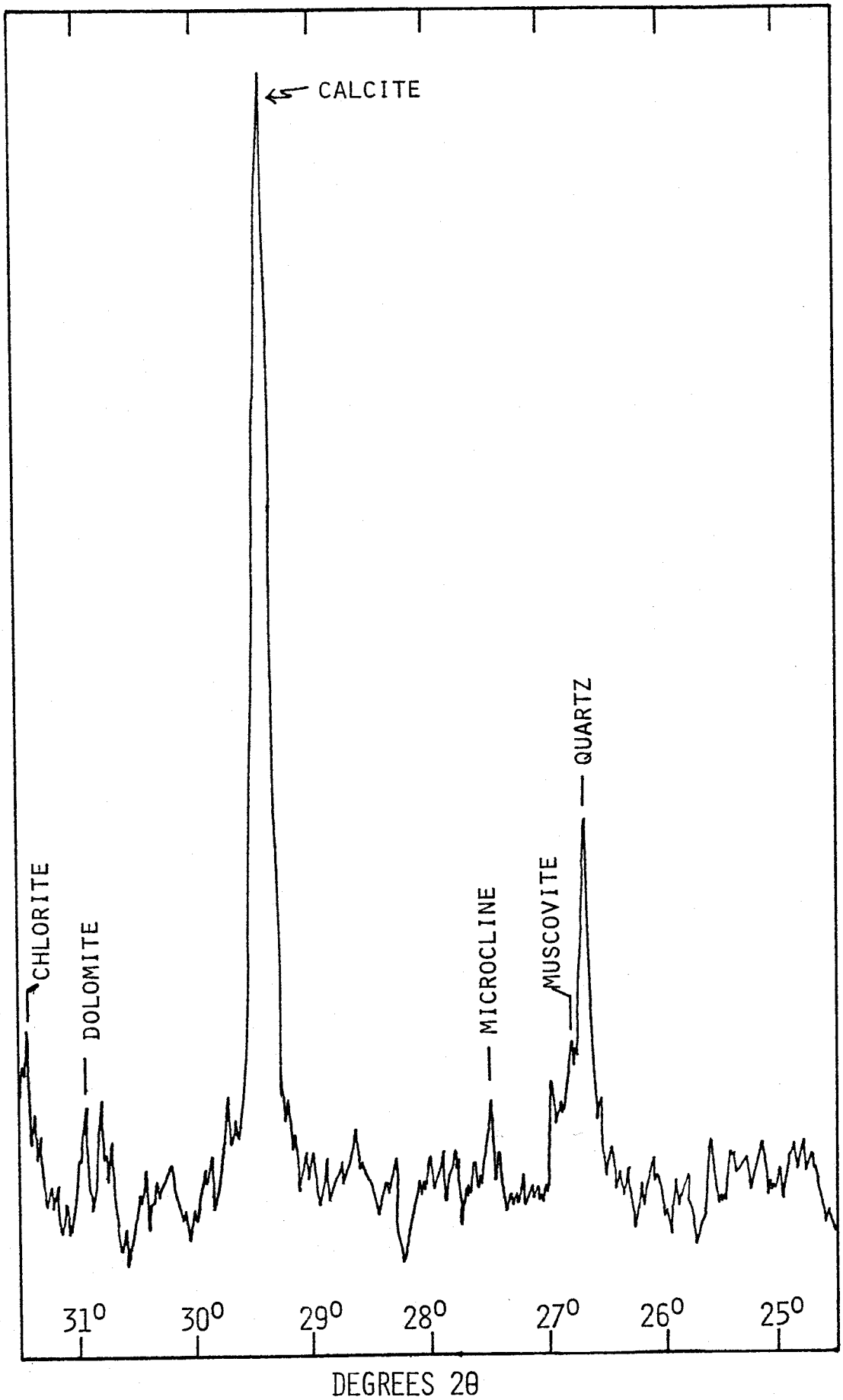
CALCITE
CHLORITE
DOLOMITE
MICROCLINE
MUSCOVITE
QUARTZ
31°
30°
29°
28°
27°
26°
25°
DEGREES 2θ

FIGURE 27. Part of a typical x-ray scan showing mineralogy of Gorringe Bank local events clay.

The sample is from a Gorringe Bank local turbidite event shed off of the Gorringe Bank (core 153, 132-134 cm, LA, 5 min.).

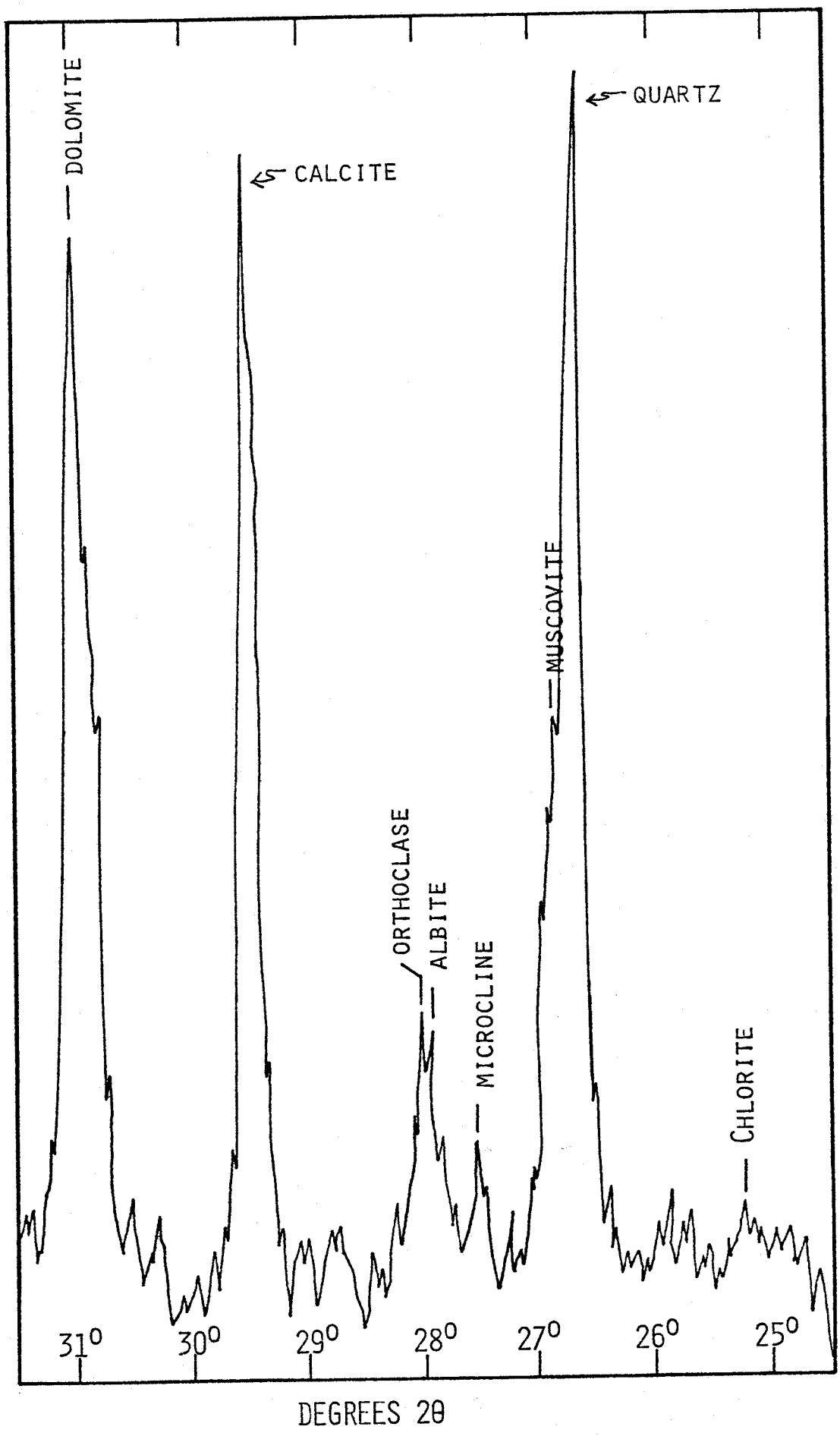
DOLOMITE
CALCITE
QUARTZ
MUSCOVITE
ORTHOCLASE
ALBITE
MICROCLINE
CHLORITE
31°
30°
29°
28°
27°
26°
25°
DEGREES 2θ

x-ray mineralogy to determine their origin. Most were found to be a mixture of pelagic and turbidite clay brought about by worm burrowing. Figure 28 displays the mineralogy of such a zone of mixing below the third turbidite. This horizon can be easily identified in a visual manner as being the burrowed pelite interval (mixed with turbidite clay) on the top of the fourth turbidite (see Figure 9).

In summary, x-ray mineralogy of the clay and mud sections of the cores shows that the visual correlation can be supported by x-ray mineralogy, but the general trend is one of mineralogic uniformity.

Petrography of Turbidite Sandy Bases

Very fine sand (3-4 Ø) from the turbidite bases was seperated into heavy and light mineral fractions according to a format outlined in the Methods Chapter. Abundant micro-scratches were observed on the face of grains, suggesting a violent episode of transportation in the recent history of the grains, quite possibly during aeolian transport or perhaps turbidity flow. In addition, black rod-like grains larger than 4 Ø grain size were collected in sieving the upper three horizons of the third turbidite (tops, middles, and two-thirds). These pyrite rods (less than 5 mm in length and less than 0.5 mm in diameter) were also found to be present in the fourth and fifth turbidites, and therefore could not be used as a mineralogic marker (Figure 29). X-ray floresence and x-ray diffraction methods were used to determine that the composition

FIGURE 28. Part of a typical x-ray scan showing mineralogy of the burrowed top of the fourth turbidite, a visually correlatable horizon in each of the abyssal plain cores. Bioturbation has resulted in a mixture of pelagic and turbidite clay mineralogy.

The sample is from the burrowed top of the fourth turbidite (core 148, 287-290 cm, LA, 5 min.).

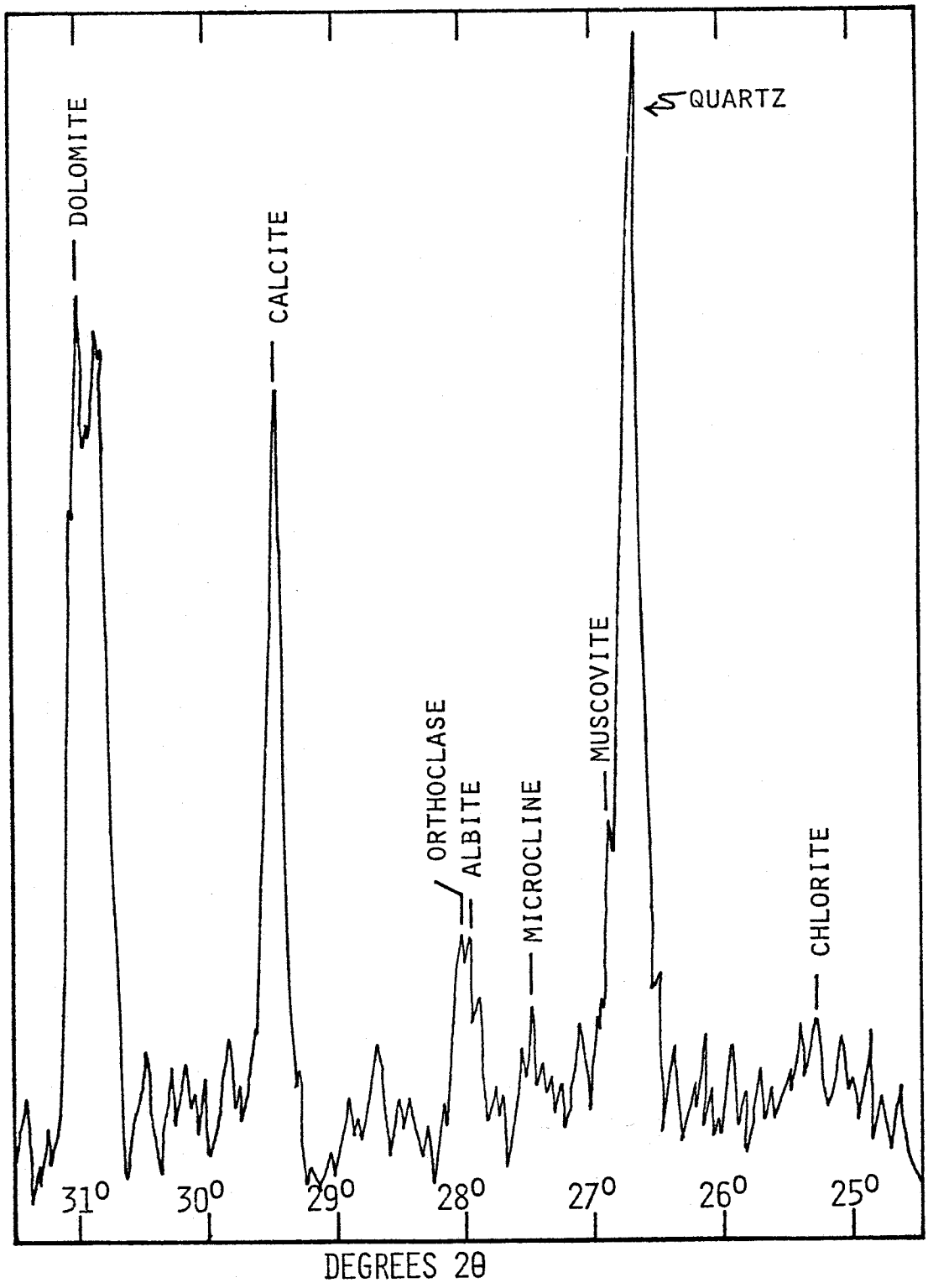
DOLOMITE
CALCITE
QUARTZ
ORTHOCLASE
ALBITE
MICROCLINE
MUSCOVITE
CHLORITE
31°
30°
29°
28°
27°
26°
25°
DEGREES 2θ

FIGURE 29. Locations of pyrite rods (framboids) found in the Horseshoe Abyssal Plain turbidites. Stars (☆) show areas where framboids are found; dash line indicates inferred framboid location.

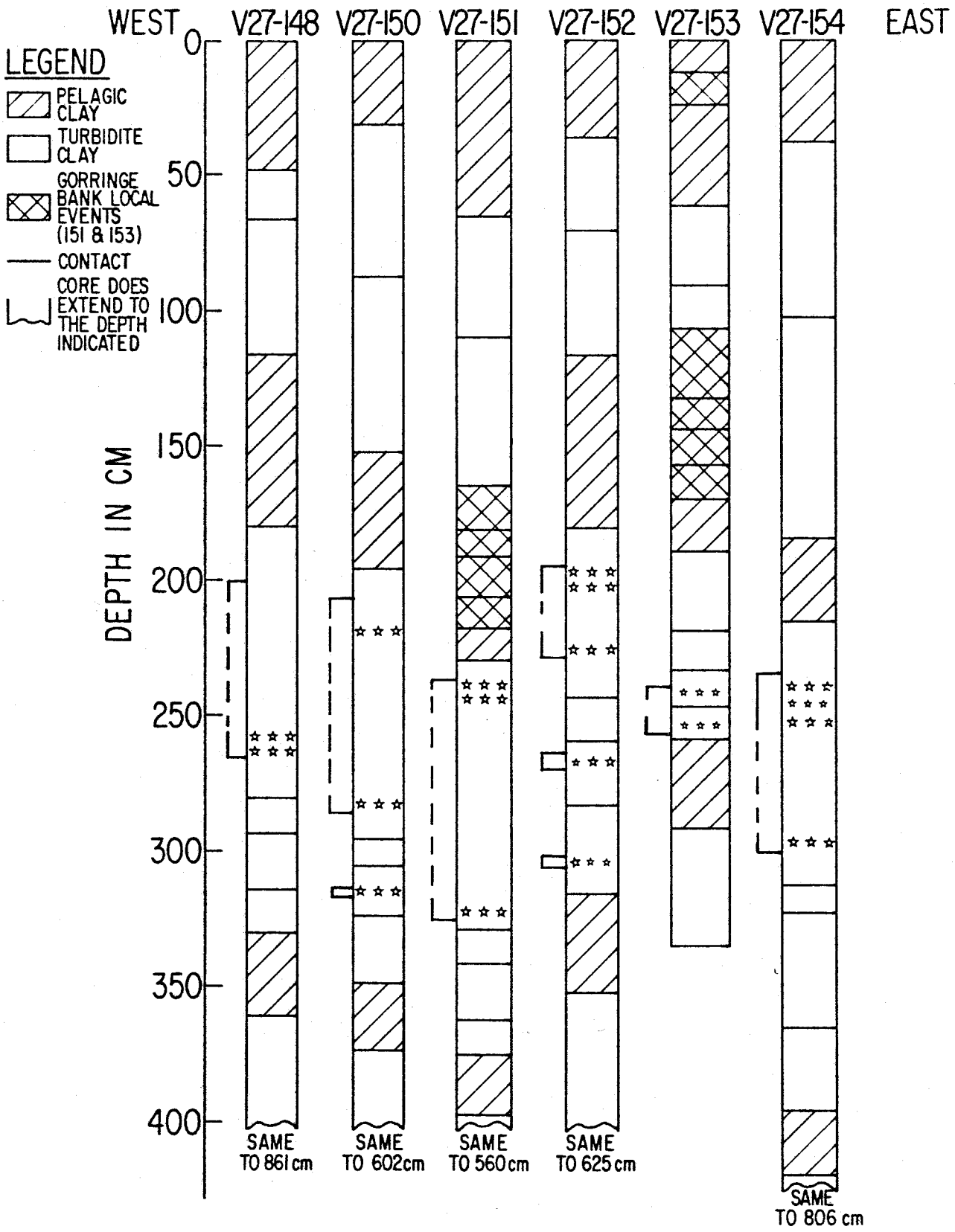
WEST
EAST
V27-148
V27-150
V27-151
V27-152
V27-153
V27-154
LEGEND
PELAGIC CLAY
TURBIDITE CLAY
GORRINGE BANK LOCAL EVENTS (151 & 153)
CONTACT
CORE DOES EXTEND TO THE DEPTH INDICATED
DEPTH IN CM
0
50
100
150
200
250
300
350
400
SAME TO 861 cm
SAME TO 602cm
SAME TO 560 cm
SAME TO 625 cm
SAME TO 806 cm

of these very dense rods was FeS_2 (Pyrite). Berner (1964a, b, c, 1969,1970,and 1971) has described these dense pyrite rods (called framboids) as authigenic growths in organic-rich marine sediments from various environments. The sulfur is thought to result from the decay of organic material with age and the iron is thought to come primarily from iron-bearing materials which have been deposited. Thus, the horizon in which these framboids are found in the Horseshoe Abyssal Plain is indicative of a zone where geochemical conditions have existed over time which have been favorable to the growth of these pyrite rods around organic cores. There is no evidence to suggest that these pyrite framboids are detrital in origin.

Figure 30 shows the mineralogy of the sandy bases light fraction (form 202 to 958 grain counts) broken down into two groups: 1) $CaCO_3$ tests and 2) all other minerals. The average $CaCO_3$ tests' contents for the first three turbidites are: first 67.0 $\pm$ 11.1%, second 71.0 $\pm$ 10.3%, and third 54.1 $\pm$ 6.9%. These data indicate the dominance of foraminifera in the sediment of the sandy bases. As with grain size, the standard deviation decreases from the first, through the second, to the third turbidite. For comparison, four different turbidites from the Gorringe Bank (numbered consecutively down from the top in cores 151 and 153) were also plotted in Figure 30 and display a greater percentage of $CaCO_3$ tests (79.4 $\pm$ 8.2%). The Gorringe Bank local events lack typical assemblages of continentally-derived material and their mineralogy is predominated by planktonic foraminifera. Of the three continentally-

FIGURE 30. Mineralogy of the sandy bases of the first three turbidites and the Gorringe Bank turbidites broken down into $CaCO_3$ tests and non-$CaCO_3$ tests. The dotted line indicates the average $CaCO_3$ for each group.

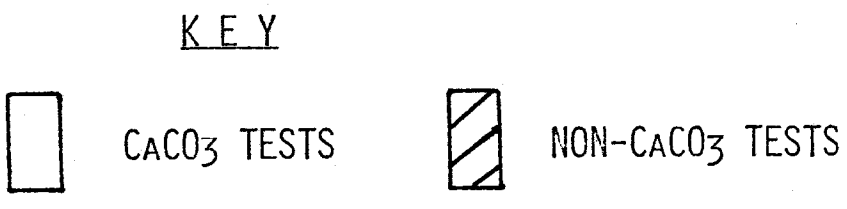

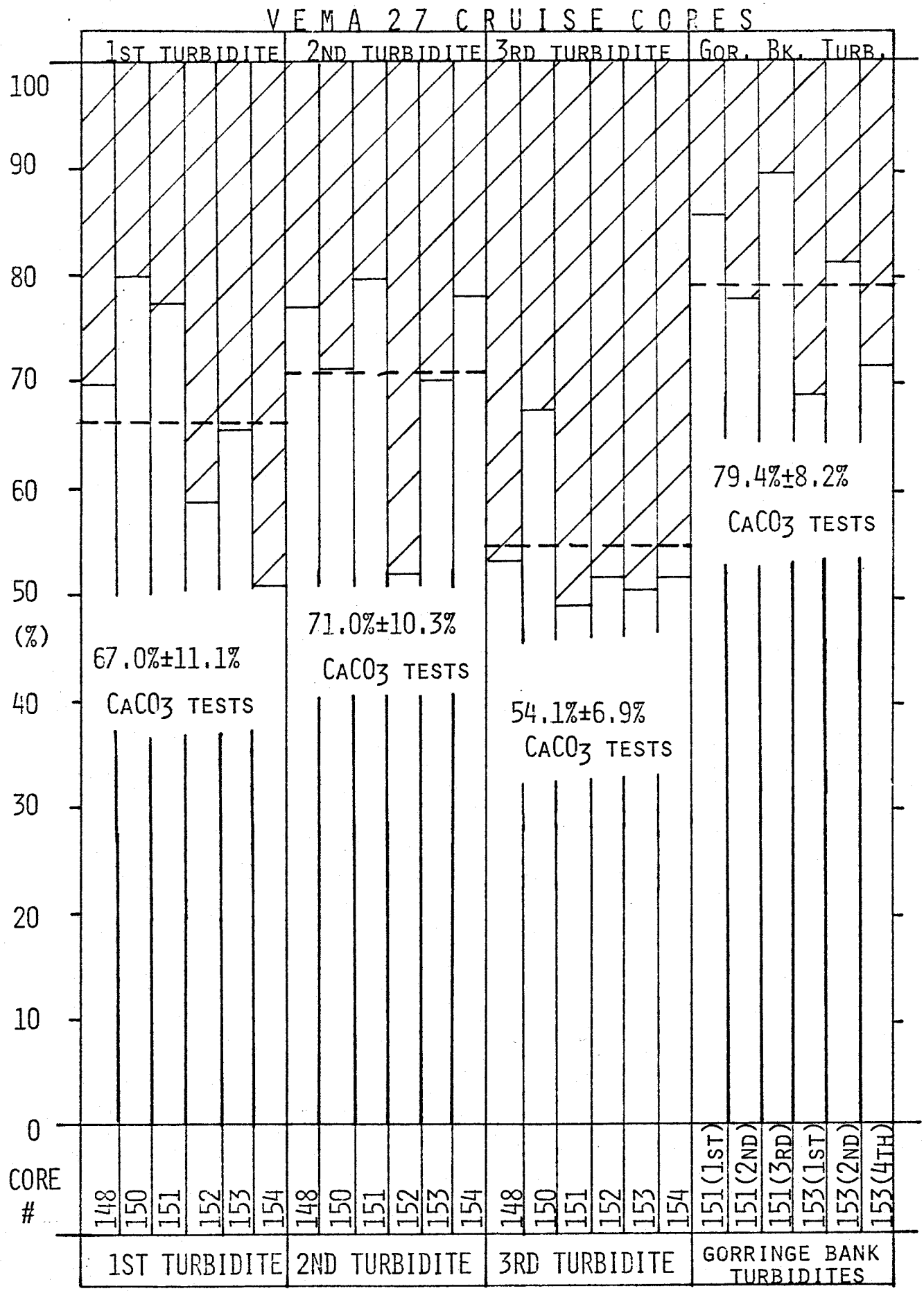
VEMA 27 CRUISE CORES
1ST TURBIDITE
2ND TURBIDITE
3RD TURBIDITE
GOR. BK. TURB.
100
90
80
70
60
50
(%)
40
30
20
10
0
67.0%±11.1%
CaCO3 TESTS
71.0%±10.3%
CaCO3 TESTS
54.1%±6.9%
CaCO3 TESTS
79.4%±8.2%
CaCO3 TESTS
CORE #
148
150
151
152
153
154
148
150
151
152
153
154
148
150
151
152
153
154
151(1ST)
151(2ND)
151(3RD)
153(1ST)
153(2ND)
153(4TH)
1ST TURBIDITE
2ND TURBIDITE
3RD TURBIDITE
GORRINGE BANK TURBIDITES

derived turbidites, the third contains the highest percentage of fragments of shallow-water fauna, with fewer in the first turbidite and almost none in the second turbidite. The presence of abundant foraminifera below the carbonate compensation depth suggests that the sandy bases of the turbidites of the Horseshoe Abyssal Plain have been rapidly deposited, buried, and protected from the corrosive bottom waters. In a like manner, other shallow-water fauna (mostly pelecypods and corals) present in the turbidite bases are thought to have been dispalced and redeposited. One might infer that the first and third turbidites originated in an area of the continental shelf which was relatively shallow and contained coarse grain sizes, predominantly $CaCO_3$ tests. On the other hand, the second turbidite may have originated in an area of the continental slope/rise which was not only deeper, but also contained much finer mean and maximum grain sizes.

Figure 31 displays the mineralogy of the light fraction of non-$CaCO_3$ tests expanded to 100% from Figure 30 (all counts consist of 100 non-$CaCO_3$-test grains). Several distinctive characteristics of the top three turbidites and the Gorringe Bank turbidites are apparent. From the first turbidite through the third (left to right in Figure 31), detrital limestone decreases. As expected, there is no detrital limestone in the Gorringe Bank turbidites. Although quartz content is nearly a constant 50% in the third turbidite, the amount of quartz in all the other turbidites is highly variable, with averages much less. The large percentages of quartz in cores 151 and

FIGURE 31. Mineralogy of the non-$CaCO_3$ fraction of Figure 30, expanded to 100% and based on counts of 100 non-$CaCO_3$ test grains. The arrangement of the three turbidites and the Gorringe Bank turbidites are identical to that of Figure 30.

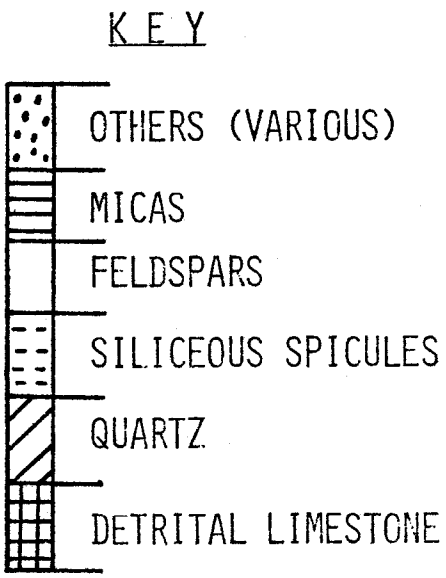

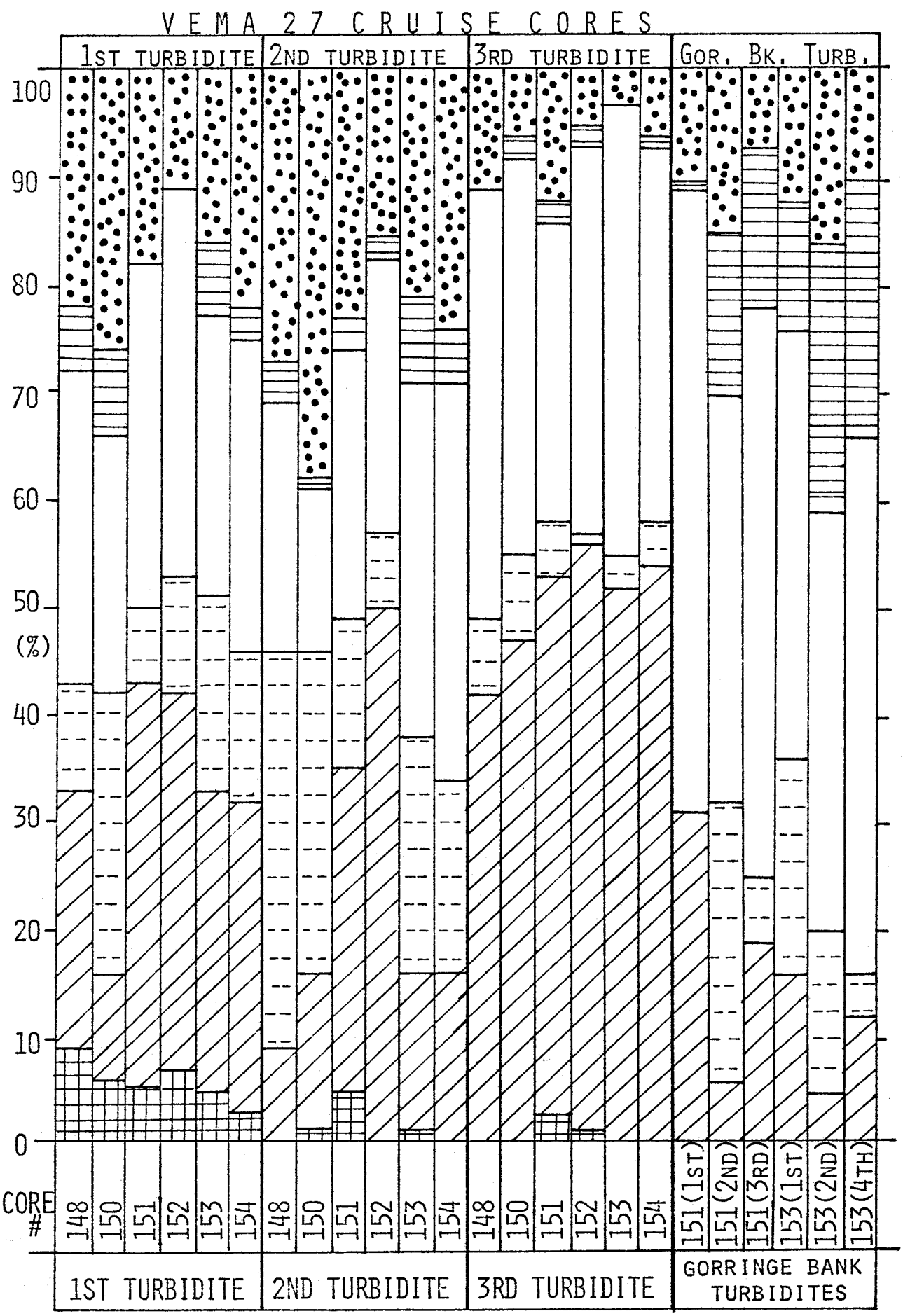
VEMA 27 CRUISE CORES
1ST TURBIDITE
2ND TURBIDITE
3RD TURBIDITE
GOR. BK. TURB.
100
90
80
70
60
50
(%)
40
30
20
10
0
CORE #
148
150
151
152
153
154
148
150
151
152
153
154
148
150
151
152
153
154
151(1ST)
151(2ND)
151(3RD)
153(1ST)
153(2ND)
153(4TH)
1ST TURBIDITE
2ND TURBIDITE
3RD TURBIDITE
GORRINGE BANK TURBIDITES

152 in all main turbidites suggest a preferential deposition of quartz at these core locations. This may be due to inferred lower velocities, resulting in enhanced deposition of the coarser grained particles, predominantly quartz. Siliceous spicules are, most likely, predominantly from skeletons of sponges. The second turbidite contains the highest percentage of these siliceous spicules while the third turbidite contains the lowest percentage. The first turbidite and Gorringe Bank turbidites contain intermediate amounts. The large percentage of siliceous spicules in the second turbidite may largely be a function of the paucity of other grains in the 3-4 Ø size class (recall that the first turbidite contains 19 times more sand than the second turbidite and that the third contains 72 times more sand than the second). The opposite reasoning would apply to the low percentage of siliceous spicules in the sandy third turbidite bases. The third turbidite predominantly contains short, three-pronged siliceous spicules, whereas, the first and second turbidites contain long and narrow ones, often with an end which was attached to a sponge. The Gorringe Bank turbidites contain short and stubby siliceous spicules different from others seen. Differences in feldspar content are not marked, except that the Gorringe Bank events have larger amounts. Although percentages of micas are highly variable, it can be generalized that the third turbidite has almost none and the Gorringe Bank turbidites have large amounts. The large amounts of feldspar and mica (chlorite) in the Gorringe Bank turbidites suggest an oceanic igneous source area for

these sediments. The "other" category consists of organic material (plant remains, roots, etc.), mineral aggregates, and opaques for the first and second turbidites. The third turbidite contains organic material and mineral aggregates with essentially no opaques, which distinguishes it from the others. The Gorringe Bank events, on the other hand, contain only mineral aggregates and opaques with essentially no organic material. The lack of continentally-derived organic material further substantiates the individual character of the Gorringe Bank turbidites.

In summary, the results of the "light" mineralogy of sandy bases are compatible with the visual correlation and establish the individual character of the Gorringe Bank turbidites (a similar light mineralogy was found for Deep-Sea Drilling Project Site 120 on the northern side of the Gorringe Bank studied by Honnorez and Fox, 1973; and Gavasci and others, 1973). Further substantiation of these trends follows in the description of the heavy minerals.

Heavy Minerals.

Because of contamination with light minerals, low natural abundances and fine grain sizes of heavy minerals, grain counts were not made for the heavy mineral fractions of the first three turbidites of the Gorringe Bank events. However, a qualitative and semiquantitative analysis was made on each heavy mineral slide corresponding to the light mineral slides discussed above.

Each of the first three turbidites contained a complex and diverse heavy minerel suite, each indicative of multi-component continental provenance. Calcite tests, organic material, and siliceous spicules were found in the same relative abundances and types as in the light mineral fractions of the first three turbidites. Common heavy minerals present were chlorite, zircon, garnet, tourmaline, pyroxene, amphibole, and various opaques. The first and third turbidites commonly contained a reddish-brown opaque, thought to be hematite, whereas, the second turbidite contained no such opaque mineral. Instead, the second turbidite commonly contained opaques of various other types. Shallow-water fauna (e.g. pelecypods and corals) were most easily identifiable in the base of the third turbidite.

Heavy mineral suites from the four Gorringe Bank turbidites were distinctly different from the widely-varied continental suites of the first three turbidites. Besides ubiquitous basaltic glass, each turbidite commonly contained chlorite, a chlorite-like mineral, epidote, felty growths of fibrous actinolite, and various opaques (mostly iron oxides). Pyroxenes and other amphiboles were less frequently identified. Basaltic glass shards, presumably from surface basalt pillows, could have been easily eroded by a cascading turbidity current and incorporated into the sandy bases of these local Gorringe Bank events. Petrography of the northern Gorringe Bank "basement" has been outlined by Honnorez and Fox (1973) based on data from D.S.D.P. Site 120.

Heavy minerals found in these metagabbros were a tan pyroxene (unidentifiable due to deformation of grains), felty growths of fibrous actinolite surrounding pyroxene, chlorite, and a chlorite-like mineral. Relict crystal outlines suggest that olivine has been replaced by chlorite. Another study, this one in the crustal area of the Gorringe Bank (Gavasci and others, 1973), found quartz and epidote associated with primary mafic igneous minerals, in addition to the minerals found in the metagabbros of Site 120.

In summary, the heavy mineral suites of the first three turbidites are very similar; however, the widely diverse, continentally-derived suites of these turbidites contrast sharply with the Gorringe Bank turbidites suite, consisting of charactersitic oceanic meta-igneous minerals known to exist in rocks of the Gorringe Bank.

CHAPTER V.

CONCLUSIONS

The following important conclusions and speculations are drawn from the data:

1) Distinct, continuous, parallel subbottom reflectors and zones of acoustically transparent sediment which are recorded throughout the Horseshoe Abyssal Plain can be strongly correlated with the *in situ* strata by piston coring. Furthermore, lateral stratigraphic correlations for six major turbidite events can be confidently made for the entire abyssal plain over an east-west distance of 300-400 km.

2) Detailed studies of the thickness variations in the upper three turbidites indicate that the third turbidite has the largest volume of the three. The first turbidite is less than half the size and the second is about 2/3 the size of the third. In addition to these volumetric differences, great mineralogic differences exist, which strongly suggest differences of turbidity current origin, both in time and space. The third and first turbidites probably were initiated on the continental shelf/slope break, whereas, second may have initiated further downslope.

3) Analysis of grain size data on the top three turbidite bases (where the only significant differences are found) leads to the suggestion that different velocities of flow may have existed between the three turbidites. However, variation in the volume of the three turbidites and the size

of the largest grains being transported causes these speculations to be tenuous. If erosive ability of the turbidite is a measure of its velocity, then the three turbidites would be arranged in the following order of increasing velocity: second, first, and third.

4) Previous widely-accepted notions concerning the proximal-distal character of modern turbidite deposits are valid on a regional scale, from supplying canyon to abyssal plain to the western abyssal hills. However, variations in character within the Horseshoe Abyssal Plain proper appear to be caused by local bottom topography rather than by distance from the mouth of the supplying canyon or distance from the inferred main flow avenue. All three turbidites are considered "distal", with the third least so, the first intermediate, and the second most distal. No proximal-distal variation of individual flows can be supported by the data.

5) The westward-thickening trend of the turbidites may be due to a decelleration of the turbidity currents and subsequent deposition of more material. Also, it is generally true that more sand has been deposited in areas where the turbidity current was climbing upslope (e.g. cores 153 and 148). Conversely, it appears that less sand has been deposited in areas of negative relief (e.g. core 154).

6) Lateral variations in grain size and sorting do not follow simple, regular patterns down the length of the abyssal plain. Homogeneity is the rule, except for general variations observed at core 153 (terrace) and core 154 (sink hole).

7) Local turbidite events exist in the northern abyssal plain (cores 151 and 153), which contain greater abundances of $CaCO_3$ tests as well as a suite of oceanic meta-igneous heavy minerals. These events are thought to have originated on the Gorringe Bank to the north.

8) Finally, is is felt that additional piston cores from the central areas of the Horseshoe Abyssal Plain and additional detailed echo sounding would provide data to further substantiate the ideas of this study, which have only begun to demonstrate the fallicies of the ruling turbidite paradigm.

BIBLIOGRAPHY

ANDERSON, A., AND BJERRUM, 1967, Slides in subaqueous slopes in loose sand and silt: in A. F. Richards, ed., Marine Geotechnique, University of Illinois Press, Urbana, p. 221-239.

BARAZANGI, M., AND DORMAN, J., 1969, World seismicity maps compiled from ESSA data, 1961-1967: Bull. Seismological Society of America, v. 59, plate 3.

BORNHOLD, B. D., AND PILKEY, O. H., 1971, Bioclastic turbidite sedimentation in the Columbus Basin, Bahamas, v. 82, p. 1341-1354.

BOUMA, A. H., 1962, Sedimentology of Some Flysch Deposits, Elsevier, Amsterdam and New York, 168 pp.

_____ AND HOLLISTER, C. D., 1973, Deep ocean basin sedimentation: in Turbidites and Deep-Water Sedimentation, S.E.P.M. Short Course, Pacific Section S.E.P.M., Los Angeles, p. 79-118.

CARTA GEOLOGICA DE PORTUGAL, 1972, Servicos Geologicas De Portugal.

CARTA GEOLOGICA DO QUATERNARIO DE PORTUGAL, 1969, Servicos Geologicas De Portugal.

CARVER, R. E., 1971, Heavy mineral seperation: in R. E. Carver, ed. Procedures in Sedimentary Petrology, Wiley-Interscience, p. 427-452.

CONOLLY, J. R., AND EWING, M., 1967, Sedimentation in the Puerto Rico Trench: Journal of Sed. Pet., v. 37, p. 44-59.

DALY, R. A., 1936, Origin of submarine canyons: Am. Jour. Sci., v. 31, p. 401-420.

DAMUTH, J. E., 1975, Echo character of the Western Equatorial Atlantic floor and its relationship to the dispersal and distribution of terrigenous sediments: Marine Geology, v. 18, p. 17-45.

DAVIDSON, C., AND KEEN, M. J., 1963, Size analyses of turbidity current sediment: Nature, v. 197, p. 372-373.

DEWEY, J. F., PITMAN, W. C. III, RYAN, W. B. F., AND BONNIN, J., 1973, Plate tectonics and the evolution of the Alpine System: G. S. A. Bull., v. 54, p. 3137-3180.

DILL, R. F., 1969, Earthquake effects on fill of Scripps submarine canyon: G.S.A. Bull., v. 80, p. 321-328.

DOTT, R. H., JR., 1963, Dynamics of subaqueous gravity depositional processes: A.A.P.G. Bull., v. 47, p. 104-128.

DUPLAIX, M. S., NESTEROFF, W. D., AND HEEZEN, B. C., 1965, Mineralogie comparée des sediments du Tage (Portugal) et de quelques sables profonds de la plaine abyssale correspondante: Deep-Sea Research, v. 12, p. 211-217.

ELMORE, R. D., 1976, Extensive horizontal continuity of a single turbidite, Hatteras Abyssal Plain: G.S.A., Abstracts with Programs, v. 8, p. 167.

EMBLEY, R. W., EWING, J. I., AND EWING, M., 1970, the Vidal deep-sea channel and its relationship to the Demerara and Barracuda Abyssal Plains: Deep-Sea Research, v. 17, p. 539-552.

EMBLEY, R. W., AND BRYAN, G., 1976 preprint, Lithologic and topographic influences on bottom amd subbottom reflectivity in deep ocean environments: Marine Geology.

EMERY, K. O., 1969, The continental shelves: in The Ocean, Scientific American Series, W. H. Freeman, San Francisco, p. 39-52.

ERICSON, D. B., EWING, M, AND HEEZEN, B. C., 1952, Turbidity currents and sediments in the North Atlantic: A.A.P.G. Bull., v. 36, p. 489-511.

EWING, M., RYAN, W. B. F., NEEDHAM, H. D., AND SCHREIBER, B. C., 1970, Turbidity currents on the ocean bottom: United States Civil Engineering Laboratory Report # CR 70.018, 156 pp.

FOLK, R. L., 1954, The distinction between grain size and mineral composition in sedimentary rock nomenclature: Journal of Geology, v. 62, p. 344-359.

_____, 1968, Petrology of Sedimentary Rocks: Hemphills, Drawer M. University Station, Austin, Texas, 170 pp.

_____, AND WARD, W. C., 1957, Brazos River bar: a study of the significance of grain size parameters: Jour. Sed. Pet., v. 27, p. 3-26.

FRANCIS, T. J. G., 1971, Effect of earthquakes on deep-sea sediments: Nature, v. 233, p. 48-102.

FRUTH, L. S., JR., 1965, The 1929 Grand Banks turbidite and the sediments of the Sohm Abyssal Plain: M. S. Thesis, Department of Geology, Colombia University, N. Y., N. Y., 258pp.

GAVASCI, A. T., FOX, P. J., AND RYAN, W. B. F., 1973, Petrography of rocks from the crestal area of the Gorringe Bank: D.S.D.P. v. XIII., pt. 2, p. 749-752.

GIBBS, R. J., 1968, Clay mineral mounting techniques for x-ray diffraction analysis: A discussion: Jour. Sed. Pet., v. 38, p. 242-244.

GORSLINE, D. S., AND EMERY, K. O., 1959, Turbidity current deposits in San Pedro and Santa Monica Basins off Southern California: G.S.A. Bull., v. 70, p. 279-290.

HARMS, J. C. AND FAHNESTOCK, R. K., 1965, Stratification, bed forms, and flow phenomena (with an example from the Rio Grande): in G. V. Middleton, ed., Primary Sedimentary Structures and Their Hydrodynamic Interpretation: S.E.P.M. Special Publication 12, p. 84-115.

HEEZEN, B. C., 1956, The origin of submarine canyons: Scientific American, Aug., 1956, p. 36-41.

_____, 1959, Note on progress in geophysics, dynamic processes of abyssal sedimentation: erosion, transportation and redeposition on the deep-sea floor: Jour. Roy. Astr. Soc., v. 2, p. 142-163.

_____, 1960, Turbidity currents: McGraw-Hill encyclopedia of Science and Technology, p. 146-147.

_____, AND EWING, M. 1952, Turbidity currents, submarine slumps, and the 1929 Grand Banks earthquake: Am. Jour. Sci., v. 25, p. 849-873.

HEEZEN, B. C., AND DRAKE, C. L., 1963, Gravity tectonics, turbidity currents and geosynclinal accumulations in the continental margins of eastern North America: Lamont contribution # 673.

_____, 1964, Grand Banks Slump: A.A.P.G. Bull., v. 48, p. 221-233.

HEEZEN, B. C., AND HOLLISTER, C., 1971, The Face of the Deep: Oxford University Press, New York, 659 pp.

HERSEY, J. B., 1965, Sediment ponding in the deep sea: G.S.A. Bull., v. 76, p. 1251-1260.

HESSE, R. 1974, Long-distance continuity of turbidites: possible evidence for an Early Cretaceous trench-abyssal plain in the East Alps: G.S.A. Bull., v. 85, p. 859-870.

_____, 1975, Turbiditic and non-turbiditic mudstone of Cretaceous flysch sections of the East Alps and other basins: Sedimentology, v. 22, p. 387-416.

HOLLISTER, C. D., AND HEEZEN, B. C., 1964, Primary structures of Atlantic deep-sea turbidites: G. S.A. Special Paper 76, p. 81.

HONNOREZ,J., AND FOX, P. J., 1973, Petrography of the Gorringe Bank "Basement": D.S.D.P. v. XIII., pt. 2, p. 747-749.

HORN, D. R., EWING, M., DELACH, S., AND HORN, B. M., 1971a, Turbidites of the Northeast Pacific: Sedimentology, v. 11, p. 55-69.

HORN, D. R., EWING, M., DELACH, S. AND HORN, B. M., 1971b, Turbidites of the Hatteras and Sohm Abyssal Plains, Western North Atlantic: Marine Geology., v. 11, p. 287-323.

HORN, D. R., EWING, J. I., AND EWING, M., 1972, Graded bed sequences emplaced by turbidity currents north of 20° north in the Pacific, Atlantic, and Mediterranean: Sedimentology, v. 18, p. 247-275.

HUBERT, J. F., 1971, Analysis of heavy mineral assemblages: in R. E. Carver, ed. Procedures in Sedimentary Petrology, Wiley-Interscience, p. 453-478.

IRELAND, H. A., 1971, Insoluble residues: in R. E. Carver, ed., Procedures in Sedimentary Petrology, Wiley-Interscience, New York, p. 479-498.

KRAUSE, D. C., AND WATKINS, N. D., 1970, North Atlantic crustal genesis in the vicinity of the Azores: Geophysical Journal. Royal Astr. Soc., v. 19, p. 261-283.

KUELEGAN, G. H. 1957, Thirteenth progress report on model laws for density currents. An experimental study of the motion of saline water from locks into fresh water channels: Unites States National Bureau of Standards, Report # 5168.

KUENEN, PH. H.,AND MIGLIORNI, C. I., 1950, Turbidity currents as a cause of graded bedding: Jour. Geol., v. 58, p. 91-127.

KUENEN, PH. H., 1966, Experimental turbidite lamination in a circular flume: Jour. Geol., v. 74, p. 523-545.

LEPICHON, X., BONNIN, J., AND PAUTOT, G., 1970, Proceedings of the Upper Mantle Symposium: Flagstaff, Arizona.

LEPICHON, X., AUZENDE, J. M., PAUTOT, G., MONTI,S., AND FRANCHETEAU, J., 1971, Deep-sea photographs of an active fault zone near Gibraltar Straits: Nature, v. 230, p. 110-111.

MCLAREN, E. H., 1976, personal communication, Dept of Chemistry, SUNY-Albany, Albany, N. Y.

MIDDLETON, G. V., 1966a, Experiments on density and turbidity currents: I. Motion of the head: Can. Jour. Earth Sci., v. 3, p. 523-546.

_____, 1966b, Experiments on density and turbidity currents: II. Uniform flow of density currents: Can. Jour. Earth Sci., v. 3, p. 627-637.

_____, 1967, Experiments on density and turbidity currents: III. Deposition of sediment: Can. Jour. Earth Sci., v. 4, p. 475-505.

_____, AND HAMPTON, M. A., 1973, Sediment gravity flows: mechanics of flow and deposition: in Turbidites and Deep-Water Sedimentation, S.E.P.M. Short Course, Pacific Section S.E.P.M., Los Angeles, p. 1-38.

MOORE, D. G., 1961, Submarine slumps: Jour. Sed. Pet., v. 31, p. 343-347.

MORGENSTERN, N. R., 1967, Submarine slumping and the initiation of turbidity currents: in A. F. Richards, ed., Marine Geotechnique, University of Illinois, Urbana, p. 189-220.

MUTTI, E., AND RICCI-LUCCHI, F., 1974, La signification de certaines unites sequentielles dan les series à turbidites: B.S.G.F., v. 7, p. 577-582.

_____, 1975, Examples of turbidite facies and facies associations from selected formations of the Northern Apennines.

NATLAND, M. L., AND KUENEN, Ph. H., 1951, Sedimentary history of the Ventura Basin, California, and the action of turbidity currents: S.E.P.M. publication no. 2, p. 76-107.

NELSON, C. H., MUTTI, E., AND RICCI-LUCCHI, F. 1975, Comparison of proximal and distal thin-bedded turbidites with current-winnowed deep-sea sands: Extracts of Congress Publications, IXth International Congress of Sedimentology, Theme 5, Nice, p. 317-323.

PAYNE, R., CONOLLY, J. R., AND ABBOTT, W. H., 1972, Turbidite muds within diatom ooze of Antartica: Pleistocene sediment variation defined by closely-spaced piston cores: G.S.A. Bull., v. 83, p. 481-486.

PHLEGER, F. B., 1951, Displaced foraminiferal faunas: in Turbidity currents and the transportation of coarse sediments to deep waters, a symposium, S.E.P.M. Special Pub. no. 2, p. 66-75.

PILKEY, O. H. AND BENNETTS, R. W., 1974, Characteristics of three individual turbidites from the Hispaniola-Caicos Basin: G.S.A. Abstracts with Programs, v. 6, p. 912.

PRATSCH, J. C., 1958, Stratigraphy and tectonics in the Mesozoic of the Algarve (South Portugal): Bech. Geol. Jb., Heft 30, 123 pp., (abstract in English).

PURDY, G. M., 1975, The eastern end of the Azores-Gibraltar plate boundary: Geophysical Jour. Royal Astr. Soc., v. 43, p. 973-1000.

RICCI-LUCCHI, R., 1975, Miocene paleogeography and basin analysis in the Periadriatic Apennines: in Geology of Italy, ed. by C. Squyres, Petroleum Exploration Society of Libya, Tripoli, 111 pp.

RUPKE, N. A., AND STANLEY, D. J., 1974, Distinctive properties of turbiditic and hemipelagic mud layers in the Algero-Baleric Basin, western Mediterranean Sea: Smithsonian contributions to the earth sciences, no. 13, Washington, D. C., 40 pp.

RYAN, W. B. F., WORKUM, F. JR., AND HERSEY, J. B., 1965, Sediments on the Tyrrhenian Abyssal Plain: G.S.A.Bull., v. 76, p. 1261-1282.

SCHLEE, W., 1957, Upland gravels of southern Maryland: G.S.A. Bull., v. 68, p. 1371-1410, (method on p. 1379).

SEIGLIE, G. A., FROELICH, P.N.,AND PILKEY, O. H., 1976, Deep-sea sediments of Navidad Basin: correlation of sand layers: Deep-Sea Research, v. 23, p. 89-101.

SIMONS, D. B., RICHARDSON, E. V., AND ALBERTSON, M. L., 1961, Flume studies using medium sand ((0.45mm): U.S.G.S. Water supply paper no. 1498-A, 76 pp.

TARR, A. C., 1974, World seismicity map: U.S.G.S. and N.O.A.A.

VAN derKNAAP, W. AND EYPE, R., 1968, Some experiments on the genesis of turbidity currents: Sedimentology, v. 11, p. 115-124.

WALKER, R. G., 1967, Turbidite sedimentary structures and their relationship to proximal and distal depositional environments: Jour. Sed. Pet., v. 37, p. 25-43.

_____, AND MUTTI, E. 1973, Turbidite facies and facies associations: in Turbidites and Deep-Water Sedimentation, S.E.P.M. Short Course, Pacific Section S.E.P.M., Los Angeles, p. 119-158.

WENTWORTH, C. K., 1922, A scale of grade and class terms for clastic sediments: Jour Geol., v. 30, p. 377-392.

WOOD, A, AND SMITH, A. J., 1959, The sedimentation and sedimentary history of the Aberystwyth Grits (Upper Llandoverian): Geol. Soc. London Quart. Jour., v. 114, p. 163-195.

APPENDIX I.

REVIEW OF STUDIES ON THE SEDIMENTOLOGY OF TURBIDITY CURRENTS

Modern Abyssal Plain Turbidites

In the last quarter-century, pioneering studies considered the first-order sedimentology of turbidites from present-day abyssal plains. These studies have utilized piston corers to sample sediment and acoustic reflection profilers to determine acoustic layering within abyssal plain sediment accumulations. The earliest investigations of abyssal plain turbidites focused on sediment type, mineralogy, textural properties, primary structures, and displaced faunas (e.g. Phleger, 1951; Natland and Kuenen, 1951; Ericson et. al. 1952; Gorsline and Emery, 1959; Davidson and Keen, 1963; Hubert, 1964; and Hollister and Heezen, 1964). These studies were primarily concerned with elucidating the physical properties of turbidites and made no attempts at bed correlations. More recently, Horn et. al. (1971a,b,1972) have provided a recent synthesis of data concerning general morphology, size, sediment type, and sediment distribution of turbidites from many world abyssal plains. In the northeast Pacific, Horn et. al. (1971a) compiled textural and grain-size analyses from thirty piston cores which allowed the authors to draw a distinction between proximal versus distal facies. Using characteristics of layering, grading, and textural variation, it was noted that these parameters changed as a function of distance from the main avenues of

turbidite flow (the concept of distal versus proximal deposition was first suggested by Wood and Smith, 1959). Proximal facies correspond to areas in which there is a wide range of layer thicknesses, maximum layer thickness, non-grading, truncation of grading, textural reversals, and sand at the base of graded layers. Distal facies farther away from the main channel are areas of episodic addition of silt-through clay-size sediment. With increasing distance from main avenues of flow, the thickness, mean grain size, and proportion of silt to clay decreases. However, due to multiple source areas, a lack of acoustic reflection data, and a lack of mineralogic studies, correlation of individual turbidite layers was not attempted. In addition to the two previous studies, Horn et. al. (1972) have studied sediments from many abyssal plains above 20^{o} North in the Atlantic, Pacific, and the Mediterranean. Preliminary results from cores in the Horseshoe Abyssal Plain (the same cores to be used in the proposed study) suggest that there may be a progressive decrease in grain size of turbidites to the west across the plain; accompanying this trend is a progressive increase to the west in the amount of pelagic sediment, as well as a progressive increase in degree of sorting. It should be pointed out that during the world-wide consideration of turbidite properties, the turbidites of the Horseshoe Abyssal Plain were not studied in detail. Only 15 samples were obtained from the six cores, providing only a general knowledge as to their physical properties. Also, no attempt was made to correlate turbidite beds.

Ryan et. al. (1965) made the first serious attempt at correlating individual turbidite beds throughout an abyssal plain. These workers, in their correlations of turbidites in four cores from the Tyrrhenian Abyssal Plain (located approximately equidistant from Italy, Sicily, and Sardinia), used both piston cores and acoustic reflection data to demonstrate that individual turbidite beds are "remarkably" (a few miles) continuous throughout the abyssal plain. Grain size distributions, bed thicknesses, primary structures (grading, laminations, etc.), and mineralogy were used to identify the origin and transportation routes for two different types of sand. However, there were several limitations in this study with regard to correlations of individual turbidite beds: 1) the topography of the Tyrrhenian Abyssal Plain is very complicated, containing both seamounts and restricted arms; 2) multiple sediment sources occur as the three aforementioned land bodies (Italy, Sardinia, and Sicily) form a triangle around the abyssal plain; 3) correlations on the basis of acoustic horizons must be well supported by the sedimentological data from the cores. In light of the complexities, the four cores used for this study were not sufficient to document clearly the evolution of physical properties within a given turbidite with distance from the source region.

Attempts at detailed correlation in trenches and small basins or troughs have been made (Conally and Ewing, 1967; Pilkey and Bennetts, 1974). Conally and Ewing's

study (1967) of the sedimentation in the Puerto Rico Trench (a long trough with multiple sediment sources) provided apparent 200 km correlations of individual turbidite beds, based on color, texture, and composition. In their study of three individual turbidite beds in the 4100 m-deep Hispaniola-Caicos basin, Pilkey and Bennetts (1974) traced turbidite beds of varying composition for a distance of about 100 km; but both the area of the basin (8100 km^2) and the volume of sediment in the largest flow ($3.3x10^9 m^3$) are small in comparison to the area of even the smallest abyssal plains (Horseshoe Abyssal Plain area is about 15,000 km^2) and in the volume of sediment contained in individual flows. Complicated and poorly understood tectonic movements in both the Puerto Rico Trench and the Hispaniola-Caicos basin add a factor which may confuse the sedimentological study of turbidity current deposits. Other similar studies in abyssal plains or basins include Bornhold and Pilkey's (1971) study of the Columbus Basin, Payne and others' (1972) study of the Wilkes Abyssal Plain off Antarctica, and Seiglie and others' (1976) study of the Navidad Basin.

From data obtained in 65 piston cores in the Hatteras Abyssal Plain, Elmore (1976) has discovered extensive horizontal continuity of a single turbidite covering an area of at least 44,000 km^2 with postulated flow of at least 400 kms. The thickness observed varies from 40 cm. on the western margin to 400 cm. on the eastern margin, with a volume of at least $10^{10} m^3$ which is comparable to the volume

of the turbidite of the Horseshoe Abyssal Plain. This turbidite is characterized by its great thickness as well as abundant (40% in proximal, coarse-grained; 1% in the distal sections) black shells, which are used as a marker for this unit. The scale and scope of this study are very similar to that of the present Horseshoe Abyssal Plain study.

Flysch Models Applicable to the Study of Modern Abyssal Plain Turbidites

If one accepts as a working hypothesis the tenet that flysch deposits with sedimentological characteristics similar to modern turbidites are indeed ancient analogues of existing marine turbidites, then sedimentation models based on flysch deposits can be applied to modern studies. Flysch deposits provide the investigator with the opportunity to study turbidites in outcrop and the results of studies on flysch deposits have helped investigators to better understand the sedimentology of turbidites. Bouma (1962), in his study of Alpine flysch deposits, developed textural zones A, B, C, D, and E, (grading finer A through E) for grading, parallel laminations, current ripples, cross bedding, convolute bedding, and worm burrowing in individual beds. These divisions are indicative of the evolving flow regime of a turbidity current as it moves past a fixed point; they have already been widely applied to modern turbidites and are in common usage. Walker (1967), in his study of "flysch-like" deposits in Maryland, has developed a scale

for the sand fraction of turbidites (Bouma divisions A, B, C) which expresses whether a turbidite deposit was deposited in a proximal facies or a distal facies; he has used a ternary diagram with division A, B, and C at the three apexes and has derived a parameter P_1 which expresses on a scale of 100 the velocity of turbidite flow when deposition of the lowermost turbidite layer occurred (100 represents the highest velocity). Walker used velocity versus size-grade data from Simmons et. al. (1961) and Harms and Fahnestock (1965). In addition, Hesse (1974) studied the Gault flysch formation in the Alps and has used petrologically-defined marker beds to show that individual turbidites can be correlated for a distance of 115 km. This was undertaken in an area of complicated tectonics and faulting and it is impossible to determine the original size of the turbidite basin. The linear shape of the trough as well as various current directions recognized by Hesse suggest that there were several different sources of sediment, thereby complicating the correlation of individual beds. Unfortunately, the complicated structural and deformational setting of most flysch deposits makes it difficult to study the sedimentology of individual turbidites over the entire depositional surface.

Experimental Studies

Kuenen and Migliorni's pioneering paper "Turbidity Currents as a Cause of Graded Bedding" (1950) showed that

most graded deposits observed in nature could not be caused by processes commonly associated with graded beds (such as varves, dust storms, climatic rhythms, storm wave churning, etc.). They suggested that the common grading in flysch deposits was caused by turbidity current deposition. Two types of evidence were enlisted to support their hypothesis: 1) the observation that the wide variety of primary structures observed in graded beds could all arise from the depositional dynamics of turbidity currents and 2) the fact that a turbidity current of density 2 gm/cm^3 has a tremendous capacity to transport sediment (several thousand times the capacity of clear water with a density of 1 gm/cm^3).

In support of this hypothesis, laboratory workers have produced graded beds by means of small turbidity currents. Middleton performed three sets of experiments of density and turbidity currents using a straight flume 500 cm long, 50 cm deep, and 15.4 cm wide: 1) motion of the head of the turbidity current (1966a), 2) uniform flow of density currents (1966b), and 3) deposition of sediment (1967). The most recent study (Middleton, 1967) provides models for characteristic sorting, skewness, and grain-size distribution throughout turbidites, both vertically and laterally. The major limitations on equating these straight flume experiments with naturally occurring turbidites are a lack of volume of sediment and a lack of time required for the turbidite primary structures to develop. In an

effort to avoid these limitations, Kuenen (1966) produced laminations and other primary structures associated with turbidites by means of a circular flume 120 cm across. The limitation of this study is that the stirring of a small volume of water and sediment to simulate turbidity current motion only approximates the probable natural conditions. Van der Knaap and Eype (1968) have taken a fundamentally different approach to the initiation of experimental turbidity currents. Instead of introducing a slurry of sediment into clear water (Middleton, 1966a, 1966b, 1967; Kuenen, 1967), Van der Knaap and Eype rapidly increased pore-water pressure in an existing sediment layer on a slope (the flume tank was 2.75 m long, 0.40 m wide and 0.40 m high). This resulted in slumping of the sediment and the subsequent development of a turbidity current; slumping (perhaps with resulting turbidity currents) is thought to be caused by over-steepening of the depositional slope and/or earthquake activity (Heezen and Ewing, 1952, 1955; Heezen, 1959b; Moore, 1961; Houtz, 1963; Heezen and Drake, 1963, 1964; Anderson and Bjerrum, 1967; Morgenstern, 1967; Van der Knaap and Eype, 1968; Dill, 1969; Ewing and others, 1970; and Francis, 1971).

APPENDIX II.

THE EASTERN END OF THE AZORES-GIBRALTAR PLATE BOUNDARY

Figure 32 shows the general bathymetry in the area of the eastern end of the Azores-Gibraltar plate boundary as well as earthquake events in the area between 1961 and 1967 (Barazangi and Dorman, 1969). There is evidence of movement of Africa and Eurasia toward one another, implying consumption of oceanic lithosphere at the Azores-Gibraltar plate boundary at the rate of 1-1½ cm/yr. However, this area lacks the following general characteristics of oceanic lithospheric consumption: an arcuate trench, island arc volcanism, and deep seismicity. Two characteristics of oceanic subduction zones, which this area does possess, are compressive fault plane solutions, sometimes mixed with some strike-slip solutions, and shallow seismicity.

The Gorringe Ridge, 120 km long and 5 km high, is thought to be an upthrust block of oceanic crust and dense upper mantle material. This is supported by Purdy's (1975) gravity data, which show a large (+ 390 mgal) free-air gravity anomaly, requiring that a large body of dense (greater than 3.0 gm/cc) material lies below Gorringe Ridge. Also, basalts, gabbros, and ultramafics have been dredged from the northern face of the ridge. Figure 33 shows the model for "normal" consumption of oceanic crust, which is not operating in the area in question. Note the various criterion of this model which are not met for the Gorringe Ridge. Figure 34 shows Purdy's (1975) model for consumption

FIGURE 32. General bathymetry in the area of the eastern end of the Azores-Gibraltar plate boundary showing recent earthquake activity (from Purdy, 1975). Earthquakes indicated by (•).

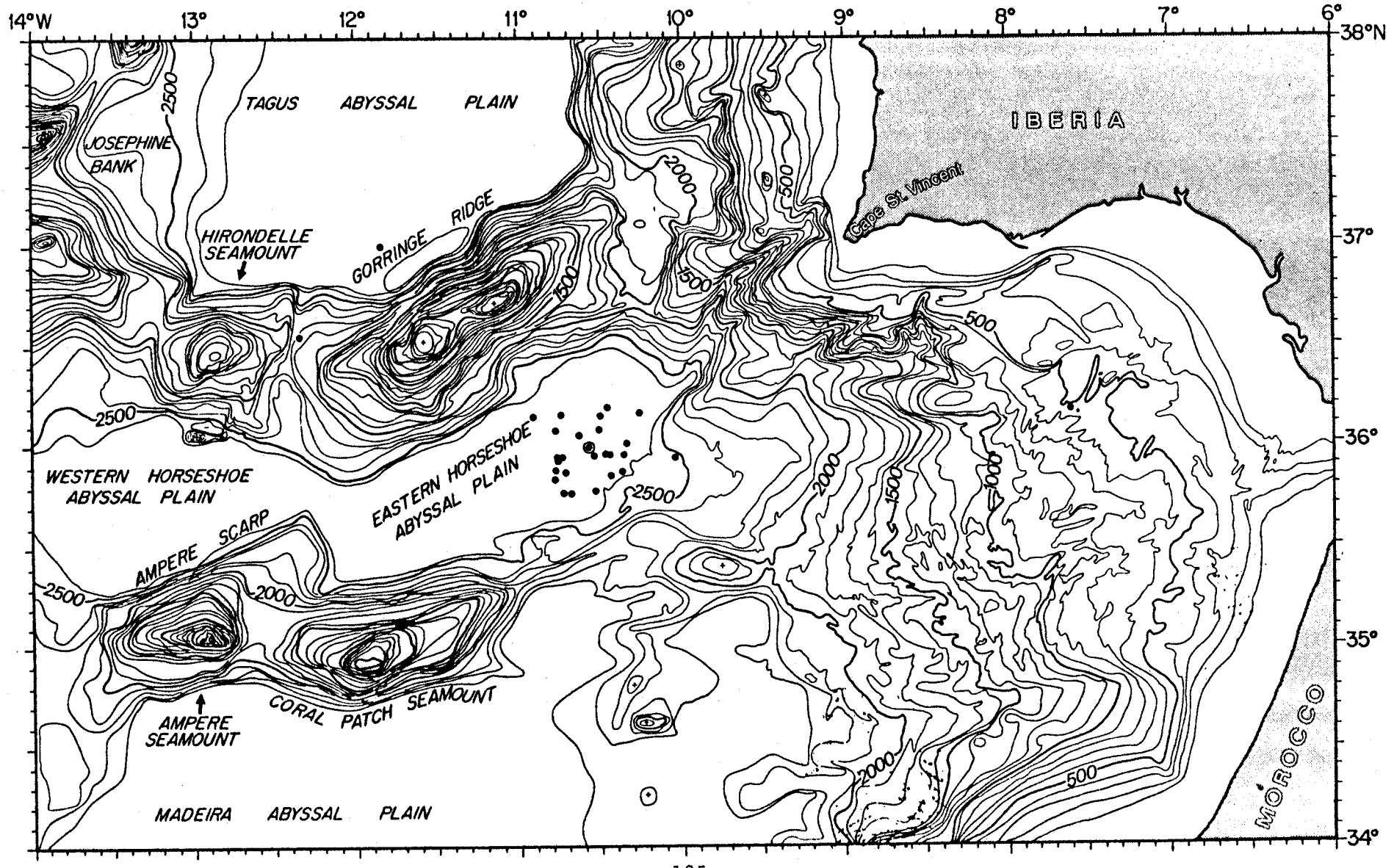
14°W
13°
12°
11°
10°
9°
8°
7°
6°
38°N
37°
36°
35°
34°
IBERIA
Cape St. Vincent
MOROCCO
TAGUS ABYSSAL PLAIN
JOSEPHINE BANK
HIRONDELLE SEAMOUNT
GORRINGE RIDGE
WESTERN HORSESHOE ABYSSAL PLAIN
EASTERN HORSESHOE ABYSSAL PLAIN
AMPERE SCARP
AMPERE SEAMOUNT
CORAL PATCH SEAMOUNT
MADEIRA ABYSSAL PLAIN
2500
2000
1500
500

FIGURE 33. Model for normal consumption of oceanic crust (from Purdy, 1975).

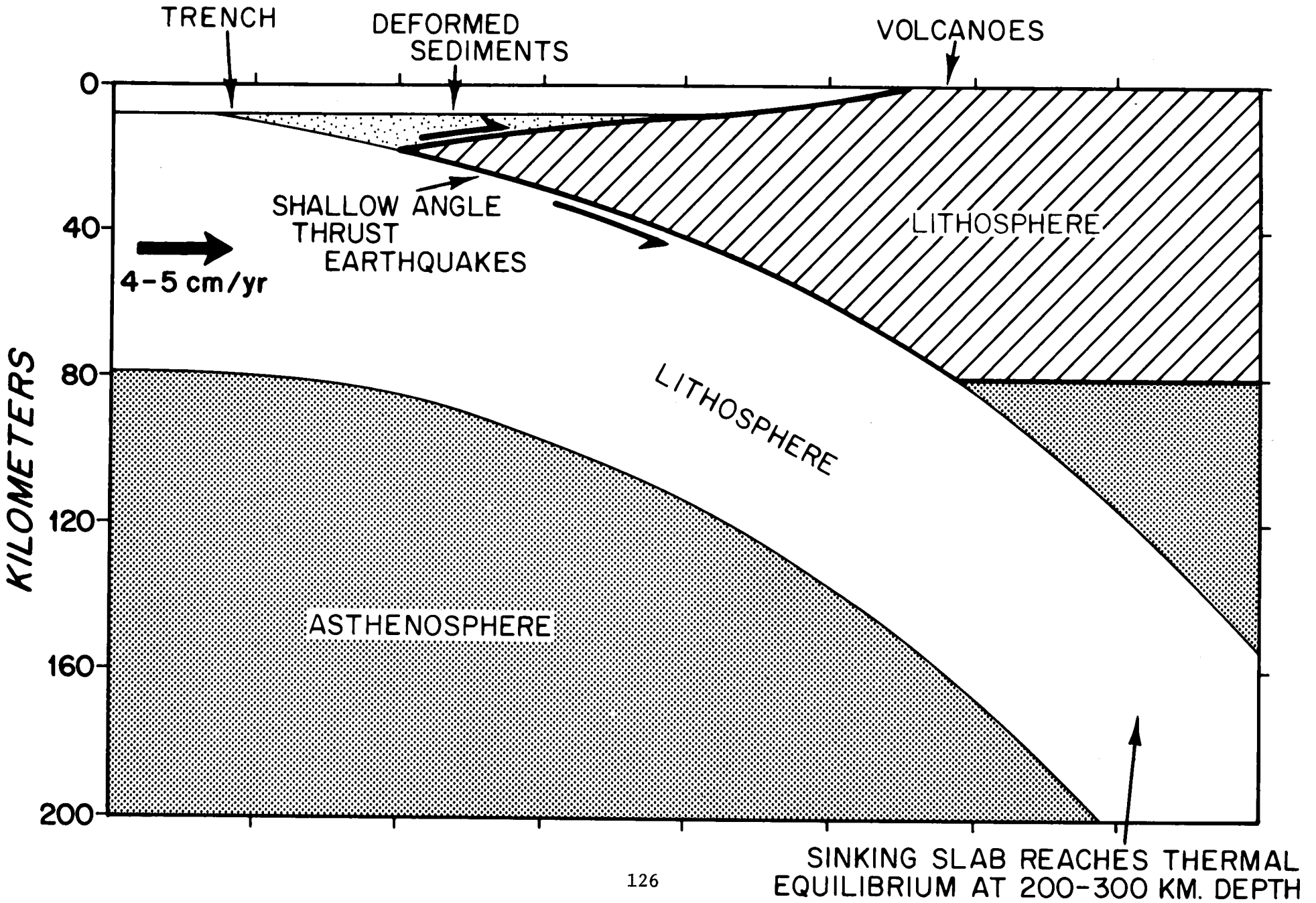
TRENCH
DEFORMED SEDIMENTS
VOLCANOES
0
40
80
120
160
200
KILOMETERS
SHALLOW ANGLE THRUST EARTHQUAKES
4-5 cm/yr
LITHOSPHERE
LITHOSPHERE
ASTHENOSPHERE
SINKING SLAB REACHES THERMAL EQUILIBRIUM AT 200-300 KM. DEPTH

FIGURE 34. Model for slow consumption of oceanic crust resulting in Gorringe Ridge and satisfying all data presented by Purdy (1975).

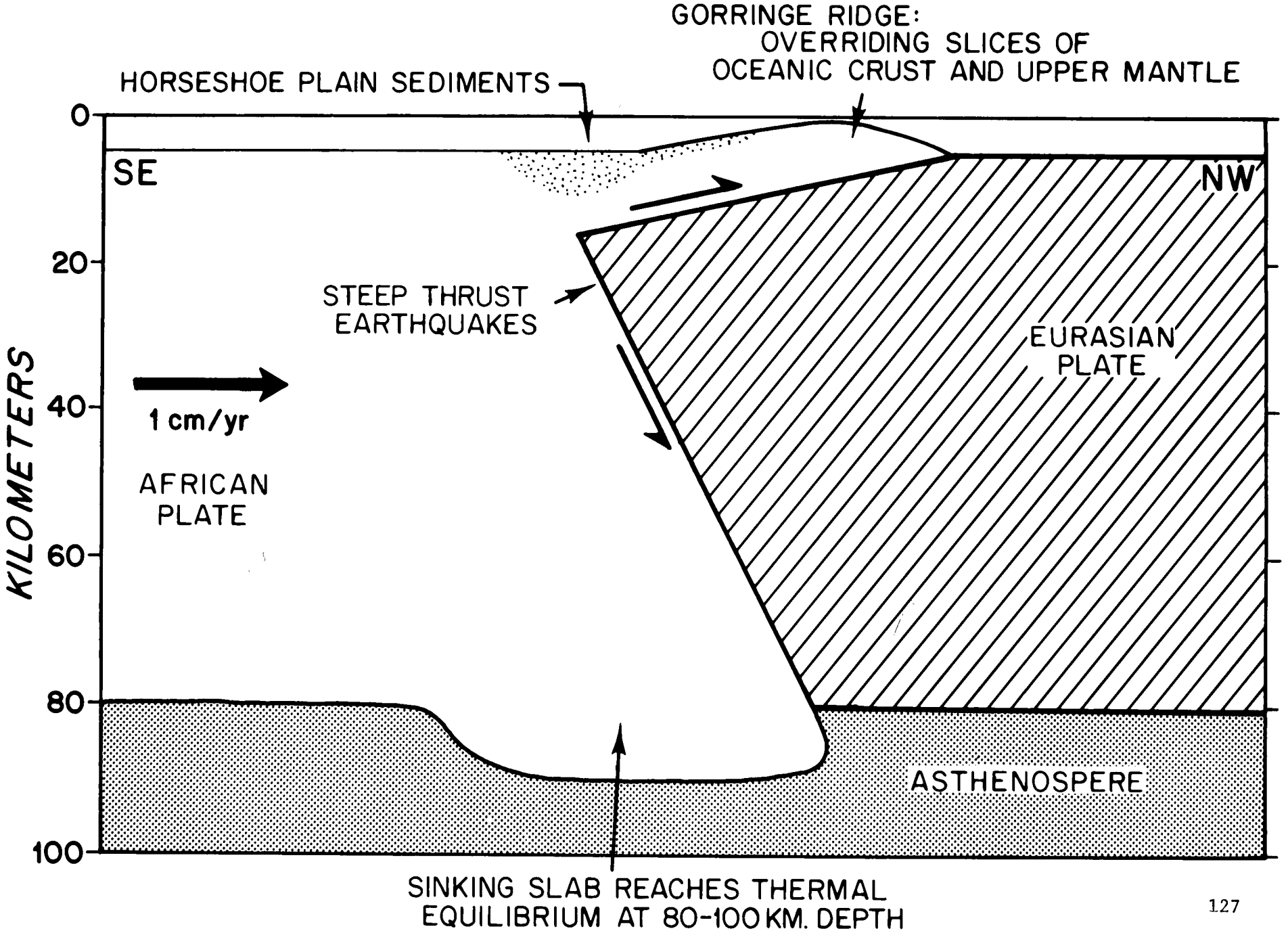
GORRINGE RIDGE:
OVERRIDING SLICES OF
OCEANIC CRUST AND UPPER MANTLE
HORSESHOE PLAIN SEDIMENTS
0
SE
NW
20
STEEP THRUST
EARTHQUAKES
EURASIAN
PLATE
KILOMETERS
40
1 cm/yr
AFRICAN
PLATE
60
80
ASTHENOSPERE
100
SINKING SLAB REACHES THERMAL
EQUILIBRIUM AT 80-100 KM. DEPTH

of oceanic crust resulting in the Gorringe Ridge and satisfying all the data presented in his paper. Purdy discusses the possibility of a fixed finite difference pole for tens of millions of years in order to explain the remarkable topographic relief of the Gorringe Ridge, the Hirondelle Seamount, the Ampere Seamount, and the Coral Patch Seamount (see discussion of Dewey and others, 1973). Problems with this model are several, but most of them are written off by Purdy due to the fact that the convergence rates are so low and that the eight-year collection of seismic data is so short. More rigorous studies will test Purdy's hypothesis.

Purdy also hypothesized that there was a change in pole position about 10 m. y. ago, since which there has been slow compression; 60-72 m. y. before that (i.e. 70-82 m. y. ago), there was right-lateral strike-slip motion at a rate of 5.5 cm/yr., according to Purdy's interpretation of various salient data. Purdy's presumed direction of compression in the last 10 m. y. is about 60° south of east; at right angles to this (60° east of north) is the presumed direction of previous strike-slip motion, which follows the predominant bathymetric trend in this area (60° east of north). Purdy points out that this trend is also recorded in the structures of the Algarve of southern Portugal and Spain (Pratsch, 1958); Pratsch reports that the Upper Triassic lies discordantly upon intensely folded Paleozoic to Turonian (85 m.y.b.p.) rocks. This data can also be construed to support Purdy's hypothesis of a change in tectonics circa 85 m.y.b.p.

APPENDIX III.

DETAILED LABORATORY PROCEDURES

Following are the laboratory procedures used in studying sediment samples.

Grain Size Analysis (Adapted from Schlee, 1957).

Run Eight Samples at Once:

1) With a pocket knife, shave the contaminated sediment off the outside of the core sample.

2) Soak 1 to 15 grams of sediment (15 gms normal size) in 100 ml redistilled water for at least 24 hours.

3) Centrifuge in 250 ml redistilled water for five minutes at 2000 r.p.m., and pour off the salt water.

4) Disaggregate with an ultrasonic bath for two minutes.

5) Sieve each sample through a 63 micron, 3 inch diameter brass sieve using finger and washing with 2g/l sodium hexa-metaphosphate water (Calgon). Washings (silt and clay) go directly into 1000 ml glass cylinders. Fill each cylinder to 1000 ml with sodium hexametaphosphate water, stir, and allow to set for 2 to 3 hours to see if the sample flocculates.

6) Wash the greater than 63 micron fraction with distilled water into a weighed beaker. Dry and weigh the sand fraction.

7) Agitate each 1000 ml cylinder vigorously with a rubber plunger for 30 seconds, insert pipette at least 25 cm below the water surface and withdraw a 50 ml aliquot, the time zero sample. Place it in a numbered, weighed 50 ml beaker. Rinse

sediment on walls of pipette (with redistilled water) into beaker for each aliquot.

8) Agitate 1000 ml cylinder for 30 seconds, wait 2 minutes, and withdraw a 50 ml aliquot from a depth of 10 cm below the surface. Repeat for other 7 cylinders.

9) Then begin procedure where all aliquots are taken sequentially at carefully timed intervals. At eight minutes from time zero, agitate the first cylinder for 30 seconds, wait 30 seconds, then agitate the second for 30 seconds, wait 30 seconds, then agitate the third, etc. After the agitation of the eighth cylinder, wait 30 seconds and take an aliquot from the first cylinder at a depth of 10 cm. Take aliquots from successive cylinders at one minute intervals.

10) Repeat this procedure without agitating the cylinders at

times:	and depths:
32 min	10 cm
2 hr 08 min	10 cm
5 hr 58 min	7 cm
24 hr 00 min	7 cm

Cover the cylinders to prevent dust contamination before these last four aliquots.

Grain size statistics were calculated from cumulative percent curves (Figure 35) on the basis of the most accurate of Folk's (1968) formulas for the following four commonly cited parameters:

1) Mean grain size (Folk's graphic mean) with a formula of $M_z = (\emptyset 16+\emptyset 50+\emptyset 84)/3$ and with verbal limits determined by

the phi (Ø) scale and Wentworth's (1922) size classes;

2) Sorting index (Folk's inclusive graphic standard deviation) with a formula of $\sigma_I = \frac{Ø84-Ø16}{4} + \frac{Ø95-Ø5}{6.6}$ and with indicies of less than 0.35 called very well sorted, 0.35 to 0.50 well sorted, 0.50 to 0.71 moderately well sorted, 0.71 to 1.00 moderately sorted, 1.00 to 2.00 poorly sorted, 2.00 to 4.00 very poorly sorted, and greater than 4.00 extremely poorly sorted;

3) Skewness index (Folk's inclusive graphic skewness) with a formula of $SK_I = \frac{Ø16+Ø84-2Ø50}{2(Ø84-Ø16)} + \frac{Ø5+Ø95-2Ø50}{2(Ø95-Ø5)}$ and with indicies of 1.00 to 0.30 called strongly fine skewed, 0.30 to 0.10 fine skewed, 0.10 to -0.10 nearly symmetrical, -0.10 to -0.30 coarse skewed, and -0.30 to -1.00 strongly coarse skewed (those with excess fine material, that is, a tail to the right on cumulative percent curves, have positive skewness whereas, those with excess coarse material, that is, a tail to the left on cumulative percent curves, have negative skewness); and finally,

4) Kurtosis (peakedness) index (Folk's graphic kurtosis) with a formula of $K_G = \frac{Ø95-Ø5}{2.44(Ø75-Ø25)}$ and with indicies less than 0.67 called very platykurtic (flat), 0.67 to 0.90 platykurtic, 0.90 to 1.11 mesokurtic, 1.11 to 1.50 leptokurtic, 1.50 to 3.00 very leptokurtic, and greater than 3.00 extremely leptokurtic (peaked). By referring to the cumulative curve (Figure 35), the reader can grasp an understanding of how each of these parameters is calculated. For example, the Ø5 value is determined by going 5% of the way up the curve along

FIGURE 35. Cumulative percent curve model used to demonstrate method of calculation for the grain size statistics used in this study.

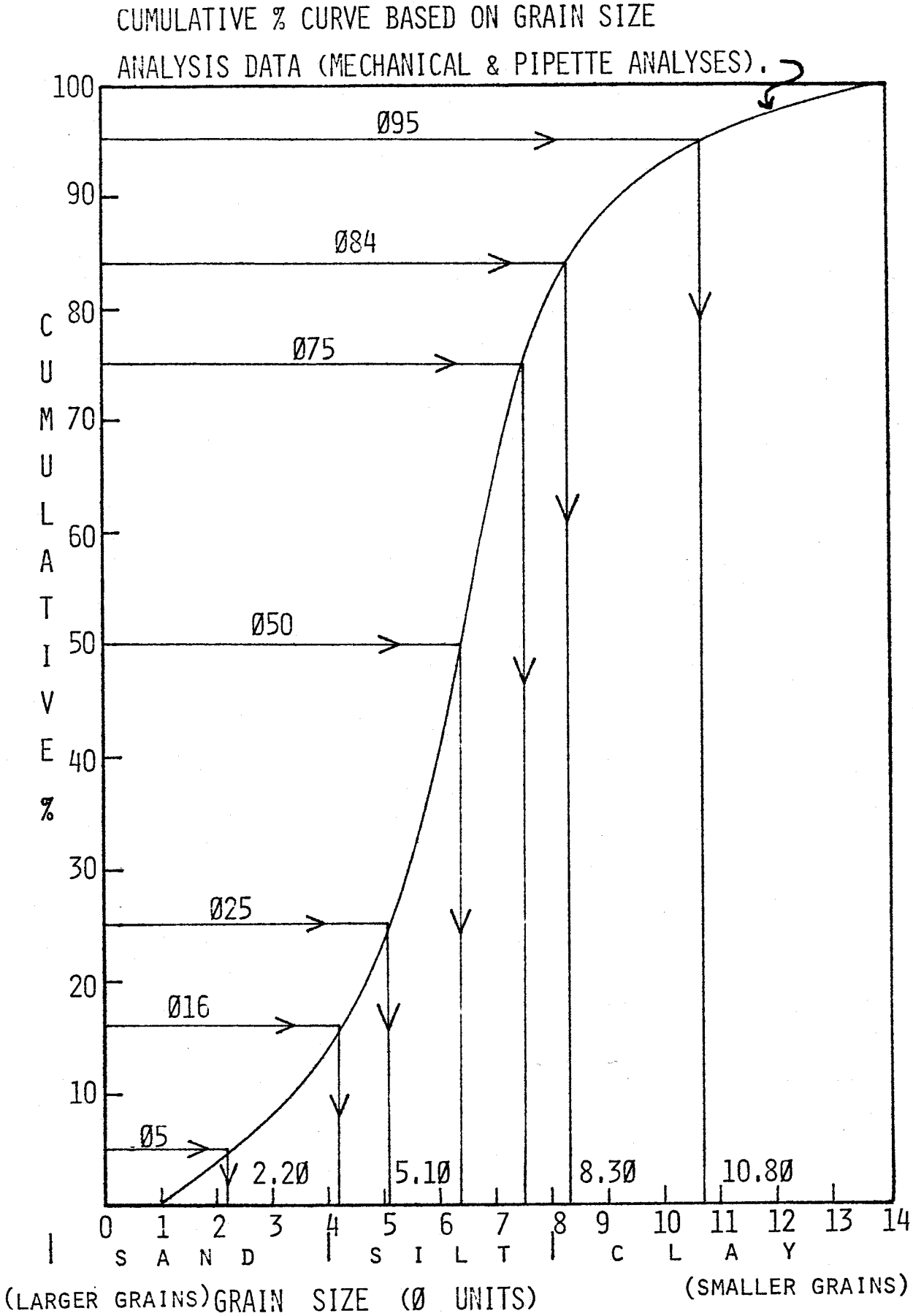
CUMULATIVE % CURVE BASED ON GRAIN SIZE
ANALYSIS DATA (MECHANICAL & PIPETTE ANALYSES).
CUMULATIVE %
100
90
80
70
60
50
40
30
20
10
Ø95
Ø84
Ø75
Ø50
Ø25
Ø16
Ø5
2.2Ø
5.1Ø
8.3Ø
10.8Ø
0 1 2 3 4 5 6 7 8 9 10 11 12 13 14
SAND
SILT
CLAY
(LARGER GRAINS) GRAIN SIZE (Ø UNITS) (SMALLER GRAINS)

the vertical y-axis, measuring orthogonally over to the cumulative % curve, and then dropping down vertically until reaching the x-axis, measured in Ø units. In this case, Ø5=2.20, and so on for the others. Note that the Ø units cancel in the formulae above.

10% HCl-Solubility Determination Procedure.

A weighed amount (1.0 gm) of agate-ground sample was placed in a weighed 50 ml beaker containing 30 ml of 10% HCl. The sample was then placed in an ultrasonic bath for 10 minutes and stirred occasionally (the HCl was tested for potency after use). The sample was then washed into a centrifuge tube with redistilled water and centrifuged for 2 minutes at 3100 r.p.m. Then, the supernatant liquid was poured off and the remaining solid was washed with redistilled water into a 50 ml beaker for drying (below 70° C in an oven) and weighing (to the nearest 0.001 gm).

Grain-Counting Statistics Chart for Mineralogy Determination.

Since the most important source of error in modal point-counting of grains arises from counting a limited number of grains, it is important to assess this error in a statistical manner (Hubert, 1971). This error is a function of the number of randomly-drawn grains from the total population. Although the population is, in each slide, a finite number, in actual practice, the number is so large that it can be considered infinite for counting purposes. The binomial

which best represents the probability density function is: $f(x)=(p+q)^n$, where x is the number of grains of the specific mineral encountered in traverses, p is the probability of encountering the mineral, q is the probability of not encountering the mineral, and n is the total number of grains in the traverses. Using the mean, $\bar{X}$, and size, n, of a sample, the 95% confidence interval around the population mean of a bimodal distribution can be read from Figure 36 (from Hubert, 1971). If, for instance, a mineral forms 25% (y-axis) of the assemblage based on a count of 100 grains, the interval from 16% to 34% (x-axis) has a 95% possibility of including the fixed, real population mean. The sample population size for the present study on the sands of the Horseshoe Abyssal Plain turbidites was taken to be at least 202, but not less than 958, which would have reduced the range of the 95% confidence interval in the above example to from 18% to 32% or 22% to 27%, respectively.

Parameters for Sample X-Ray Diffraction.

The following parameters were employed in XRD runs on the Siemens unit: 20 kv, 20 ma, Ni filter, Cu K radiation, scintillation counter 1175, slits $1/4^{\circ}$, 0.1 mm, 5v base, 20v window, run at $1/8^{\circ}$ 2θ per minute equals ¼ cm on chart drive, $1x10^3$ or $2x10^3$ impulses full scale, and 2% or 3% time constant. Diffractions were made at:

FIGURE 36. Chart of Hubert (1971) used to demonstrate grain counting statistics validity. Ninety-five percent confidence limits are shown for means drawn from the binomial distribution. The sample mean = x/n. Axes units are explained in the text. Numbers inside the figure denote the number of grains counted, which enclose a 95% confidence interval around the true sample mean.

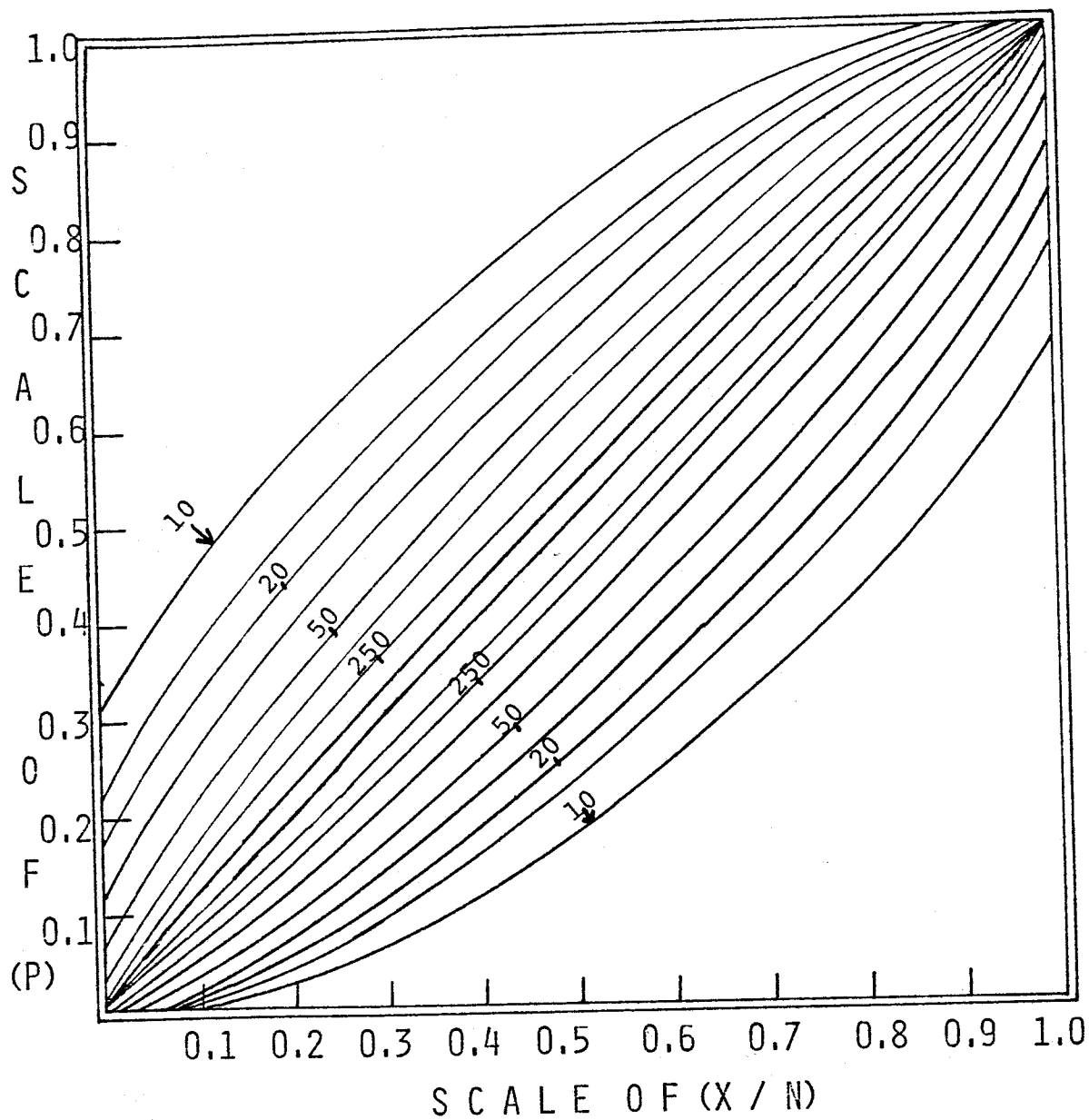
1.0
0.9
S
0.8
C
0.7
A
0.6
L
0.5
E
0.4
0.3
O
0.2
F
0.1
(P)
10
20
50
250
250
50
20
10
0.1 0.2 0.3 0.4 0.5 0.6 0.7 0.8 0.9 1.0
SCALE OF (X / N)

Angles ($^{o}2\theta$):	Identifying the following minerals:
8.0-10.0	Muscovite-Illite (8.9^{o}); Ferririte (9.2-9.35^{o})
11.5-13.0	Kaolinite (12.35^{o}); Chlorite (12.45^{o})
13.5-15.5	Orthoclase (13.75^{o}); Albite (13.85^{o}); Ferririte (15.2^{o})
17.5-19.0	Muscovite (17.75^{o}); Chlorite (18.8^{o})
20.0-21.5	Kaolinite (20.3^{o}, 21.2^{o}); Quartz (20.9^{o}); Microcline (21.05^{o})
22.0-22.5	Orthoclase (22.15^{o}); Ferririte (22.5^{o})
24.5-31.5	Kaolinite (24.9^{o}); Ferririte (25.15^{o}, 25.5^{o}); Chlorite (25.25^{o}); Quartz (26.65^{o}); Muscovite (26.7^{o}); Microcline (27.1^{o}, 27.4^{o}, 27.5^{o}); Albite (27.9^{o}); Orthoclase (28.1^{o}); Calcite (29.4^{o}); and Dolomite (30.9^{o})
35.5-36.5	Kaolinite (36.0^{o})